A Torso Haptic Display based on Shape Memory Alloy Actuators

by
Mealani Nakamura

B.S. Mechanical Engineering
Massachusetts Institute of Technology, 2000

SUBMITTED TO THE DEPARTMENT OF MECHANICAL ENGINEERING IN PARTIAL FULFILLMENT OF THE REQUIREMENTS FOR THE DEGREE OF

MASTER OF SCIENCE IN MECHANICAL ENGINEERING

AT THE
MASSACHUSETTS INSTITUTE OF TECHNOLOGY

SEPTEMBER 2003

Signature of Author: _____
Department of Mechanical Engineering
June 27, 2003

Certified by: _____
Lynette A. Jones
Principal Research Scientist in Mechanical Engineering
Thesis Supervisor

Accepted by: _____
Ain A. Sonin
Chairman, Department Committee on Graduate Students

A Torso Haptic Display based on Shape Memory Alloy Actuators

by
Mealani Nakamura

Submitted to the Department of Mechanical Engineering
on June 23, 2003 in Partial Fulfillment of the
Requirements for the Degree of Master of Science in
Mechanical Engineering

ABSTRACT

The focus of this thesis is on the development of a Tactile Vest, a wearable, torso-based haptic device. The tactor for the Tactile Vest was designed and built based on NiTi shape memory alloys. Four of these tactors were manufactured to form a 2x2 and 4x1 array, and tested for use in a wearable device. The tactors are self-contained, and are 42 mm x 22 mm x 17 mm. The tactors were able to generate a mean of 133 kPa in pressure, which is over twice the touch threshold of the torso, and the tactor pin contacting the skin was able to displace 3 mm at a bandwidth of 0.3 Hz. The tactor array was attached to a fitting garment, and preliminary tests were conducted. The tactor activations were described as firm sensations of pressure, as if someone were gently prodding the skin with a finger. The wearable array of tactors based on shape memory alloys is recommended for further development and testing.

Thesis Supervisor: Lynette A. Jones
Title: Principal Research Scientist in Mechanical Engineering

Acknowledgements

I would first like to thank my advisor, Lynette, for her thoughtful guidance and endless patience. I admire her immensely, as a leading scientist in her field, a wonderful mother, and a caring, understanding, amazing person with a great sense of humor. I have never respected someone so much. Many thanks to Ian for upholding and exemplifying the highest standards in research and technology; I have learned much from being a part of the BioInstrumentation Lab.

I would also like to extend my thanks to the members, past and present, of the BioInstrumentation Lab. Special thanks to Tim, Nic, and Laura, for giving their time so generously to help me construct and debug my circuits, and helping me with the HAAS. Peter, James, and Robert, your advice and tips and help along the way were invaluable. And thank you to Rachel, Michal, and Aimee, for helping me to get started in the lab and showing me around. Thank you to all the lab members; your excitement for the research you conduct, and the breadth of knowledge in the lab, have provided much inspiration and motivation for me.

This research was supported in part through the Advanced Decision Architectures Collaborative Technology Alliance sponsored by the U.S. Army Research Laboratory under Cooperative Agreement DAAD19-01-2-0009.

Table of Contents

1 Introduction

The focus of this thesis is on the development of a Tactile Vest, which is a wearable device that provides haptic feedback to the torso. The main objective will be to develop a robust, versatile actuator for the Tactile Vest based on Nitinol, a shape memory alloy (SMA).

The haptic system is an untapped channel of communication, yet our skin (total surface area is 1.8 m^2 for the average human adult) contains thousands of mechanoreceptors specialized for the sense of touch (see Chapter 2 for information on the physiology and sensitivity of the human skin). The torso in particular offers a large haptic drawing space, claiming roughly half the total skin surface area, or about 1 m^2. The Tactile Vest would access an underused sensory channel, alleviating sensory overload of the eyes and ears, as well as leaving the hands free for other tasks.

Torso-based tactile displays have a long history as sensory substitution devices for the blind and deaf. In the 1960s Bach-y-Rita started working on a number of tactile vision substitution systems (TVSS), in which images that were recorded by a television camera were conveyed electrically or mechanically on the skin (Kaczmarek et al., 1991). More recently, the use of haptic feedback to the torso as a balance prosthesis has been explored in patients with vestibular loss (Wall and Weinberg, 2003; Wall et al., 2001). Tactile vests have also been used to provide feedback to pilots controlling aircraft (Rupert, 2000; Rupert et al., 1993), and have shown potential in providing navigation and orientation cues in unusual environments such as during extra vehicular activities in space (Rochlis and Newman, 2000; Traylor and Tan, 2002). A Tactile Vest may also aid in situation awareness (e.g., a buzz felt on one side could indicate the approach of a person or vehicle from that direction) using a communication modality that is not seen or heard by anyone else (Rupert, 2000). Chapter 3 contains a summary of the various torso-based haptic displays mentioned above and an overview of the actuating technology in these devices.

Researchers developing these torso-based devices have expressed the need for improved actuator technology. Ideally, actuators should be more perceptually robust, yet lightweight and flexible, making them comfortable and invisible to the user until a stimulus occurs. In addition, the actuator should also be able to output a wide range of frequencies and intensities in order to create a variety of tactile stimuli (Rupert, 2000).

We propose the use of Nitinol, a shape memory alloy (SMA), as the actuator to satisfy these requirements. Shape memory alloys have the ability to "remember" their original shape even after undergoing deformation. At lower temperatures, the SMA is easily deformed; heating, however, causes changes in the crystalline structure, and the deformed alloy is returned to its original shape with considerable force (see Chapter 4 for more information on shape memory alloys and their use in various tactile displays). Nitinol can produce very large stresses, over 200 MPa, compared to muscle, which produces 0.1-0.35 MPa, and can generate strains of 4%. The SMA has high power to mass and energy to volume ratios, and is small in size and flexible, features advantageous for its use in the thin, dynamic workspace of a vest.

The ability of Nitinol to generate adequate stresses and strains was confirmed in preliminary tests (see Chapter 5), and a tactor, an actuator that provides tactile stimulation, was designed and built using Nitinol (see Chapter 6). Four tactors were manufactured to form a 2x2 array, and tested for use in a wearable device (see Chapter 7). The tactor is self-contained, its overall size being 42 mm x 22 mm x 17 mm. The tactor can generate on average 133 kPa in pressure, which is over twice the touch threshold in the torso, and the tactor pin that contacts the skin is able to displace 3 mm at a bandwidth of 0.3 Hz. The tactor array was then attached to a fitting garment, and preliminary tests were conducted on the device (see Chapter 8). It was concluded that a tactor based on shape memory alloys holds promise for use in a wearable, torso-based tactile display.

2 The Psychophysiology of Touch

The average human adult has a total skin surface area of 1.8 m^2. Within and just below the skin are thousands of specialized mechanoreceptors responsible for the sense of touch. The glabrous, or hairless, skin found on the hands, lips, and soles of the feet is the most responsive to touch. The majority (90%) of skin, however, is covered in hair, and is less sensitive to tactile stimuli (Gardner et al., 2000; Kaczmarek and Bach-y-Rita, 1995).

The receptors responsible for the sense of touch in both glabrous and hairy skin are mechanoreceptors. They sense deformation of the skin and motion across the skin surface. The mechanoreceptor consists of an afferent nerve fiber whose end is unmyelinated and encapsulated by a non-neural structure. Both the nerve fiber and end organ are physiologically specialized for a particular function (Gardner et al., 2000; Johnson, 2001). Mechanical deformations applied to the skin (e.g. vibration, pressure, and stretch) deform the end organ or receptor. These deformations are transmitted to the nerve fiber in a manner determined by the end organ's physiology and so the properties of the end organ influence the dynamics of the receptor response (Gardner et al., 2000; Johnson, 2001). Furthermore, the properties of the terminal membrane of the innervating nerve determine the level of sensitivity and type of stimulation that activates the nerve ending. If appropriate stimulation occurs, a transducer within the nerve ending sends an electrical impulse to the central nervous system where it is further processed and translated into a tactile sensation (Gardner et al., 2000; Johnson, 2001).

2.1 Touch in Glabrous Skin

Glabrous skin is arranged in circular patterns of regular arrays of ridges that result from the folds of the epidermis (Gardner et al., 2000). Innervating the glabrous skin are four types of afferent nerve fibers:

1. slowly adapting type I (SAI) afferent nerve fibers,
2. rapidly adapting or fast adapting type I (RA or FAI) afferent nerve fibers,
3. Pacinian or fast adapting type II (PC or FAII) afferent nerve fibers, and
4. slowly adapting type II (SAII) afferent nerve fibers.

The afferent nerve fibers adapt at different rates to static stimuli, and are classified by this rate of adaptation. Pacinian and RA nerve fibers are rapidly adapting, and react primarily at the onset and offset of a stimulus and then their response rapidly decays. On the other hand, SAI and SAII afferent nerve fibers adapt at a much slower rate. The SAI afferents discharge action potentials irregularly and the SAII afferents regularly, in response to steady, static stimuli (LaMotte and Srinivasan, 1987). The SAI and SAII afferent fibers produce action potentials at a rate proportional to the force applied to the mechanoreceptor (Gardner et al., 2000).

The afferent nerve fibers are also classified by their receptive field sizes. A small receptive field is classified as a type I receptor, and II indicates a large field (Kaczmarek and Bach-y-Rita, 1995). The receptive field is the area of skin that excites a receptor; receptors with smaller fields are capable of finer spatial resolution, while receptors with larger fields detect coarse detail (Burdea, 1996). See Table 2-1 for the receptive field sizes of each mechanoreceptor in the hand.

Each of the four afferent nerve fibers has a different end organ surrounding its terminus.

1. SAI afferent nerve terminals are surrounded by Merkel disks,
2. RA afferent nerve terminals are surrounded by Meissner corpuscles,
3. PC afferent nerve terminals are surrounded by Pacinian corpuscles, and
4. SAII afferent nerve terminals are surrounded by Ruffini endings.

Meissner corpuscles and Merkel disks are smaller, more numerous, and are located in the superficial layers of skin, just below the epidermis. Pacinian corpuscles and Ruffini endings are larger and located in the dermis and subcutaneous tissue (Gardner et al., 2000) (see Figure 2-1). The mechanoreceptors are densest at the fingertip, with a total of about 300 mechanoreceptors per cm^2, with fewer mechanoreceptors in the proximal phalanges (20 per cm^2) and palm (50 per cm^2) (Gardner et al., 2000).

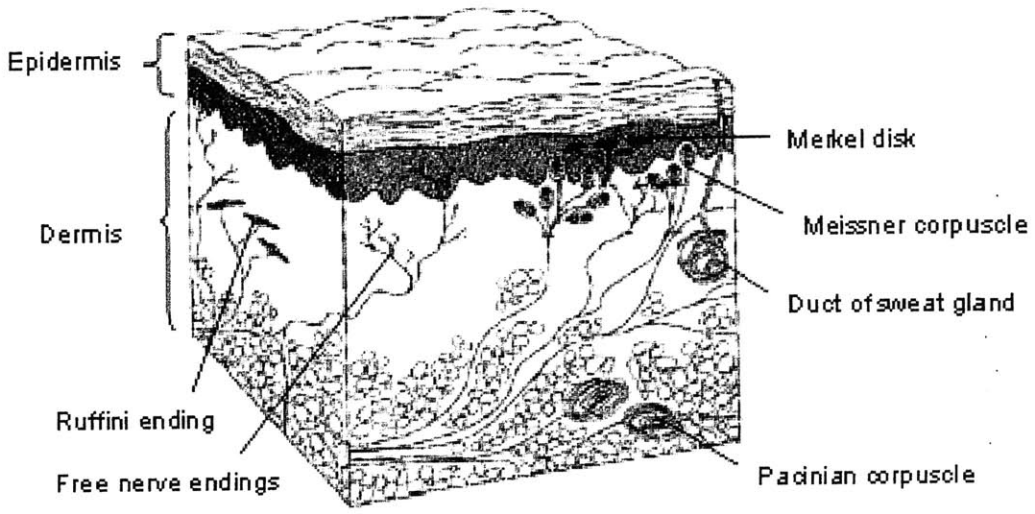

Figure 2-1. Glabrous skin with touch mechanoreceptors (adapted from Okamura, 2001).

Throughout this chapter, the hyphenated term Merkel disk-SAI afferent nerve fiber will refer to the mechanoreceptor consisting of the SAI afferent nerve fiber and Merkel disk. Similarly, the terms Meissner corpuscle-RA afferent nerve fiber, Pacinian corpuscle-PC afferent nerve fiber, and Ruffini ending-SAII afferent nerve fiber will be used to refer to the mechanoreceptor composed of the respective end organ and innervating nerve fiber.

The unique properties of the afferent nerve fibers and end organs convey distinct functions to each receptor unit. The Merkel disk-SAI afferent nerve fiber mechanoreceptor is the primary provider of spatial information, and believed responsible for the perception of form and surface details (Johnson, 2001; Kaczmarek and Bach-y-Rita, 1995). The information needed for grip control and the delicate manipulation of objects is provided by the Meissner corpuscle-RA afferent nerve fiber mechanoreceptor (Johnson, 2001). This receptor also provides form and surface detail information that is too small in variation for the Merkel disk-SAI afferent nerve fiber receptor to detect (Kaczmarek and Bach-y-Rita, 1995). The information required for skilled tool use is provided by the Pacinian corpuscle-PC afferent nerve fiber mechanoreceptor. The most sensitive to high frequency vibrations, this receptor detects distant events at the ends of objects held in the hand. Finally, the Ruffini ending-SAII afferent nerve fiber

mechanoreceptor provides information about hand and finger position (Johnson, 2001). However, there is some debate as to the contribution of this receptor to the sense of touch. Some investigators claim that while this receptor supplies kinesthetic information, it does not mediate tactile sensation (Kaczmarek and Bach-y-Rita, 1995).

The following sections contain more detail on the physiology, function, and capabilities of the mechanoreceptors found in glabrous skin. See Table 2-1 for a summary of the information provided above.

Table 2-1. The end organ, innervating afferent nerve fiber, function, and properties of the four mechanoreceptors found in glabrous skin.

Afferent nerve fiber	Slowly adapting type I (SAI)	Rapidly adapting (RA)	Pacinian (PC)	Slowly adapting type II (SAII)
End organ	Merkel disk	Meissner corpuscle	Pacinian corpuscle	Ruffini ending
Location	Superficial skin	Superficial skin	Subcutaneous tissue	Subcutaneous tissue
Adaptation speed	Slow	Fast	Fast	Slow
Innervation density [3]	Fingertip: 100 per cm^2	Fingertip: 150 per cm^2	Total in hand: 300	Fewer than SAI and RA
Percent total in hand [1]	25%	> 40%	13%	19%
Receptive field size [2,3]	Small Fingertip: 2-3 mm dia.	Small Fingertip: 10-30 mm^2 area 2-5 mm dia. Palm: 10 mm dia.	Large May include entire hand	Large 5x larger than SAI
Function	Perception of form and surface details	Feedback for grip control and delicate manipulation of objects	Information for skilled tool use	Hand and finger position (tactile sensation?)

References: 1. Burdea (1996), 2. Gardner et al. (2000), 3. Johnson (2001)

2.1.1 Merkel disk-slowly adapting type I (SAI) afferent nerve fiber, glabrous skin

The Merkel disk is a small, epithelial cell. The semi-rigid structure of the cell confers compressive strain to the enclosed nerve ending. Merkel disks are located very close to the dermal-epidermal junction and are clustered between the dermal papillae (the dermal ridges immediately below the epidermis) and so are sensitive to any dermal ridge

movement. The only mechanoreceptor closer to the epidermal junction is the Meissner corpuscle (Gardner et al., 2000).

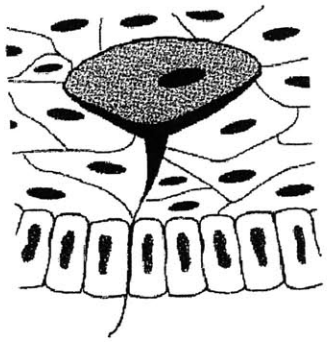

Figure 2-2. Merkel disk (from Okamura, 2001).

Merkel disks are innervated by slowly adapting type I (SAI) afferent nerve fibers. SAI fibers are sensitive to the strain energy density or a similar component that is proportional to the maximum local compressive strain squared (Johnson, 2001). This feature makes the SAI afferent fiber sensitive to the curvature, corners, and edges of an object. Sensitive to static deformation, the SAI afferent fiber adapts slowly, and discharges action potentials at an irregular rate for a long time in response to static stimuli (Burdea, 1996). Sustained indentation of the skin up to depths of 1500 μm produces a slowly adapting response linearly related to indentation depth (Johnson, 2001).

SAI afferents respond to flat surfaces with slow, continuous firing rates. If the surface is convex, and thus indents the skin, the rate of firing increases in proportion to the convexity of the surface. With concave surfaces, on the other hand, the receptor discharge rate slows and eventually stops (Gardner et al., 2000). Thus, these slowly adapting afferents can signal the pressure and shape of objects (Gardner et al., 2000). The population of SAI afferents is fairly dense, reaching about 100 per cm^2 in the fingertip. The SAI afferent nerve fibers split into many branches as they approach the skin surface. A single fiber covers an area of about 5 mm^2, and innervates in the order of 100 Merkel disks (Johnson, 2001) (10-25 according to Gardner et al., 2000).

The receptive field of the SAI afferent fiber is 2 to 3 mm in diameter. An individual fiber can dominate the response, making a "hot spot" within the receptive field. Individual

fibers have a spatial resolution of 0.5 mm. Thus, the receptor can sometimes have a spatial resolution smaller than its receptive field size due to the presence of hot spots (Johnson, 2001). The excellent resolution of the Meissner corpuscle-SAI afferent fiber unit, as well as its select sensitivity, allows this mechanoreceptor to resolve fine spatial details and respond to small changes in curvature. These properties make the receptor ideal for conveying surface texture and form (Johnson, 2001).

2.1.2 Meissner corpuscle-rapidly adapting (RA) afferent nerve fiber, glabrous skin

The Meissner corpuscle is globular, filled with fluid, and consists of many layers of flattened epithelial cells that surround two to six nerve fiber endings. These cell layers protect the sensitive nerve endings from static skin deformation. Of the four mechanoreceptors, the Meissner corpuscle is closest to the skin surface, located in the center of dermal papillae. Mechanical coupling to the dermal ridges confer further sensitivity to the Meissner corpuscle to any changes in dermal ridge shape (Gardner et al., 2000; Johnson, 2001).

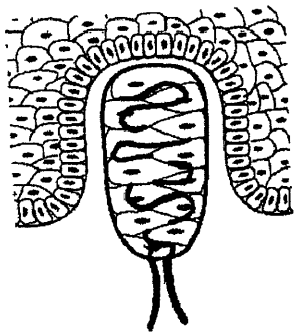

Figure 2-3. The Meissner corpuscle (from Okamura, 2001).

Meissner corpuscles are innervated by rapidly adapting (RA) afferent nerve fibers. As the RA afferent fibers approach the skin, they branch out and end as large, leaf- or disk-like structures. One fiber can innervate 10-25 Meissner corpuscles (Gardner et al., 2000; Johnson, 2001). The terminals of RA afferent nerve fibers are selectively sensitive to the velocity of objects contacting the skin. The RA afferents signal dynamic skin deformation with much greater resolution than SAI afferents, and are especially sensitive to the sudden movement or forces of objects in contact with the skin (Johnson, 2001). As

suggested by its name, the RA fiber reacts mostly at the onset of a stimulus and quickly adapts to static stimuli. The nerve response begins to saturate at indentations of 100 μm and does not register indentations over 300-400 μm (Johnson, 2001).

The population of RA afferent nerve fibers is fairly dense, with about 150 afferents per cm^2 at the fingertip (Johnson, 2001). The receptive field of the RA afferent fiber is relatively small, averaging 2 to 3 mm in diameter at the fingertip (3-5 mm according to Johnson (2001)), and 10 mm in diameter on the palm (Gardner et al., 2000). In contrast to the SAI afferent fiber, which has a similar field size, the RA nerve fiber has a fairly uniform response over its entire receptive field. Furthermore, when uniformly stimulated, each branch of the afferent nerve fiber contributes equally to the neural signal (Johnson, 2001). Although this uniformity in response lends poor spatial resolution to the RA afferent, the sensitive nerve endings signal skin movement precisely (Johnson, 2001).

The main function of the Meissner corpuscle-RA afferent mechanoreceptor is to provide the feedback necessary for finger grip control. The receptor is able to detect very small slips of an object against the skin. The central nervous system uses this information to make minute adjustments in grip force, which allows for delicate object control and manipulation. Studies have shown that people are able to exert forces at the fingertips that are barely above the minimum required to keep an object from slipping out of the hand (Johnson, 2001).

Johnson (2001) cites several characteristics of the Meissner corpuscle-RA afferent nerve fiber mechanoreceptor that make it ideal for detecting micro-slips. The receptor's high sensitivity to skin motion and strong, uniform response to local events mean that even the smallest slips are signaled robustly. Furthermore, the Meissner corpuscle shields the RA afferent nerve fiber from static force or very low frequency stimuli, and thus the low frequency, high amplitude grip forces do not interfere with the sensation of micro-slips.

The physiology and adaptation speed of the receptor also allows the Meissner corpuscle-RA afferent nerve fiber to distinguish fine surface detail and form that are too small in

variation for the Merkel disk-SAI afferent nerve fiber mechanoreceptor to detect (Burdea, 1996; Gardner et al., 2000; Kaczmarek and Bach-y-Rita, 1995).

2.1.3 Pacinian corpuscle-Pacinian (PC) afferent nerve fiber, glabrous skin

The Pacinian corpuscle is similar to the Meissner corpuscle in structure and purpose. The Pacinian corpuscle is relatively large, filled with fluid, and has many layers (as many as 70) that enfold the nerve ending. The layers act as high-pass mechanical filters that shield the sensitive nerve ending from large, low frequency stresses and strains (Gardner et al., 2000; Johnson, 2001).

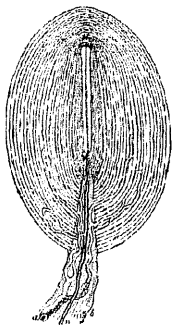

Figure 2-4. The Pacinian corpuscle (from Gray, 2001).

Pacinian corpuscles are located below the superficial layers of skin in the dermis and deeper tissues. They have also been found in the mesentery, between muscle layers, and on interosseous membranes. The corpuscle is connected flexibly to the skin, conferring extra sensitivity to the receptor to skin deformations centimeters away (Gardner et al., 2000).

The Pacinian corpuscle, innervated by the Pacinian (PC) afferent nerve fiber, is the most sensitive of all the mechanoreceptors to vibration. The Pacinian afferent nerve fiber is rapidly adapting and extremely sensitive to vibration, especially vibrations in the range of 200 to 250 Hz. A stimulus 3 nm in amplitude, when applied directly to the surrounding Pacinian corpuscle, can trigger a response from the most sensitive PC fibers. Vibrations of only 10 nm are known to stimulate the fiber when the stimulus is applied to the skin (Johnson, 2001). However, proportionally larger amplitude vibrations are needed to

activate the receptor for frequencies lower and higher than the threshold frequency (Gardner et al., 2000). Pacinian afferent fibers are less numerous than SAI and RA afferent fibers, with roughly 40-60 afferent fibers per finger and 300 total in the hand (Stark et al., 1998). Unlike SAI and RA afferent fibers, Pacinian afferent nerve fibers do not have branches; instead, a single fiber innervates a single Pacinian corpuscle (Gardner et al., 2000; Johnson, 2001).

The extreme sensitivity of the PC afferent fiber and location of the Pacinian corpuscle give this mechanoreceptor a very large receptive field and virtually no spatial resolution. A receptive field may include the entire hand; there is, however, a point of greatest sensitivity immediately above the receptor (Gardner et al., 2000; Johnson, 2001). This mechanoreceptor is believed to contribute to the skilled use of objects held in the hand. The Pacinian afferent nerve fiber provides the means to monitor events occurring at the far end of an object held in the hand by responding to even the smallest vibrations of a surface. The great sensitivity of the Pacinian nerve fiber would be useless, however, if the Pacinian corpuscle did not first filter out the high intensity, low frequency impact the hands are subjected to in everyday tasks. These combined abilities of the mechanoreceptor, namely its sensitivity and filtering characteristics, allow for dexterous tool use (Johnson, 2001).

2.1.4 Ruffini ending-slowly adapting type II (SAII) afferent nerve fiber, glabrous skin

Ruffini endings, or Ruffini corpuscles, are larger than the mechanoreceptors in the superficial layers of skin, and are shaped like spindles. They are found in the connective tissue of the dermis, attached between subcutaneous tissues, or coupled to fingernails or skin on the joints or palm. A single slowly adapting type II (SAII) afferent nerve fiber innervates a single Ruffini ending. SAII afferent nerve fibers are fewer in number and have larger receptive fields than SAI and RA afferent nerve fibers.

The Ruffini endings are well positioned for the perception of skin stretch and bending of the joints. In fact, the main function of the Ruffini ending-SAII afferent nerve fiber

mechanoreceptor is considered to be the monitoring of hand and finger position. SAII afferent nerve fibers are the most sensitive to skin stretch, about twice as sensitive as the SAI fiber. However, the SAII afferent nerve fiber is six times less sensitive to indentation of the skin than SAI afferents (Gardner et al., 2000; Johnson, 2001).

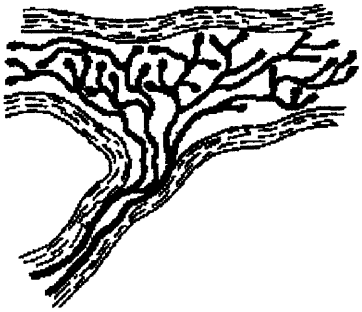

Figure 2-5. Ruffini ending (from Ascoli, 2001).

There is some debate as to the contribution of this receptor to the sense of touch. Some investigators claim that while this receptor supplies kinesthetic information, it does not mediate tactile sensation (Kaczmarek and Bach-y-Rita, 1995). Kaczmarek and Bach-y-Rita (1995) reported that while the receptor responds to shearing forces applied to the skin, no tactile sensation was recorded when the receptor was directly stimulated.

2.2 Touch in Hairy Skin

The properties and organization of hairy skin mechanoreceptors vary from those found in glabrous skin. The reason for these disparities is not known, as research on the function and purpose of hairy skin mechanoreceptors is not as extensive as studies of mechanoreceptors in glabrous skin (Bolanowski et al., 1994).

At least four types of mechanoreceptors have been found in hairy skin (Bolanowski et al., 1994; Schmidt, 1983):

1. Pacinian corpuscles innervated by Pacinian (PC) afferent nerve fibers,
2. Hair follicle receptors innervated by rapidly adapting (RA) afferent nerve fibers,
3. Ruffini endings innervated by slowly adapting type II (SAII) afferent nerve fibers, and

4. Tactile disks (complexes of Merkel cells) innervated by slowly adapting type I (SAI) afferent nerve fibers.

There is some debate, however, as to the role played by the last two mechanoreceptors listed above in hairy skin tactile sensation. Bolanowski et al. (1994) believe that at the least, the first three mechanoreceptors mediate tactile sensation in hairy skin, but that the Merkel cell-SAI nerve fiber complex does not. However, Kaczmarek and Bach-y-Rita (1995) cite authors that claim the Ruffini ending-SAII afferent nerve fiber mechanoreceptor contributes only kinesthetic information, as in glabrous skin, while the tactile disk-SAI afferent nerve fiber receptor does mediate touch sensations. Other studies have shown that unmyelinated afferent nerve fibers without surrounding end organs may also contribute to the sense of touch in hairy skin (Vallbo et al., 1999).

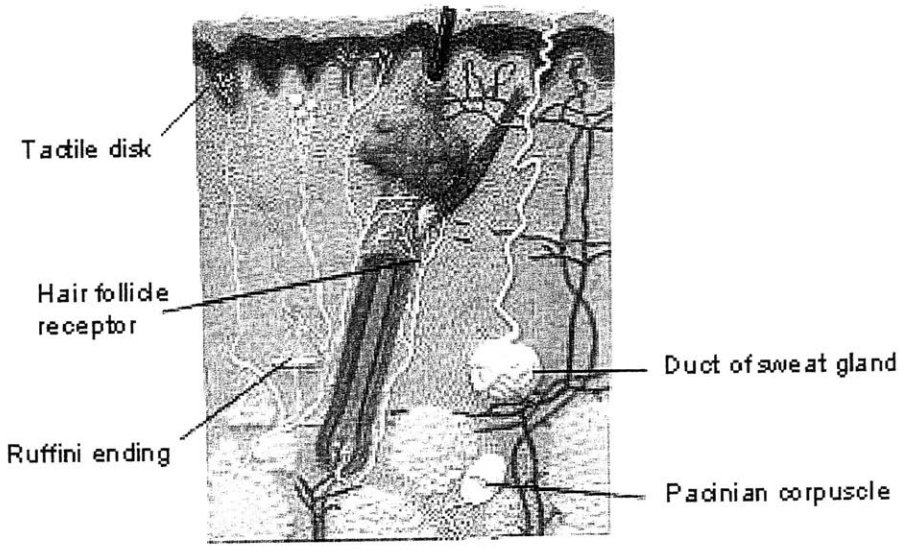

Figure 2-6. Hairy skin cross-section with touch mechanoreceptors (adapted from Anatomy-Resources.com, 2003).

2.2.1 Pacinian corpuscle-Pacinian (PC) afferent nerve fiber, hairy skin

Evidence has been found of Pacinian (PC) afferent nerve fibers in deep tissue well below the epidermis and dermis. Homologous to those found in glabrous skin, the PC afferents are believed to innervate Pacinian corpuscles. Bolanowski et al. (1994) refer to these receptor units as P channels. Stimulation of this receptor produces a tactile sensation described as "vibration." Fewer in number and deeper beneath the skin, the hairy skin P

channels are less sensitive than their glabrous skin counterparts. The hairy skin receptors, however, are still sensitive and adapt extremely rapidly, responding to high frequency stimuli from 45 to over 500 Hz. The receptor sensitivity increases with stimulus area due to spatial summation. In glabrous skin, the sensitivity of the P channels to tactile stimulation improves with increasing skin temperature; however, in hairy skin, the P channels remain unaffected by thermal changes. This temperature insensitivity is probably due to stabilizing mechanisms of the body that counter any variation of temperature at the skin surface. Although this stabilizing mechanism also occurs in glabrous skin, the receptors in hairy skin are deeper below the dermis, allowing them to experience constant temperatures (Bolanowski et al., 1994).

2.2.2 Hair receptor-rapidly adapting (RA) afferent nerve fiber (hairy skin)

Another source of tactile sensation in hairy skin is thought to arise from rapidly adapting (RA) afferent nerve fibers that innervate hair follicle receptors (Bolanowski et al., 1994). Similar to the RA afferent nerve fibers in glabrous skin, the hairy skin afferents adapt rapidly to static stimuli, and are sensitive to the velocity of objects that move the hairs in the skin (in glabrous skin, RA afferent nerve fibers innervate Meissner corpuscles and are sensitive to the velocity of objects contacting the skin) (Schmidt, 1983). Vibratory stimulation of the hair follicle-RA afferent nerve fiber receptor yields a sensation of "flutter." The afferent fiber responds to stimuli between 10 and 200 Hz, with a minimum threshold at 40 Hz (Bolanowski et al., 1994).

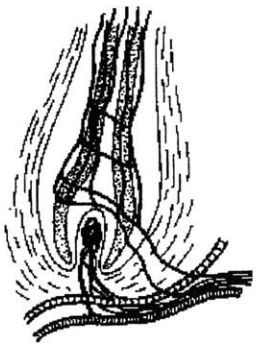

Figure 2-7. Hair follicle receptor (from Ascoli, 2001).

As with RA afferents in glabrous skin, changes in skin surface temperature affect the receptor's response, with lower temperatures decreasing the sensitivity of the receptor. On the other hand, unlike glabrous skin receptors, hairy skin RA afferents show a spatial effect: a larger area of stimulation results in greater sensitivity to the stimulus (Bolanowski et al., 1994).

2.2.3 Ruffini ending-slowly adapting type II (SAII) afferent nerve fiber, hairy skin

Ruffini endings innervated by slowly adapting type II (SAII) afferent nerve fibers are found in hairy as well as glabrous skin. As noted for the glabrous skin receptor, there is some question about the role of this mechanoreceptor in tactile sensation (Kaczmarek and Bach-y-Rita, 1995). Similar to its counterparts in glabrous skin, the SAII afferent nerve fibers in hairy skin have large receptive fields and respond to skin stretch. The SAII afferent fibers also react strongly to static deformations of the skin (Bolanowski et al., 1994).

There are, however, several differences in performance between the glabrous and hairy skin Ruffini ending-SAII afferent fiber mechanoreceptor. The SAII afferent fibers in hairy skin respond to low frequencies of 0.4 to 4 Hz and do not respond to stimuli over 100 Hz, whereas the glabrous skin receptors respond to higher frequencies ranging from 100 to over 500 Hz. The touch sensations produced by stimulating SAII afferents in glabrous and hairy skin also differ. The sensation in glabrous skin is described as "buzzing" and that in hairy skin as "pressure." Furthermore, similar to the RA afferent nerves in hairy skin, the hairy skin SAII afferent fibers display spatial summation, an effect not found in glabrous skin receptors (Bolanowski et al., 1994). An additional difference between glabrous and hairy skin SAII afferents is the effect of skin surface temperature. The sensitivity of hairy skin SAII afferents is independent of skin temperature. Ruffini endings in hairy skin are found deep in the dermis, and thus changes in skin temperature may go undetected by the receptor (Bolanowski et al., 1994).

2.2.4 Tactile disk-slowly adapting type I (SAI) afferent nerve fiber, hairy skin

Slowly adapting type I (SAI) afferent nerve fibers are also found in hairy skin. The end organs of these fibers are Merkel cells, as in glabrous skin, but in a slightly different arrangement (Bolanowski et al., 1994; Gardner et al., 2000). About 30-50 Merkel cells are arranged in a complex called a tactile disk (also called a tactile pad or touch dome). The tactile disk is about 0.2-0.4 mm in diameter and 0.1 mm in height (Schmidt, 1983).

The SAI afferent fiber responds over a wide range of frequencies and is greatly affected by temperature changes in the skin. The receptor exhibits strong reactions to mechanical stimuli but direct mechanical stimulation of the tactile disk does not evoke any touch sensations. Some researchers have therefore concluded that SAI afferent fibers in hairy skin do not contribute to tactile sensation (Bolanowski et al., 1994).

2.2.5 Unmyelinated afferent nerve fibers, hairy skin

The afferent nerve fibers innervating the mechanoreceptors described thus far have all been myelinated and rapidly conducting. However, a group of researchers are starting to point to a class of unmyelinated afferent nerve fibers found in hairy skin as possible contributors to tactile sensation, naming them "tactile C afferents" (Vallbo et al., 1999). These unmyelinated afferents have low conduction velocities (1 m/s) and do not have end organs surrounding their terminus (Schmidt, 1983).

The tactile C afferents have a low touch threshold (0.3-2.5 N) and respond strongly to stimuli moving slowly against the skin, but are very poor at detecting quickly moving stimuli. The tactile C afferents have an intermediate rate of adaptation, and have so far been commonly found in the face and hairy skin of the forearm. Other locations of the body have yet to be investigated (Vallbo et al., 1999).

Although it is clear that the tactile C afferent is not a temperature or pain receptor, its link to the central nervous system and function as a mechanoreceptor is as yet unclear. Investigators have speculated that the tactile C afferent responds to skin-to-skin touch,

and plays a role in the emotional and hormonal responses of humans (Vallbo et al., 1999). In a patient that did not have the myelinated afferents normally associated with touch sensations, stimulation of the tactile C afferents yielded "a faint sensation of pleasant touch" (Olausson et al., 2002).

2.3 Human Thresholds and Sensory Illusions

The preceding section revealed that the type, location, number, and properties of touch mechanoreceptors differ according to skin type (glabrous or hairy) and body location. These differing properties in function and underlying neural physiology influence the sensitivity and quality of sensation at each skin locus.

2.3.1 Spatial resolution and localization

Spatial resolution is a measure of the subject's ability to distinguish two distinct points touching the skin. In the early-mid 1800s, a German physiologist, Ernst Heinrich Weber, found the two-point threshold for different parts of the body and constructed the first spatial acuity map. His results showed that spatial acuity varies greatly over the body (see Figures 2-8 and 2-10). More recently, Weinstein (1968) published results that agreed with and augmented the data from Weber's initial experiments. Gardner et al. (2000) correlate this variation in spatial acuity with the density of receptors in the skin and receptor field size. Stevens and Choo (1996) found that spatial acuity declines with age, and some regions of the body degrade at a faster rate than others (see Figures 2-9 and 2-11). The lip, for example, loses resolution at a rate slower than the toe.

Two common measures of spatial resolution are the point localization and two-point thresholds. The two-point threshold is the minimum distance at which a subject can distinguish two points. Point localization measures the smallest distance at which a subject can tell whether the second of two tactile stimuli is either distal or proximal to the first one. The torso has poor spatial resolution; its two-point threshold is 32-41 mm and point localization threshold is 8.5-12 mm (see Table 2-2). By comparison, the fingertips have a two-point threshold of 2-4 mm and point localization of 1-2 mm (Weinstein, 1968).

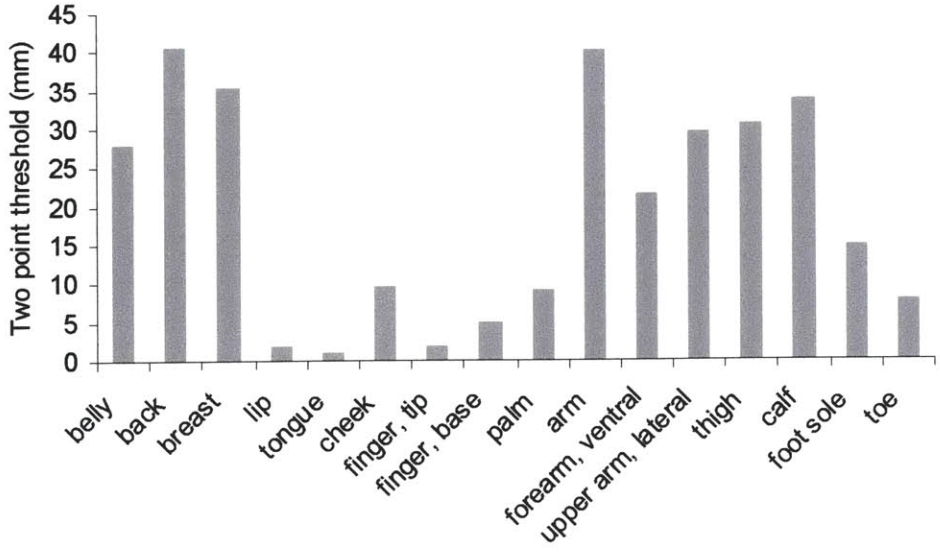

Figure 2-8. Two point threshold for various parts of the body (the values shown are averages of data from several authors: Burdea, 1996; Caldwell and Tsagarakis, 2000; Gardner et al., 2000; Srinivasan, 1994; Stevens and Choo, 1996; Weinstein, 1968) (see Appendix B for exact values).

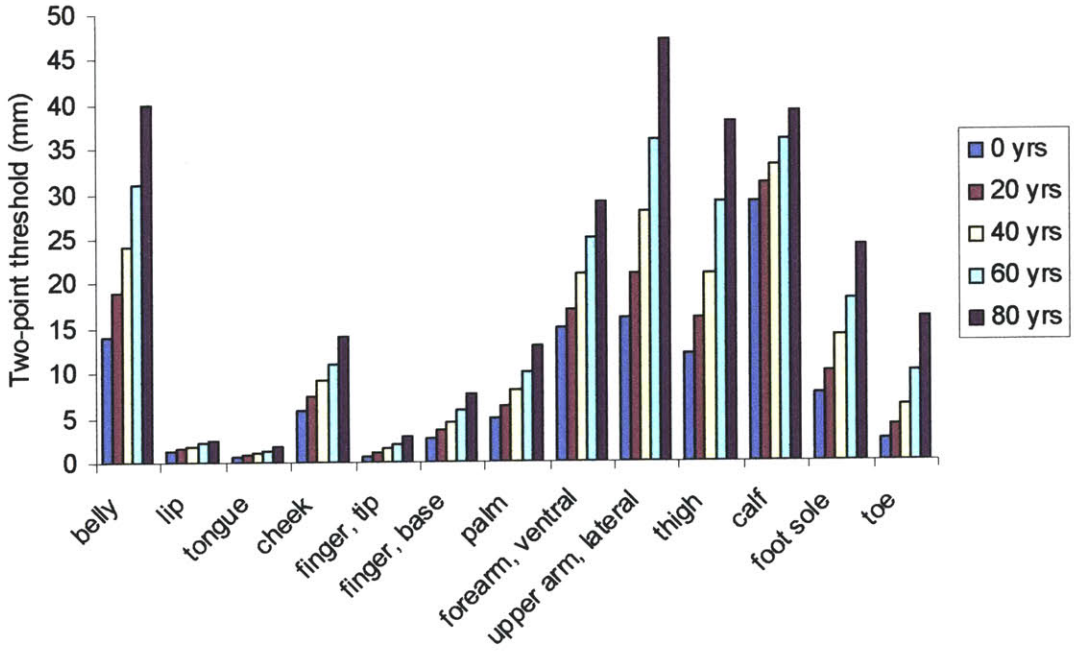

Figure 2-9. Variation of the two point threshold with age (data from Stevens and Choo, 1996) (see Appendix B for exact values).

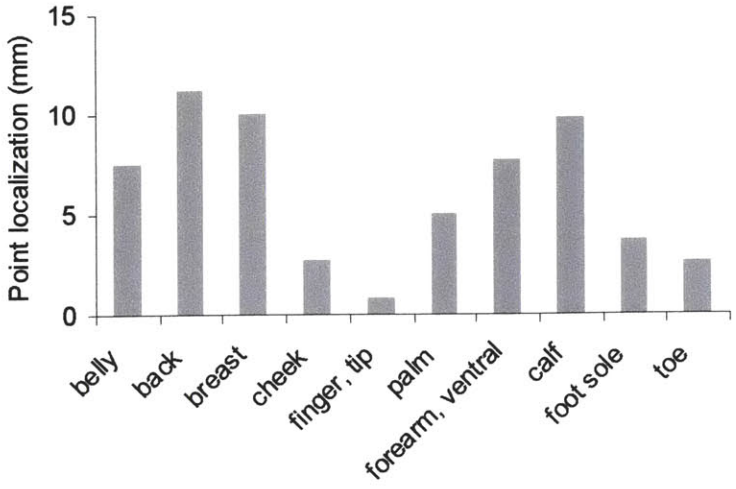

Figure 2-10. Point localization threshold for various parts of the body (the values shown are averages of data from several authors: Burdea, 1996; Srinivasan, 1994; Stevens and Choo, 1996; Weinstein, 1968) (see Appendix B for exact values).

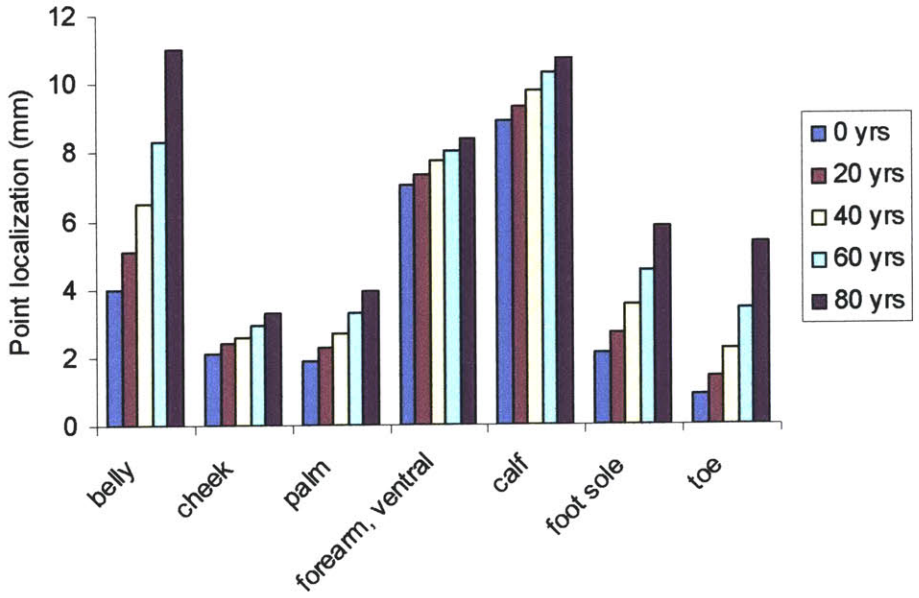

Figure 2-11. Variation of the point localization threshold with age (data from Stevens and Choo, 1996) (see Appendix B for exact values).

Table 2-2. Two point and point localization thresholds for the torso.

Part of Body		Threshold		Ref
		Two-pt	Pt local	
Belly, navel level	males	36	8.5	[2]
	females	32	9.0	
	0 yrs old	14	4.0	[1]
	20 yrs old	19	5.1	
	40 yrs old	24	6.5	
	60 yrs old	31	8.3	
	80 yrs old	40	11.0	
Back	males	40	12.0	[2]
	females	41	10.5	
Breast	males	32	9.0	[1]

References: 1. Stevens and Choo (1996), 2. Weinstein (1968)

2.3.2 Touch threshold

The touch threshold, a measure of the minimum energy required for the subject to feel a stimulus, varies widely across the body (see Figure 2-12). The torso is fairly sensitive to touch, with pressure thresholds of 54-61 kPa for men and 20-39 kPa for women (see Table 2-3), which places it second only to the face in terms of sensitivity (Weinstein, 1968). (Note: touch sensitivity measurements were made using nylon myofilaments. These values were converted from units of force (log 0.1 mg) to units of pressure (kPa) using data from Levin et al. (1978) (see Appendix A for details).)

Table 2-3. Touch threshold of the torso.

Body Part		Units of pressure (kPa)	Units of force (log 0.1 mg)	Ref
Anterior torso		24	2.08	[1]
Breast	males	54	2.8	[2]
	females	39	2.5	
Back	males	61	2.9	[2]
	females	20	1.9	
Belly	males	54	2.8	[2]
	females	20	1.9	

References: 1. Saddiki-Traki et al. (1999), 2. Weinstein (1968)

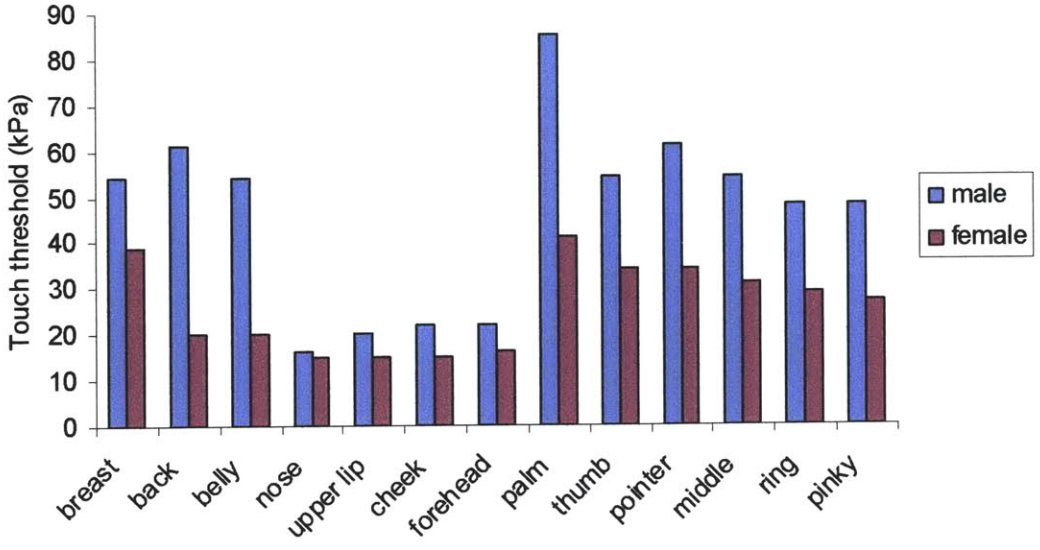

Figure 2-12. Touch threshold of various parts of the body (data from Weinstein, 1968) (see Appendix B for exact values).

2.3.3 Vibration

The human body is most sensitive to vibrations over the range of 200-250 Hz; the Pacinian corpuscle can detect vibrations of just 10 nm at 200 Hz (Johnson, 2001). Frequencies lower or higher than this range require proportionately larger amplitudes in order to be sensed. The intensity of vibration is encoded by the number of activated receptors, and the frequency with the frequency of firing of these receptors (Gardner et al., 2000). In glabrous skin, for stimuli lower than 60 Hz, the Meissner corpuscles and Merkel disk receptors are activated. These receptors have smaller receptive fields, and thus are able to resolve finer details. At frequencies greater than 60 Hz, the Pacinian corpuscles dominate the response. Pacinian corpuscles are located deeper beneath the skin and have very large receptive fields. Thus, for lower frequencies, vibratory stimuli can be presented in spatially resolved, array-type displays, while at higher frequencies, a localized stimulus is not necessary and may be replaced by a single stimulus with a larger surface area (Caldwell and Tsagarakis, 2000). See Table 2-4 for the vibration threshold and corresponding sensations for touch mechanoreceptors in glabrous and hairy skin.

Table 2-4. Threshold and touch sensation of glabrous and hairy skin mechanoreceptors in response to vibratory stimuli.

Afferent nerve fiber	Pacinian		RA		SAI		SAII	
Skin type	Glabrous	Hairy	Glabrous	Hairy	Glabrous	Hairy	Glabrous	Hairy
End organ	Pacinian corpuscle	Pacinian corpuscle	Meissner corpuscle	Hair follicle receptor	Merkel disk	Tactile disks	Ruffini ending	Ruffini ending
Frequency (Hz)	High 40->500 [1] 100-300 [2] 60-400 [3]	High 45->500 [1]	Mid 3-40 [1] 20-50 [2,3]	Mid 4-45 [1]	Low 0.4-3 [1] 0-10 [2] 5-15 [3]		High 100->500 [1]	Low 0.4-4 [1]
Touch sensation [1]	Vibration [1]	Vibration [1]	Flutter [1]	Flutter [1]	Pressure [1]	None	Buzzing [1]	Pressure [1]

References: 1. Bolanowski et al. (1994), 2. Burdea (1996), 3. Gardner et al. (2000)

2.3.4 Sensory saltation and line production

Sensory saltation is a tactile illusion that occurs when a series of stimuli is provided successively at two or more locations; for example, three taps at one position, three more taps at a second position, and one tap at a third position. Within certain temporal parameters, evenly distributed phantom taps are felt between the actual locations of stimulation (see Figure 2-13) (Cholewiak and Collins, 2000). This phenomenon also occurs in vision and audition. The initial researchers of sensory saltation describe the feeling as a tiny rabbit hopping along the skin. They emphasize that in contrast to illusory movement (beta movement or the Phi phenomenon), which is felt as a continuous sensation between two points, the feeling of saltation is that of displacement, and occurs at discrete points (Geldard and Sherrick, 1972).

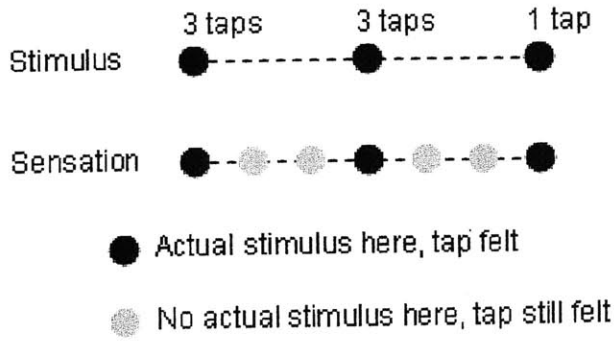

Figure 2-13. Pictorial illustration of sensory saltation.

The conditions to induce sensory saltation, as well as the quality of the dotted line generated, depend on a number of factors. The saltation effect can be produced with as few as two taps from two locations spaced at 20-350 mm. The sensation improves with added stimulators and by increasing the number of taps to 4-6 at each position. An excessive number of taps at one place (e.g., 18), however, eliminates the effect completely (Cholewiak and Collins, 2000; Geldard and Sherrick, 1972). The interval between stimuli (ISI, or interstimulus interval) is also an important factor affecting sensory saltation. For a sequence of 5 taps, each with stimulus duration of 2 ms, the "hopping" effect is first observed at an ISI of 200 ms. Evenly-spaced sensations start appearing at an ISI of 100 ms, while 40-60 ms is optimal for a clear line of regularly spaced taps. At shorter intervals of 20 ms, not all the stimuli are detected (Geldard and Sherrick, 1972).

Cholewiak and Collins (2000) compared vectors drawn using saltatory and veridical presentation modes on the skin of the finger, forearm, and back. In the saltatory mode, three stimulators were positioned and activated as shown in the top row of dots in Figure 2-13. The veridical presentation consisted of seven stimulators placed in a similar manner as the taps felt in the second row of dots in Figure 2-13. The stimulators were activated sequentially, producing one stimulus at each location for a total of seven taps. The subjects had difficulty distinguishing between the dotted lines drawn using the two modes at all three skin locations and for a wide range of timing parameters. Furthermore, independent of the mode, their judgments of line length, smoothness and straightness and

spatial distribution of each tap felt were influenced in a similar manner by changes in stimulus duration and interstimulus interval. The saltatory and veridical modes were thus deemed interchangeable. This result implies that fewer tactors can be used to draw haptic lines without reducing the quality of the line, and that it is also possible to present details finer than the stimulator spacing in a display (Cholewiak and Collins, 2000).

The quality of the (dotted) line drawn on the skin, whether using veridical or saltatory modes, depends on the ISI, duration of each stimulus, and velocity at which the line is drawn. The smoothness of the line is affected mainly by the ISI, with shorter ISIs producing a smoother line. Longer durations lengthen and higher velocities shorten the perceived line length. The straightness of the line is improved by shortening the duration and ISI, and monitoring the velocity. Lines drawn too slowly, at 20 mm/s for instance, seem to wander across the skin, while at 140 mm/s the line appears straight (Cholewiak and Collins, 2000).

3 Torso-Based Tactile Displays and Actuator Technology

Torso-based tactile displays have a long history as sensory substitution devices for the blind and deaf. Images and sounds were transmitted to the back and abdomen using the sense of touch as early as the 1960s (Kaczmarek and Bach-y-Rita, 1995). More recently, haptic feedback to the torso has been implemented in balance prostheses for patients with vestibular loss (Wall and Weinberg, 2003; Wall et al., 2001). Tactile vests have also been used to provide feedback to pilots controlling aircraft (Rupert, 2000; Rupert et al., 1993), and have shown potential in providing navigation and orientation cues in unusual environments such as during extra vehicular activities in space (Rochlis and Newman, 2000; Traylor and Tan, 2002). Most tactile displays use either electrical or mechanical stimulation to activate the touch mechanoreceptors. Less common are devices that feature magnetic, thermal, ultrasound, or chemical stimulation (Kaczmarek and Bach-y-Rita, 1995). Mechanical actuators can be divided into quasi-static or low bandwidth devices, and dynamic or high bandwidth devices. The next sections provide an overview of electrical and mechanical actuators that provide tactile feedback, as well as more detail on various torso-based haptic displays and the actuators employed in each.

3.1 Electrical Stimulation

Electrical stimulation involves passing very small ionic currents through the skin via an electrode to activate the cutaneous afferent nerve fibers responsible for touch sensations. The electrode is a transducer that converts electron flow into ionic flow. Ionic flow through the skin occurs through channels of low resistance, which are most likely sweat ducts or possibly sebaceous glands or minute epithelial breaks. Many factors need to be carefully monitored and controlled in electrotactile stimulation to avoid painful, damaging, or unpleasant sensations (Kaczmarek and Bach-y-Rita, 1995).

Selection of the electrode material, size, and placement are all very important in determining the type of tactile sensation generated. A small electrode with an area of 1 mm^2 delivers uncomfortable, prickly sensations. Increasing the stimulus amplitude of this

electrode slightly above threshold produces pain, while small shifts in location of 0.1 mm changes the quality of tactile sensation. Although larger electrodes produce more comfortable feelings of touch and vibration, shifts of 1 mm in location can still change the pain threshold levels and quality of sensation (Kaczmarek and Bach-y-Rita, 1995). An electrode that only produces ions natural to the skin and does not react chemically with the skin surface is necessary so that the skin is not damaged or irritated. Metals commonly used for electrodes are titanium, gold, platinum, platinum-iridium, silver, and stainless steel. Electrochemical reactions between the skin and electrode can still occur however if the net DC current through the skin is not kept close to zero (Kaczmarek and Bach-y-Rita, 1995).

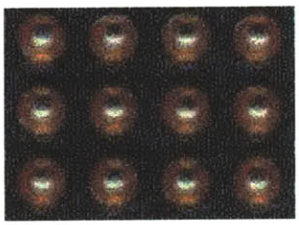

Figure 3-1. A portion of an array of electrodes in a torso-based haptic device developed by Unitech Research, Inc. (now ForeThought Development, LLC). Each electrode is 3 mm^2 in area (ForeThought Development, LLC, 2000).

The skin must also be well hydrated for electrically induced sensations to be comfortable. At best, stimulation of dry skin produces a prickly sensation, probably due to non-uniform current flow through the skin. The channels that normally conduct ionic flow can experience sudden drops in resistance when the skin is dry, causing most of the current to flow through these channels of least resistance. As a result, the subject feels sudden, sharp stings and a red spot forms on the skin. This problem is noted particularly when large metal electrodes over 100 mm^2 in area are used (Kaczmarek and Bach-y-Rita, 1995). One method of hydration is to apply a conductive electrode gel on the skin; however, the gel can dry out after a few hours of use and must then be reapplied. Furthermore, if the electrodes are packed closely together, the gel can short-circuit the adjacent electrodes and raise the current levels (Kaczmarek and Bach-y-Rita, 1995). Another method of hydration is to use sweat, which the subject produces in adequate amounts during stimulation. Kaczmarek and Bach-y-Rita (1995) cite some researchers

that mount their device 20 minutes before use so the subject can produce sufficient levels of perspiration. Other investigators use water or saline to moisten the skin initially (Kaczmarek and Bach-y-Rita, 1995).

Electrotactile stimulation is influenced by such a multitude of factors, including skin hydration, electrode material, size, and location, stimulating voltage, current, and waveform, and contact force between the skin and electrode, that the resulting sensation is very difficult to predict. Subjects can experience a "tingle, itch, vibration, buzz, touch, pressure, pinch, and sharp and burning pain," depending on the values of these parameters (Kaczmarek and Bach-y-Rita, 1995). After careful work and much research, Unitech Research, Inc. of Madison, WI developed a device that it reports does not produce painful sensations when the electrodes are coated with a conductive electrode gel (see Figure 3-1). The electrodes are 3 mm^2 in area and utilize a charge-dump circuit to limit the current flowing into the skin (Kaczmarek and Bach-y-Rita, 1995).

3.2 Mechanical Stimulation

Mechanical actuators provide tactile feedback by displacing the skin, causing the underlying touch mechanoreceptors to deform as well. Many methods of actuation exist, ranging from dynamic, high bandwidth (>50 Hz) devices, to quasi-static, low bandwidth (<10 Hz) devices. Electric motors, voice coils, and piezoelectric devices number among the dynamic actuators, while quasi-static actuators include shape memory alloys (SMAs), solenoids, polymers, and electrostatic and magnetostrictive devices; pneumatic actuators can be dynamic or quasi-static, depending on the design of the device.

3.2.1 Dynamic mechanical actuators

Electric motors

Electric motors are commonly found in devices providing low-end tactile feedback, such as in joysticks or gamepads (see Figures 3-2 and 3-3) and in pagers and cell phones to provide alerting mechanisms (see Figures 3-4 and 3-5). They are also employed in devices designed solely to provide haptic feedback (see Figure 3-6). Electric motors are

simple to use, inexpensive, and can produce high frequency vibrations (>150 Hz). On the other hand, their power to mass ratios are low, and the frequency and amplitude of vibration is difficult to control independently, giving the motor a limited range of outputs. A common method of providing tactile feedback using the DC motor is to create pulsations with on/off control.

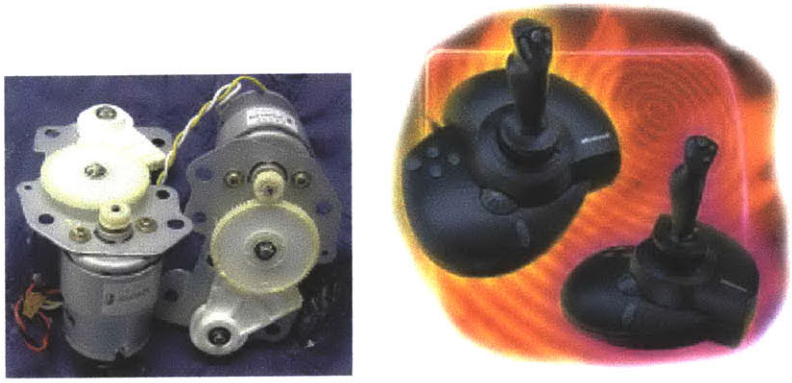

Figure 3-2. Two electric DC motors plus gears (left) provide force and "rumble" feedback in the gaming joystick (right) (Microsoft Sidewinder Force Feedback Pro).

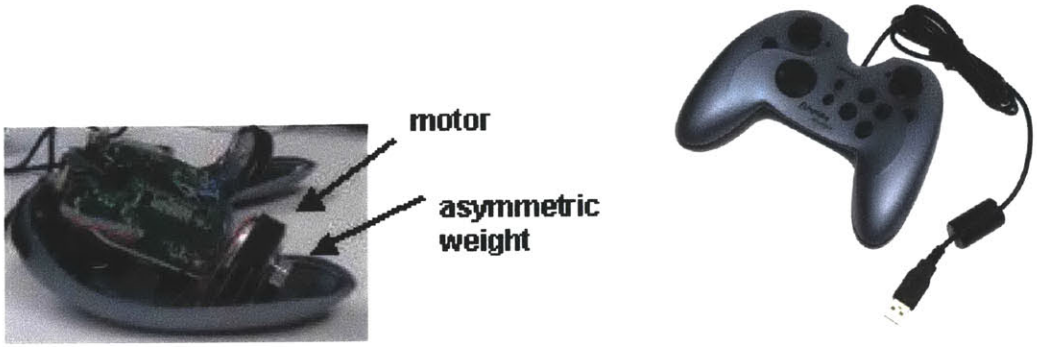

Figure 3-3. The inside of a gamepad (left), the Gravis Eliminator Aftershock (right). Two motors with asymmetric weights provide "rumble" feedback to each hand.

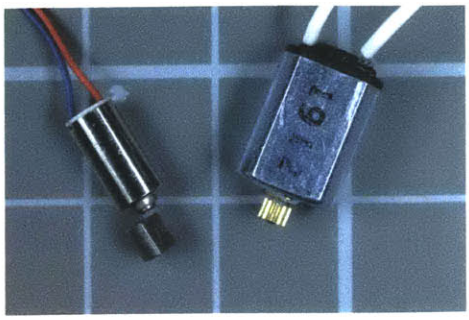

Figure 3-4. Small DC motors (each white line demarks 10 mm). The motor on the left has an asymmetric weight attached to it to create vibrational feedback, a tactic typically employed in pagers and cell phones.

Diameter	14 mm
Height	3.5 mm
Weight	0.004 kg
Speed	4,500 rpm
Max. running	8 VDC, 45 mA

Figure 3-5. A pancake pager motor; an asymmetric weight attached to the motor inside the casing provides vibrational feedback.

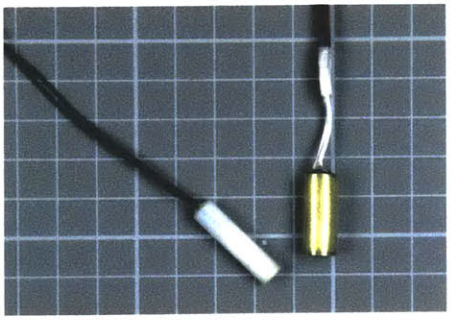

The Rototactor (left):

Diameter	6.4 mm
Length	25.4 mm
Weight	0.002 kg
Vibration	200 Hz
Operation	10 VDC, 170 mA

Figure 3-6. The Rototactor (white, Steadfast Technologies) and MIT tactor (gold, Jones and Hunter), developed specifically for use in haptic devices.

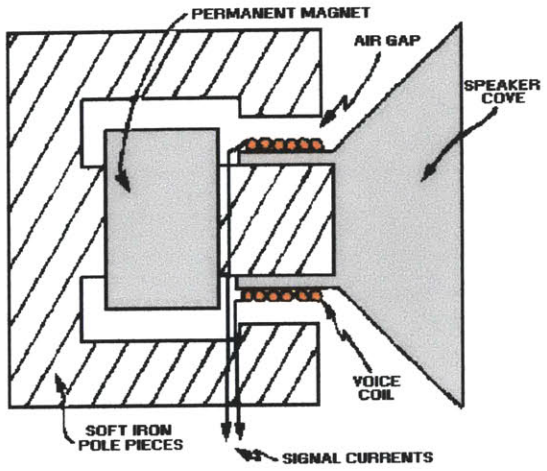

Figure 3-7. Cross-section of a voice coil. The voice coil is an electromagnetic device, consisting of a coil winding (the conductor) placed in a permanent magnetic field. Movement is generated by passing a current through the coil, which, according to the Lorentz Force Principle, produces a force on the coil proportional to the current.

Voice coils and speakers

Voice coils were originally used in radio loud speakers, but are now being used in a variety of applications. They are able to produce low amplitude, high frequency vibrations, linear motion and force, and have high rates of acceleration (see Figure 3-7). Similar to electric motors, the frequency and amplitude of the voice coil are difficult to control independently; the voice coil also has low power to weight and power to volume ratios (Okamura, 2001). See Figures 3-8 and 3-9 for examples of devices that use voice coils to provide tactile feedback.

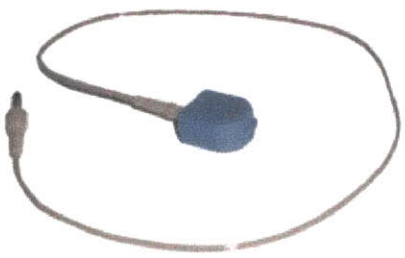

Size	25.4 mm long 18.5 mm wide 10.7 mm thick
Weight	6.5 g
Frequency	250 Hz peak
Amplitude	Sensory threshold to 50 dB above threshold
Power consumption	200 mW

Figure 3-8. Skin stimulator (Model VBW32, Audiological Engineering Corp).

Size	32 mm diameter
	11.7 mm thick
Weight	26 g
Skin contactor	8 mm diameter
Frequency	200 Hz resonant
Amplitude	Sensory threshold to 45 dB re 1 μm peak
Input power	6 VDC at 0.25 A

Figure 3-9. Tactile transducer (Model C1-97, Engineering Acoustics, Inc.).

Piezoelectric actuators

The piezoelectric effect occurs when a material produces a voltage at its surface in response to deformation, and conversely, deforms in response to an applied voltage. Pierre Curie and his brother first observed this effect in 1880. Today, the piezoelectric effect is utilized in many applications ranging from quartz crystal watches to ultrasound imaging. Piezoelectric actuators are also used in haptic devices to generate vibrations with small amplitudes and high frequencies. For instance, piezoelectric bimorph benders (see Figure 3-10) have long been used in tactile displays for the blind. The Optacon was developed in the 1970s to convey scanned images haptically via an array of vibrating pins (see Figure 3-11). Today, piezoelectric bimorph benders are commonly found in commercially available Braille display systems (e.g., in Braille cells by KGS Corporation and Metec AG) (see Figure 3-12). The piezoelectric effect is also featured in a card speaker that produces vibration amplitudes large enough to be felt against the skin (see Figure 3-13).

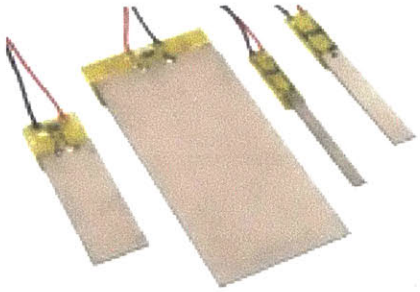

Typical specifications:

Weight	<10 g
Resonant frequency	>250 Hz
Displacement	10^2-10^3 μm
Force	0.1-1 N

Figure 3-10. Piezoelectric bimorph benders (Piezo Systems, Inc., Cambridge, MA).

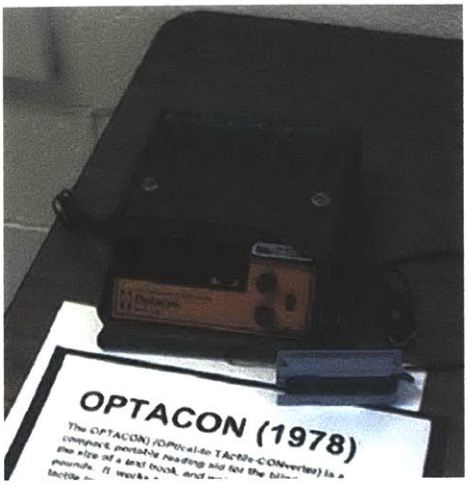

Figure 3-11. The Optacon (formerly commercially available from Telesensory, Inc., discontinued 1996). Images read by a scanner are presented to the finger via 144 vibrating pins (Bliss et al., 1970).

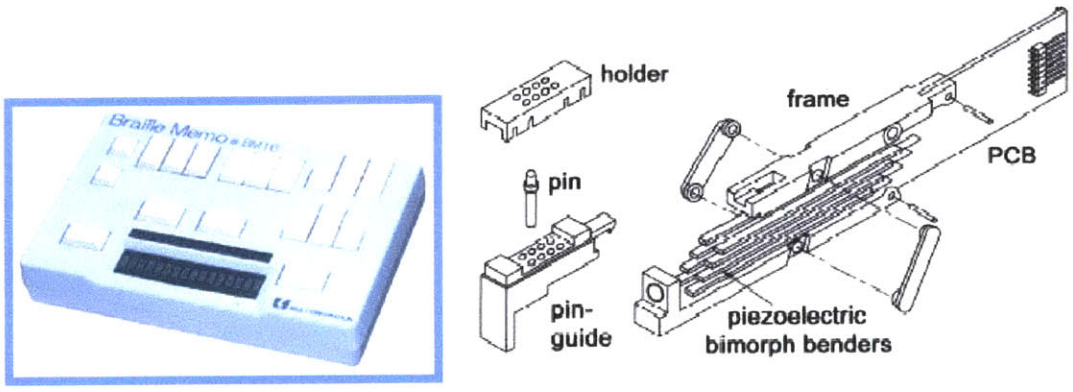

Figure 3-12. The Braille Memo (BM16, KGS Corporation), a Braille terminal actuated by piezoelectric bimorph benders.

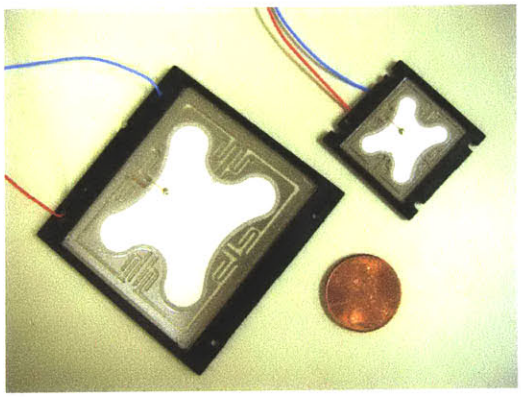

	WM-R57A (large)	WM-R30B (small)
Dimension	57.5 x 56 mm	30 x 30 mm
Height	2.0 mm	1.5 mm
Weight	0.005 kg	0.001 kg
Frequency	150 Hz – 100 kHz	400 Hz – 100 kHz

Figure 3-13. Card-type speakers with piezoceramic diaphragms (WM-R57A (large), WM-R30B (small), Panasonic).

	Dynamic	Quasi-static
Actuator	Pneumatic micro-cylinder	pneumatic Muscle Actuator (pMA)
Size	2.75 mm diameter	12.7 mm diameter
	15 mm x15 mm (array)	79 mm long
Weight	<10 g (array)	10.5 g
Outputs	5-300 Hz	5 Hz
	3.2 N	1-5 MPa
	5 mm (free)	35% strain
Strain rate		0.35-7 s^{-1}
Power/mass		500-2,000 W/kg
Force/area		> 300 N/cm^2
Efficiency		32-50%

Figure 3-14. The TactileGlove (above) features several pneumatic actuators that provide dynamic and quasi-static feedback. Pneumatic micro-cylinders actuate 16 pins (1.75 mm diameter) in a 4x4 array to display local texture and shape. The pneumatic Muscle Actuator, a two-layered cylinder of thin rubber and high-strength nylon fibers, generates lateral motion to present friction and drag. Motion of the cylinders is controlled by monitoring the air flowing in and out of the actuators (Caldwell and Tsagarakis, 2000).

Pneumatic actuators (dynamic and quasi-static)

Pneumatic actuators control the flow of air to create motion and pressure. For example, air jets draw patterns of pressure on the skin; air rings encircle, then squeeze and release a body part (e.g., the finger); and air bellows inflate or deflate to deform the skin

(Youngblut, 1996; Okamura, 2001). Pneumatic actuators are clean, low cost, and simple, but do not have good spatial and temporal resolution. They take many different forms and provide dynamic or quasi-static mechanical stimulation depending on the design of the device. Caldwell and Tsagarakis (2000) use pneumatic power to actuate a number of parts in their TactileGlove (see Figure 3-14). A micro-cylinder in the glove provides dynamic, high frequency (<300 Hz), low amplitude tactile feedback. Another cylinder, the pneumatic Muscle Actuator developed in-house, was used to provide low frequency (5 Hz), high pressure stimulation. Air bladders were also used in the glove to provide quasi-static (< 1 Hz), high pressure (300 kPa max) feedback (Caldwell and Tsagarakis, 2000).

3.2.2 Quasi-static Mechanical Actuators

Shape memory alloys

Shape memory alloys (SMAs) have the ability to "remember" their original shape even after undergoing deformation. A stretched fiber will contract with significant force and displacement when heated, and expand once more as it cools. SMAs can produce very large stresses compared to muscle (a NiTi SMA produces over 200 MPa versus 0.1-0.35 MPa for muscle). On the other hand, SMAs generate only an eighth of the strain of muscle, which can contract by over 40%. The SMA has relatively high power to mass and energy to volume ratios (>1000 W/kg and >10 kJ/m^3 respectively for NiTi SMA), and although it has a low efficiency, the power requirements and costs are relatively small (Hunter and Lafontaine, 1992a). One major drawback of shape memory alloys is its low bandwidth (< 1 Hz), which is limited mainly by the cooling times of the alloy. However, circulation of a liquid around the wires to facilitate cooling can improve the bandwidth to 40 Hz (Wellman and Peine, 1997). A more detailed look at SMAs and their use in haptic devices is provided in Chapter 4.

Polymers

Various synthetic polymers are able to convert chemical or electrochemical energy into mechanical energy. These polymers contract or expand in response to changes in the chemical balance or electric field of the surrounding medium. The polymers generate

large stresses comparable to shape memory alloys (180 MPa), and strains comparable to muscle (>40%) (Hunter and Lafontaine, 1992a). The polymer gel polyacrylic acid-polyvinyl alcohol (PAA-PVA) has been extensively studied, and deemed feasible for use as an artificial muscle or tendon (Caldwell, 1992). Conducting polymers such as polyaniline (other conducting polymers are polyphenylene, polythiophene, polyacetylene, and polypyrrole) show even greater promise as contractile actuators (Anquetil et al., 2002).

Magnetostrictive actuators

Magnetostriction occurs when a material contracts or expands in response to a longitudinal magnetic field. Normally, a coil is wound around a rod of magnetostrictive material such as Terfenol-D. When current is run through the coil a longitudinal magnetic field is generated through the material; thus, by controlling the current, the magnetic field can also be controlled to change the length of the rod (Hunter and Lafontaine, 1992a). Magnetostrictive actuators are able to produce fairly large stresses (70 MPa), but have very small changes in length (0.2%). The coil conducting the electric current is often bulky and much larger than the magnetostrictive material (Hunter and Lafontaine, 1992a).

Electrostatic actuators

Electrostatic actuators take advantage of the repulsive force between electrodes of the same polarity (Hunter and Lafontaine, 1992a). Hunter and Lafontaine (1992a) cite an electrostatic actuator called the stacked variable capacitance motor with active slider (SVCMA). This actuator consists of sheets of polyimide with copper electrodes that slide relative to each other in response to applied voltages.

Figures 3-15 to 3-18 compare several different properties of various mechanical actuators, which are all quasi-static except for the piezoelectric materials.

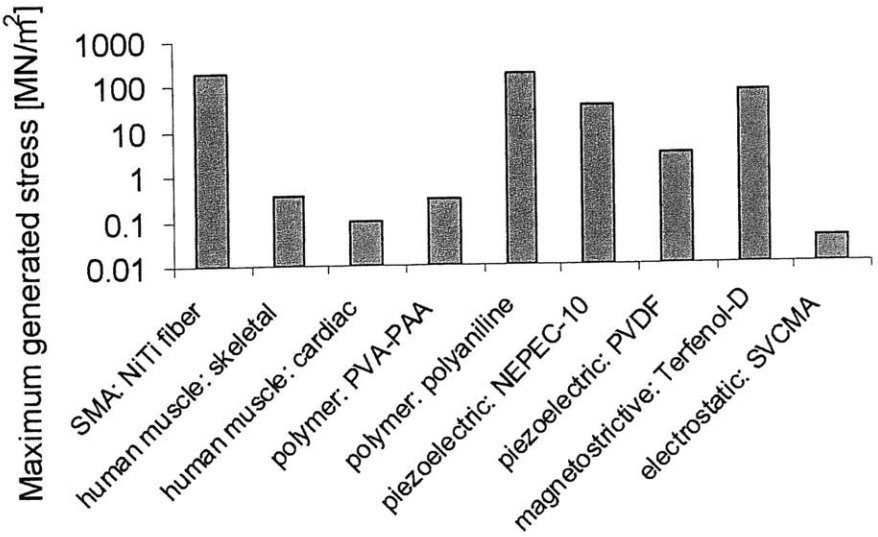

Figure 3-15. Maximum generated stress (logarithmic scale) of various contractile materials (data from Hunter and Lafontaine, 1992a).

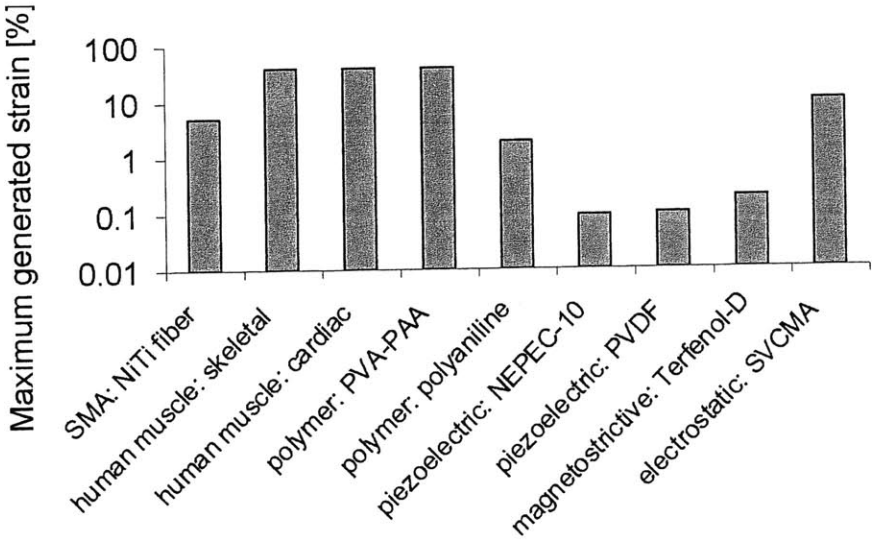

Figure 3-16. Maximum generated strain (logarithmic scale) of various contractile materials (data from Hunter and Lafontaine, 1992a).

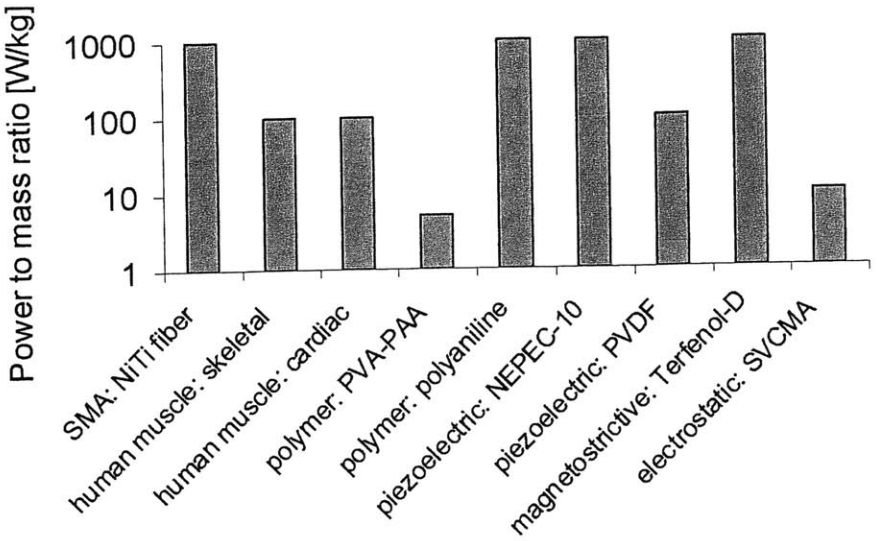

Figure 3-17. Power to mass ratio (logarithmic scale) of various contractile materials (data from Hunter and Lafontaine, 1992a).

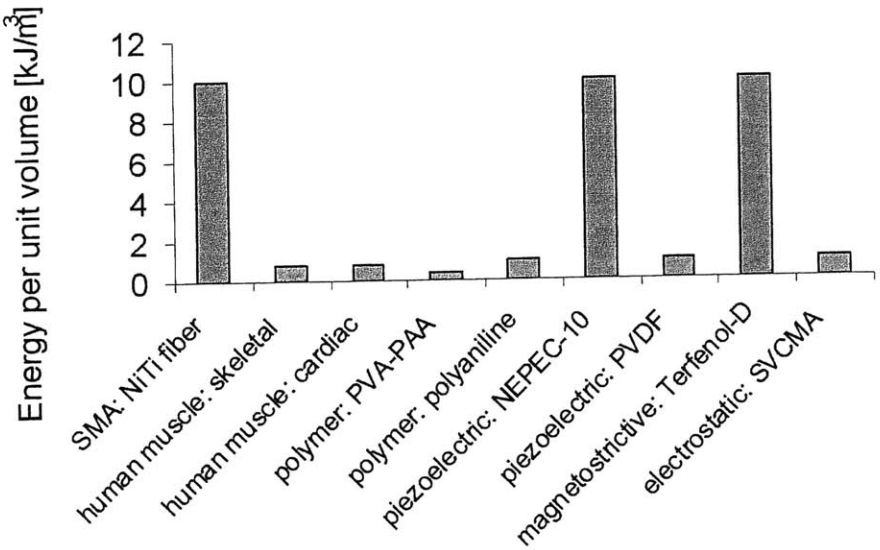

Figure 3-18. Energy per unit volume of various contractile materials (data from Hunter and Lafontaine, 1992a).

3.3 Torso-Based Tactile Displays

The following sections contain more detail on various torso-based haptic displays and the methods of actuation used in each. See Tables 3-1 and 3-2 for a summary of this information.

Table 3-1. Various torso-based haptic displays using electrical stimulation (information from Kaczmarek and Bach-y-Rita, 1995).

Name	Electrodes
Tactile Vision Substitution System (Bach-y-Rita) - prosthesis for the blind	400 electrical stimulators
Videotact (Unitech Research, Inc.) - conveys computer graphics to the abdomen	768 titanium electrodes, 2 mm diameter
Tacticon - abdominal belt auditory prosthesis	16 gold-plated electrodes, 5.5 mm diameter
Audiotact (Unitech Research, Inc.) - auditory prosthesis	32 electrodes

Table 3-2. Various torso-based haptic displays using mechanical stimulation.

Name	Array	Tactor	Operating frequency	Ref
Tactical Situation Awareness System (TSAS), civilian plane	8x3, 8x5	Mini electromechanical speakers 25.4 mm diameter, 3.2 mm thick	150 Hz	[2,4,5]
TSAS, fixed wing	4x5	Pager motors in nylon casings 25.4 mm diameter	90 Hz	[2,4,5]
TSAS, helicopter	8x2	Pneumatic tactors, hard plastic shell, latex diaphragm 15 mm diameter 90 mm spacing between rows	50 Hz	[2,4,5]
Tactor Locator System	6	Vibrotactile stimulators 13 mm diameter, 6 mm thick	250 Hz	[3]
Situation Awareness Vest	3x3	Modified flat speakers 101.6 mm diameter 100 mm interelement spacing	300 Hz	[6]
Balance prosthesis	2, 7x2, 3x16	Vibrotactile stimulators	250 Hz	[7, 8]
Tactile Vision Substitution System	400	Mechanical stimulators		[1]

References: 1. Kaczmarek and Bach-y-Rita (1995), 2. NAMRL (2000), 3. Rochlis and Newman, 4. Rupert (2000), 5. Rupert et al. (1993), 6. Traylor and Tan (2002), 7. Wall et al. (2001), 8. Wall and Weinberg (2003)

3.3.1 Sensory Substitution Devices

Vision Substitution

In the 1960s Bach-y-Rita started work on the tactile vision substitution system (TVSS), in which images recorded by a television camera were conveyed electrically or mechanically on the skin via four hundred tactors mounted on a dental chair. The intensity of the tactor activation was varied to portray the light intensity of the image. Vertical, horizontal, and diagonal lines were easily perceived. Some subjects were able to recognize people's faces and even complete complex tasks such as electronic assembly under a microscope using the TVSS (Kaczmarek and Bach-y-Rita, 1995).

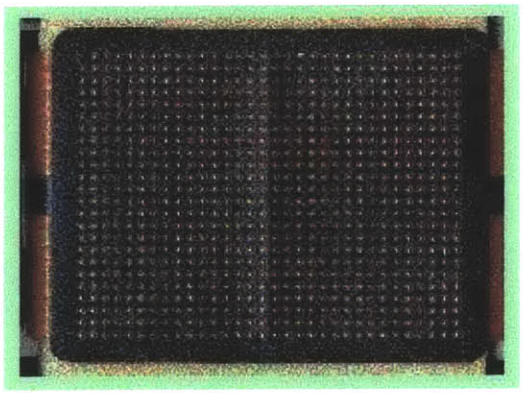

Figure 3-19. The Videotact portrays computer graphics to the abdomen via 768 titanium electrodes 2 mm in diameter (ForeThought Development, LLC, 2000).

The figure above shows the Videotact, a visual prosthesis developed by Unitech Research, Inc. (now carried by ForeThought Development, LLC) to portray computer graphics on the abdomen using electrical stimulation. The Videotact contains 768 titanium electrodes in a grounding plane of conductive Kapton. Subjects using the system were able to navigate down a simple, high-contrast hallway. In surroundings more complicated like the outdoors, however, the Videotact was not effective because of the limited amount of information the system could portray. Some signals were masked (i.e.,

one signal was not felt due to a stronger signal close by), and complicated images took a while to recognize. These problems were partially attributed to the low spatial resolution and small dynamic range of the system (Kaczmarek and Bach-y-Rita, 1995; ForeThought Development, LLC, 2000).

Auditory Substitution

Tactile feedback is also employed in aids for the deaf to convey auditory signals. The Tacticon (previously available commercially) and the Audiotact (sold by Unitech Research, Inc., now ForeThought Development, LLC) contain 16 and 32 electrodes, respectively (see Figure 3-20). Each electrode corresponds to a particular band in the sound frequency spectrum. The stimulation intensity of the electrode is determined by the intensity of sound in that pass band. A number of researchers developed devices similar to the Tacticon and Audiotact that feature different types and numbers of tactors (8, 16, or 32 channels, electrotactile or vibrotactile stimulation). These devices improved the speech clarity of deaf children, the discrimination and comprehension of sound in the elderly, and the discrimination of phonemes in lip-reading (Kaczmarek and Bach-y-Rita, 1995).

Figure 3-20. The Audiotact is an auditory prosthesis for the abdomen and contains 32 electrodes.

Tactile Substitution

In the 1970s, researchers started exploring the use of tactile substitution devices to reduce the fatigue and injury of people with insensate feet and hands (a complication of diabetes and advanced cases of Hansen's disease); and also to speed up the completion time in tasks where haptic feedback is absent (e.g., in the use of remotely operated robots, or for astronauts whose thick spacesuits obstruct all touch sensations). The tactile substitution device senses the pressure or friction at an end effector (e.g., glove surface, robot arm, shoe insole, fingers) and transmits this information on the skin in a different area of the

body (e.g., the abdomen or forehead). The intensity of electrotactile stimulation is determined by the intensity measured by the pressure sensors or strain gauges (Kaczmarek and Bach-y-Rita, 1995).

3.3.2 Spatial Orientation and Navigation Aids

In unusual environments such as in space, during flight, or under water, the systems normally used to sense the position, orientation, and movement of the human body can provide false or confusing information. These systems include the somatosensory system (skin, muscle, and joint sensors) and the vestibular system in the inner ear. Vision, the third system normally used to sense orientation and movement of the human body, must then be heavily relied upon. However, visual input can be limited or non-existent (e.g., in the dark) or the system can be overloaded during simple or complicated tasks.

In flight, pilots can receive false signals regarding the direction of gravity from their somatosensory and vestibular systems due to the acceleration of the aircraft. They must then use vision to read the aircraft displays and determine the aircraft's attitude, pitch, and velocity. Sensory overload of the visual system often occurs, especially when the pilot is in combat (Rupert, 2000). Similarly, in space, the cues the body normally uses to sense body position and movement are absent or confusing, and disorientation can result in space motion sickness. The astronaut must depend more heavily on visual cues to provide a frame of reference to judge the position, speed, and orientation of their body. Sensory overload of the visual system may easily occur, particularly when the astronaut is involved in extra vehicular activities in space (Rupert et al., 1993; Rochlis and Newman, 2000). Tactile displays that provide position, orientation, and movement information of the human body in these unusual environments are currently being developed. Several of the systems are described below.

Tactical Situation Awareness System (TSAS)

The tactical situation awareness system (TSAS) has been developed and tested by the Naval Aerospace Medical Research Laboratory to provide tactile feedback to pilots controlling aircraft (Rupert, 2000; Rupert et al., 1993; NAMRL, 2000). A computer

connected to the aircraft sensors, such as those sensing attitude or velocity, translates information on the vehicle's position and movement into haptic feedback via a matrix of vibrotactile stimulators in the pilot's vest or suit.

Figure 3-21. The Tactical Situation Awareness System (TSAS). Information on the orientation and movement of the aircraft is transmitted to the pilot via a matrix of vibrotactile stimulators on the pilot's torso and limbs (NAMRL, 2000).

A variety of prototypes have already been tested. Navy pilots flying fixed wing aircraft have been able to perform basic maneuvers and simple aerobatics relying solely on haptic feedback from the TSAS for information on plane position. Pilots using the TSAS in an Army helicopter reported an increased awareness of the helicopter's movement that improved their control of the vehicle (Rupert, 2000). The following sections contain more detail on the prototypes used in each test flight.

TSAS: fixed wing, Cessna 180

In test flights with a civilian plane, the Cessna 180, an 8x3 or 8x5 matrix of tactors sewn into a stretch Lycra suit provided continuous feedback to the pilots on the direction of "down" (i.e., the gravity vector). Four columns were placed on the pilot's front, back, left, and right sides, with four more columns placed between each of these locations. The tactors were miniature electromechanical speakers 3.2 mm (1/8") thick and 25.4 mm (1") in diameter. The stimulus waveform used to activate the tactors was a 150 Hz rectangular pulse train operating at 10% duty cycle, followed by a 450 ms break, to create a series of 10 pulses. The pilots were able to maintain normal orientation and control using the haptic feedback. However, the tactors frequently did not activate when subjected to too

much pressure; in addition, the tactors occasionally lost contact with the skin, which also resulted in unfelt activations (Rupert, 2000).

TSAS: fixed wing, Navy T-34

In a second set of tests with the Navy T-34, a fixed wing aircraft, pilots were able to perform simple aerobatics and basic maneuvers relying solely on haptic feedback. Four columns of tactors were placed at the front, back, left, and right of the pilot to form a 4x5 matrix in a stretch cotton/Nomex custom-fitted suit. Due to the louder, higher vibrations of the Navy T-34, a more robust tactor was created from pager motors mounted in 25.4 mm (1") circular nylon casings. The optimal carrier frequency of 90 Hz was turned on and off to create pulses of 1, 4, and 10 Hz. Two tactors were activated at a time, providing roll and pitch information to the pilots (Rupert, 2000). Although successful, a few problems were encountered with this prototype of the TSAS. Pilots complained that the suit was bulky and did not provide adequate pressure to keep the tactors in contact with the skin at all times, leading to unfelt vibrations. The addition of Velcro straps and duct tape did not solve the problem. The authors concluded that the tactors must be lighter and more robust for practical application. The pilots also had difficulty distinguishing between the three middle tactors of each column (Rupert, 2000).

TSAS: rotor wing (helicopter), Army H-60

A third prototype of the TSAS was developed for the Army H-60 helicopter to assist in hover and transition to forward flight. Pneumatic tactors (model 2856-Ao, Steadfast Technologies, Tampa, FL) were arranged to form an 8x2 matrix in a prototype F-22 cooling and heating vest. An air source kept the vest slightly inflated to maintain constant contact between the tactors and skin. The two tactors were spaced 9 cm apart in each column, and had hard plastic shells with latex diaphragms 15 mm in diameter that oscillated against the skin. The optimal operating frequency of 50 Hz was turned on and off to create pulses of 1, 4, and 10 Hz. Pilots reported an increased awareness of the helicopter's movement that improved their control of the aircraft. Furthermore, the vest provided consistent contact between the tactors and skin and was lighter, more

comfortable, and unobtrusive. The tactors were also lighter and more robust than in previous prototypes (Rupert, 2000).

Situation-Awareness Vest

A group from the Haptic Interface Research Laboratory at Purdue University is also working on a wearable haptic display, the Situation-Awareness Vest, to prevent the spatial disorientation of pilots. A directional line is drawn on the user's back through sensory saltation using a 3x3 matrix of vibrotactile stimulators spaced 100 mm apart. The tactors are modified flat speakers (Audiological Engineering Corp., MA) with a diameter of 101.6 mm (4"). The resonating frequency of the speakers (around 300 Hz) was used to create seven sinusoidal signals 250 ms long with varying intensities (Traylor and Tan, 2002). In a series of experiments run on ground (1 g) and in the NASA KC-135A, the "vomit comet" that creates alternating 0 g and 2 g environments during parabolic flight maneuvers, users reported that tactor vibrations felt weaker in zero gravity versus 1 g on ground. Further testing showed that this perception is most likely due to heavier cognitive loads in flight as compared to the lab environment (Traylor and Tan, 2002).

Figure 3-22. The Situation-Awareness Vest (Traylor and Tan, 2002). A 3x3 matrix of vibrotactile stimulators is used to draw a directional line on the user's back.

Tactor Locator System

In the Man-Vehicle Lab at MIT, researchers are testing the effectiveness of the Tactor Locator System (TLS) in helping astronauts to orient themselves spatially during extra

vehicular activities in space. The TLS presents directional vectors originating from the subject's center of mass by activating 1-3 tactors at a time. The system consists of six vibratory tactors total, placed on the trapezius (up), paraspinal (down), sternum body (front), spinalus (back), and lateral sides of the fourth and fifth ribs (left and right). The tactors are 13 mm in diameter and 6 mm thick. A rounded 250 Hz square wave, 6 V in amplitude peak to peak, was used as the stimulus waveform. The TLS decreased the navigation and orientation time for subjects when used in a computer simulation (Rochlis and Newman, 2000).

3.3.3 Balance Prostheses

A tactile display is also being developed for the balance impaired to use as a balance prosthesis (Wall et al., 2001; Wall and Weinberg, 2003). The tactors are electromechanical vibrators (the Tactaid, Audiological Engineering, Somerville, MA) that operate at 250 Hz (see Figure 3-8). In one configuration, a single tactor is attached to either shoulder of the subject with adhesive tape to provide feedback of head tilt amplitude (left or right), which is signaled by the frequency of stimulation of each tactor. The tactors are activated by a train of 100 ms pulses (25 cycles per pulse) at a rate of 1, 3, or 5 Hz. In another configuration, seven tactors are placed in a row on each side of the trunk. The tactors are held in place against the torso with an elastic mesh vest and adjustable Velcro tensioning strips. In this case, head tilt amplitude is signaled by the position of the activated tactor. In tests with normal, healthy subjects, the vibrotactile feedback in both configurations was effective in reducing sway (Wall et al., 2001).

Further experiments were conducted with vestibulopathic subjects who had either greatly-reduced or no motion information from the inner ear. The balance prosthesis in these tests consists of a single axis sensing module that detects front-back tilt, a controlling unit, and columns of the Tactaid vibrotactors placed on the front and back of the subject. The subjects were able to reduce sway significantly from 2.7° to 1.4° and controlled their posture more quickly with the prosthesis than without. More remarkably, subjects who regularly fell during the tests without the prosthesis were able to stand with it turned on (Wall and Weinberg, 2003). Due to the success of the one-dimensional

device, another balance prosthesis is currently being developed that provides tactile feedback of motion in three dimensions (see Figure 3-23). The device contains a 3x16 array of the Tactaid vibrotactors that operate at 250 Hz. The tactors are held against the torso just above the waistline using an elastic strip or wide belt. The columns indicate the tilt direction, and are placed at 22.5° intervals circumferentially around the waist. Tilt magnitude is signaled by the number of tactors in each column that are activated (1, 2, or 3) (Wall and Weinberg, 2003). The tactors are spaced at distances larger than the two-point discrimination threshold for the torso, which is 32-41 mm (Weinstein, 1968).

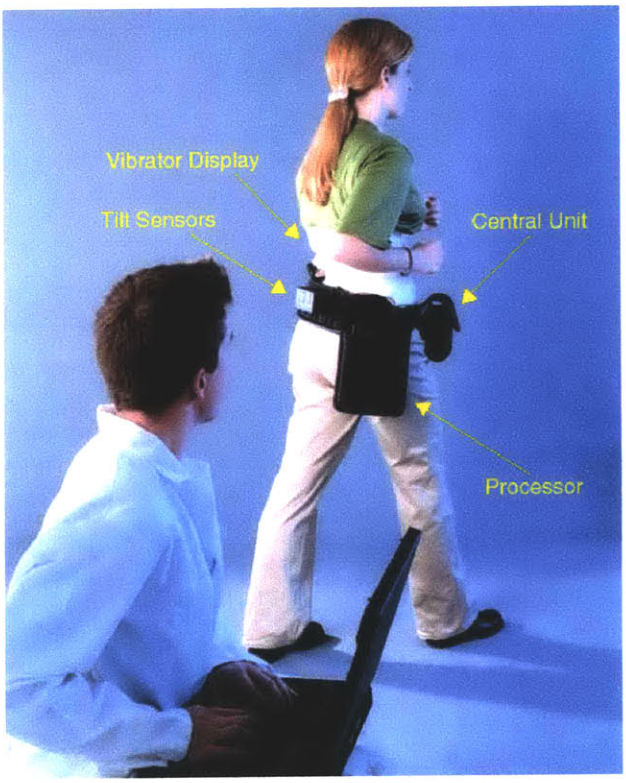

Figure 3-23. A balance prosthesis being developed by Wall and Weinberg (2003). Tactile feedback of body tilt in three dimensions is provided through a 3x16 array of vibratory tactors held against the torso (from Wall and Weinberg, 2003).

3.4 Requirements of a Torso-Based Tactile Display

Although much success has been achieved with various sensory substitution devices (see previous section), electrical stimulation is not ideal for torso-based tactile displays due to

the strict requirements in using electrodes. The skin must be coated with an electrode gel or another liquid to produce comfortable, electrically-induced sensations (Kaczmarek and Bach-y-Rita, 1995), a condition unfavorable for applications in space, flight, or underwater. The type of tactile sensation produced is also difficult to control precisely, and the range of outputs limited by the pain threshold of the skin.

Mechanical actuators are able to produce a wider range of frequencies and intensities to stimulate the skin than electrical activation. However, researchers have still expressed the need for improved actuator technology. In particular, the actuator should be perceptually robust, yet lightweight and flexible, making the device comfortable and invisible to the user until a stimulus occurs. The garment containing the tactors must also be comfortable, able to maintain constant pressure between the tactor and skin, and cover a large skin surface area. Ideally, the vest or suit would also maintain constant temperatures and be free of moisture (Rupert, 2000). The actuator for the tactile vest should be able to generate at least twice the touch threshold in the torso, or about 120 kPa, and displace the skin 2-4 mm. Inter-element spacing of the stimulators can be greater than or equal to the two-point threshold for the torso, which is 32-41 mm (Weinstein, 1968). The thickness and weight of the actuator should be minimized in order to maximize the user's comfort and mobility.

4 Properties and Uses of Shape Memory Alloys

4.1 Shape Memory Alloys: an Introduction

Shape memory alloys (SMAs) have the ability to "remember" their original shape even after undergoing deformation. This feat of memory, called the shape memory effect, is due to changes in the crystalline structure of the material, and was first noted in the 1930s. Shape memory alloys have two distinct phases called austenite and martensite, each with an associated crystalline structure. The austenite phase is considered the parent form; it has a body centered cubic crystal structure and is present at higher temperatures. The atoms are locked into an inflexible arrangement, making the alloy stronger and the yield stress higher at 241-690 MPa (35-100 kpsi) (Shape Memory Applications, Inc., 1999). (Note: these values are typical for the shape memory alloy composed of nickel and titanium.) The martensite phase is present at lower temperatures. In the martensite phase, the alloy is softer and easily shaped, possessing up to 8% recoverable strain and requiring 69-138 MPa (10-20 kpsi) to be deformed (Shape Memory Applications, Inc., 1999). The crystalline structure is in a more flexible, "twinned" zigzag shape (Nitinol Devices & Components, 1998).

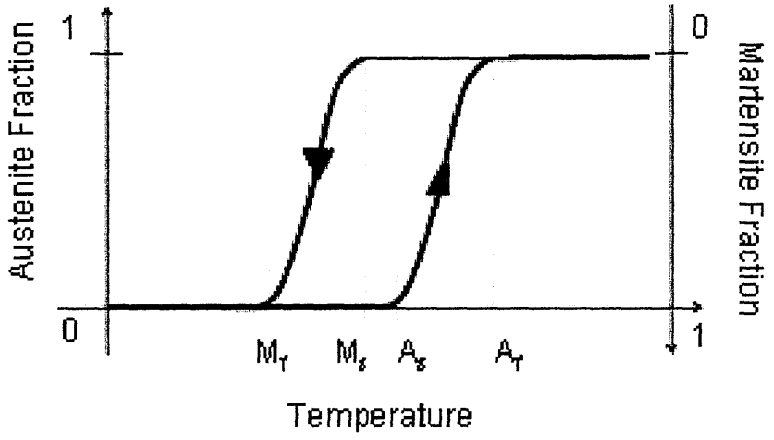

Figure 4-1. The austenite and martensite fraction present in shape memory alloys during temperature changes of the alloy (adapted from Shape Memory Applications, Inc., 1999).

Phase changes from martensite to austenite and the reverse can occur with changes in the temperature of the shape memory alloy (see Figure 4-1). At lower temperatures, the alloy is in its martensite form. As the alloy is heated past a temperature called A_s, or the austenite start temperature, the crystal structure starts changing from martensite to austenite, and is completely in the austenite phase once the austenite finish temperature, A_f, is reached. Similarly, if the alloy starts in the higher temperature, austenite phase and is then gradually cooled, martensite begins to form at a temperature called M_s, or martensite start. Transition to the martensite phase is complete once the alloy reaches its martensite finish, or M_f, temperature. The temperatures at which the shape memory alloy starts transitioning into one phase (e.g., M_s) and completes transition into the other (e.g., A_f) do not coincide, giving the SMA its characteristic transformation hysteresis (see Figure 4-1).

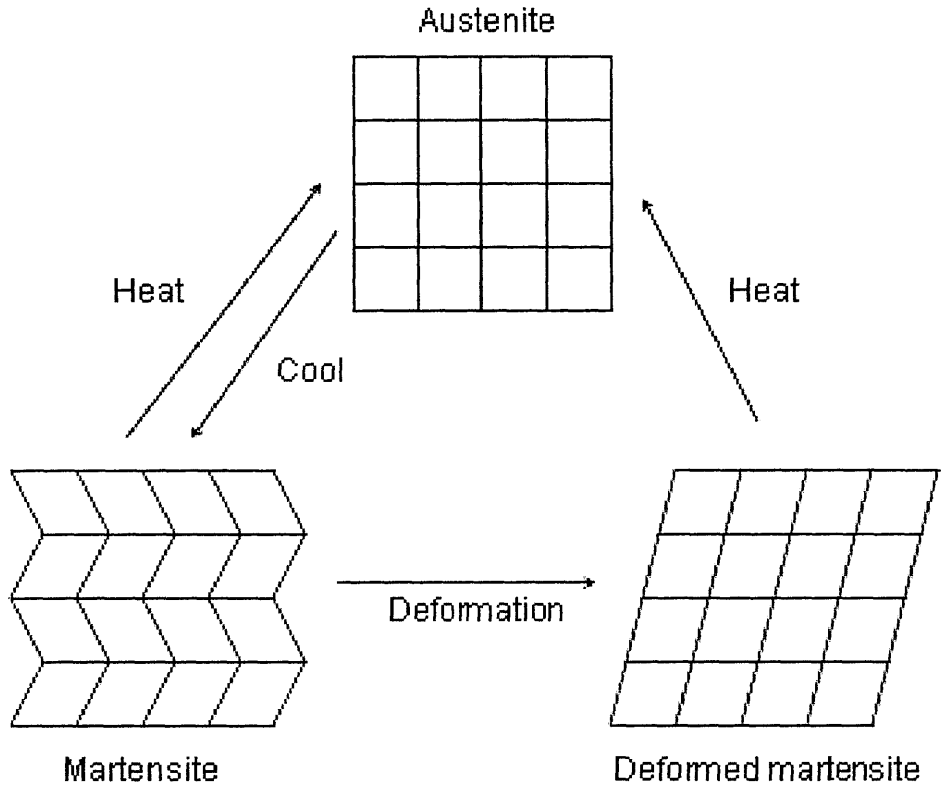

Figure 4-2. Illustration of the shape memory effect (adapted from Lafontaine, 1997).

In its lower temperature, martensite form, the shape memory alloy can be easily deformed into a new shape. If the SMA is then heated past its austenite finish

temperature, the deformed alloy returns to its original shape with considerable force (see Figure 4-2). It is in this phase change that power from the SMA is harnessed to do work (e.g., actuate motors, move valves, etc). A common method of activating the SMA is via Joule heating. By passing an electrical current through the alloy, the resistance of the material generates enough heat to trigger a phase change. Since the contraction time is determined by the time required to heat the alloy, a high amplitude current pulse of short duration can cause a very quick contraction (Hunter and Lafontaine, 1992).

Phase changes between martensite and austenite may also occur by altering the stress applied to the shape memory alloy. At temperatures above A_f, when the shape memory alloy is completely in the austenite phase, stress applied to the alloy induces martensite to form. Once in the martensite phase, the alloy can recover from up to 8% strain, giving it a rubber-like, springy effect called superelasticity (see Figure 4-3). This superelasticity is due to the fact that more energy is required to deform the shape memory alloy in the austenite phase than is required to first stress-induce martensite and subsequently deform the alloy. Once the stress is removed, however, the SMA immediately reverts back to austenite, the stable crystalline structure at these temperatures, and springs back to its original shape.

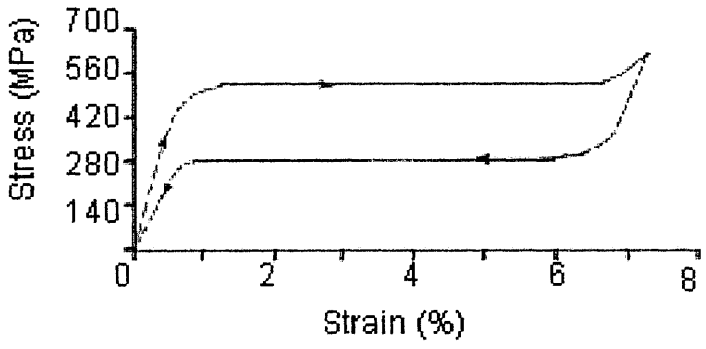

Figure 4-3. The superelastic effect of shape memory alloys (adapted from Shape Memory Applications, Inc., 1999).

4.2 Nitinol as an Actuator

Although shape memory alloys can be composed of a variety of materials (e.g., AgCd, AuCd, CuZn, FePt), SMAs composed of nickel and titanium are the most widely studied and used due to the biocompatibility of the alloy (for use in medical devices), resistance to corrosion, lower costs, and advantageous material properties (Hunter and Lafontaine, 1992a). Researchers from the Naval Ordinance Laboratory first observed the shape memory effect in a NiTi alloy in the early 1960s, and gave the alloy its name, Nitinol (NIckel TItanium Naval Ordinance Laboratory).

Nitinol is composed of roughly equal amounts of nickel and titanium (typically 55% nickel, 45% titanium by weight). However, even the slightest variation in the ratio of these two metals causes a significant change in the transition temperature. For instance, a 1% change can cause the transition temperature to go from $-100^{\circ}C$ to $+100^{\circ}C$ (Images SI Inc., 2002). Careful control of the composition and processing of the alloy enables the start and finish of the transition phase to be controlled precisely within a degree or two.

NiTi shape memory alloys have relatively high power to mass and energy to volume ratios (>1000 W/kg and >10 kJ/m^3 respectively). They can produce very large stresses, over 200 MPa, compared to muscle, which produces stresses of 0.1-0.35 MPa. On the other hand, Nitinol generates only an eighth of the strain of muscle, which can contract by over 40%. Although their efficiency is low, the power requirements and costs of Nitinol are relatively small (Hunter and Lafontaine, 1992a). See Table 4-1 for a comparison of Nitinol with other contractile actuators.

Many benefits are associated with the use of Nitinol as an actuator. For instance, Nitinol is highly corrosion-resistant, biocompatible, and operates silently. It is also relatively cheap and its high power to mass and energy to volume ratios mean that only a small amount of the alloy, about the size and weight of a human hair, for example, can generate usable movement and force. Nitinol is also flexible and kink-resistant, which permits for its use in small, restricted areas.

Table 4-1. Properties of various contractile materials. Peak values possible are shown (adapted from Hunter and Lafontaine, 1992a).

Class	Density [kg/m^3]	Stress [MN/m^2]	Stiffness [GN/m^2]	Peak/min stiffness	Strain [%]	Strain Rate [s^{-1}]	Power/mass [W/kg]	Energy/volume [kJ/m^3]	Life Cycles	Efficiency [%]
SMA: NiTi fiber	6,450	>200	78	3	>5	3	>10^3	>10	>10^5	>3
Muscle: human skeletal	1,037	0.35	0.06	5	>40	5	>10^2	0.8	>10^9	>35
Muscle: human cardiac	1,037	0.1	0.05	5	>40	4	>10^2	0.8	>10^9	>35
Polymer: gel (PVA-PAA)	1,300	0.3	<0.1	10	>40	0.1	>5	0.4	>10^5	30
Polymer: conducting (polyaniline)	1,500	180	5	1.7	>2	>1	>10^3	>1	>10^5	>30
Piezoelectric: ceramic (NEPEC-10)	7,500	35	40	1.1	0.09	>10	>10^3	>10	>10^8	>30
Piezoelectric: polymer (PVDF)	1,780	3	3	>1.2	0.1	>1	>10^2	>1	>10^6	<1
Magnetostrictive: rare-earth (Terfenol-D)	9,250	70	35	1.4	0.2	1	>10^3	>10	>10^5	<30
Electrostatic: polyimide (SVCMA)	1,061	0.04	<0.01	?	>10	>1	>10	1	?	>20

There are also several disadvantages associated with using Nitinol. One major drawback is Nitinol's low bandwidth (< 1 Hz), which is limited mainly by the length of time required for the alloy to cool enough to reset the system. However, a method patented by Hunter and Lafontaine (1992b) exists to produce a fast-twitch SMA fiber from an ordinary fiber. This method changes the nature of the fiber by subjecting it to brief, very large current pulses while being forcibly stretched. A 100 mm long, 0.8 mm diameter fiber initially had a rise time of 50 ms and cooling time of over 1,000 ms. After treatment with a 50 A, 1 ms current pulse, the rise time of the same fiber was about 10 ms and the cooling time about 300 ms, with cooling 60% complete after just 15 ms (Hunter and Lafontaine, 1992b). Based on these values, a "preconditioned" SMA can conceivably achieve a bandwidth of over 3 Hz.

Another technique proven effective at increasing the bandwidth of Nitinol involves circulating a fluid around the fibers to facilitate heat transfer. Wellman and Peine (1997)

and Peine et al. (1997) improved the bandwidth of a 75-micron diameter NiTi wire from 1 Hz in ambient air to 5-6 Hz using forced-air cooling and 40 Hz with liquid cooling. Shape memory alloys with smaller diameters and lower transition temperatures (e.g., 50-60°C) (alloys with transition temperatures from -25°C to +120°C are commercially available) may also be used to reduce the amount of heat to dissipate, and thus reduce cooling times.

A second drawback of working with shape memory alloys is the difficulty in creating secure, mechanical connections. Shape memory alloys are able to free themselves from clamping mechanisms and crack all known adhesives due to their active contraction and expansion of typically 2-8%. Welding and brazing are also ineffective, as the shape memory effect and superelasticity of the fiber are destroyed at the high temperatures required for these methods. Soldering is acceptable for forming electrical connections, but fails under the cycling stresses created by the shape memory alloy (Lafontaine, 1997). There is, however, at least one effective method of joining developed by Lafontaine (1997). A layer of material is grown on the fiber through electrodeposition; the layer can then be used with conventional methods of attachment to make a secure, mechanical connection. Lafontaine (1997) deposited nickel electrolytically on the ends of a 250-micron diameter NiTi fiber using a nickel sulfamate bath. The nickel-plated ends were then soldered to another metal. The joints did not fail under normal operating stresses of <200 MPa; instead, the fiber typically failed before the joints did. When the joints did fail, they did so at stresses of 540 MPa, well above the recommended operating stresses (Lafontaine, 1997).

4.3 Devices Activated by Nitinol

Several research groups have developed haptic displays powered by shape memory alloys to provide tactile feedback to the fingertip (e.g., Hasser and Weisenberger, 1993; Howe et al., 1995; Peine et al., 1997; Taylor et al., 1998; Wellman and Peine, 1997). These displays were developed to present small-scale surface shape and texture to the fingertip, mainly for the augmentation of virtual reality (Taylor et al., 1998; Hasser and Weisenberger, 1993; Wellman and Peine, 1997) and to supply haptic feedback in

telerobotics (Hasser and Weisenberger, 1993; Wellman and Peine, 1997). These devices demonstrate the capabilities and uses of NiTi shape memory alloys, and address some of the design issues associated with Nitinol. See Table 4-2 for a summary of the specifications of the various devices.

Table 4-2. Specifications for several different shape memory alloy-activated fingertip tactile displays (see text for more details). Note: only maximum outputs are listed.

Array	5x6	5x6	5x6	8x8	4x6	10x1
Pin spacing	1.5 mm		3 mm	2.54 mm 5.08 mm	2.1 mm	2 mm
Nitinol diameter		76 μm	100 μm	101.6 μm	75 μm	75 μm
Nitinol length		15 mm	15 mm	120 mm	30 mm	
Transition temperature					90°C	90°C
Rise time	100 ms	100 ms (90%)	170 ms	350 ms	65 ms	
Fall time	100 ms	1.6 s (80%)		350 ms	65 ms	
Bandwidth	2-3 Hz	10 Hz	2-3 Hz	1.4 Hz	6-7 Hz	40 Hz
Displacement output	1 mm	0.5 mm	1-2.5 mm	3.2 mm	3 mm	3-3.5 mm
Force output	50 mN	196 mN	200 mN		1 N	1-1.5 N
Cooling				Fanned air	Forced air	Liquid
Feedback				Resistive	Position	Position
Reference	[7]	[3]	[1]	[5]	[2]	[4,6]

References: 1. Hasser and Weisenberger (1993), 2. Howe et al. (1995), 3. Kaczmarek and Bach-y-Rita (1995), 4.Peine et al. (1997), 5. Taylor et al. (1998), 6. Wellman and Peine (1997), 7. Youngblut (1996).

Figure 4-4. Dynamic display actuated by NiTi shape memory alloy wires; developed by TiNi Alloy, Co. (from Youngblut, 1996).

TiNi Alloy, Co. developed a number of SMA-activated devices, including static and dynamic fingertip tactile displays. The dynamic display is composed of a 5x6 array of pins spaced at 1.5 mm (see Figure 4-4). The pins can displace 1 mm with a force of 50 mN (6 g) at a bandwidth of 2-3 Hz (see Table 4-2 for more details). In one study, subjects were able to match patterns presented to the fingertip using this tactile display with those shown visually on a screen (Youngblut, 1996). The static display developed by TiNi Alloy, Co. also consisted of a 5x6 array of pins. Each pin was powered by 76 μm diameter NiTi SMA wires, 15 mm in length. An input of 0.24 A caused the wire to contract by 3% and the pins to displace 0.5 mm with 196 mN (20 g) of force. The system reached 90% of its peak output in 100 ms and was 80% recovered after 1.6 s. A bandwidth of 10 Hz was deemed possible with this system (Kaczmarek and Bach-y-Rita, 1995).

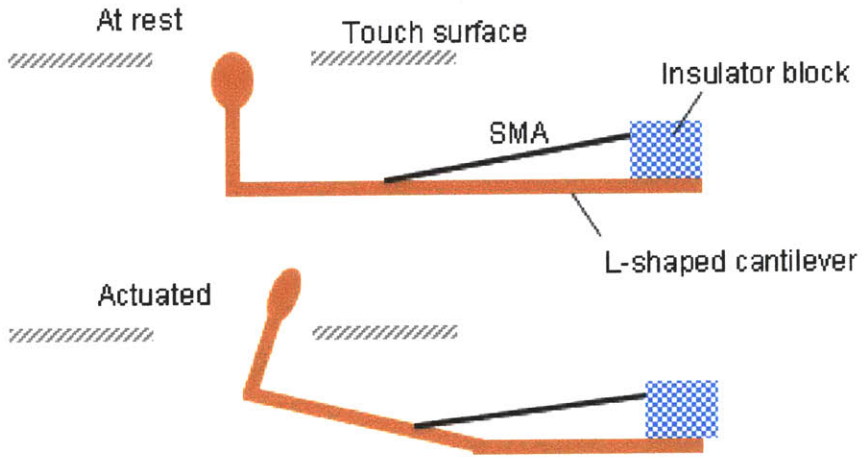

Figure 4-5. Actuation method used in a display developed by TiNi Alloy, Co. (figure adapted from Hasser and Weisenberger, 1993). An SMA wire displaces an L-shaped cantilever pin against the fingertip skin.

Hasser and Weisenberger (1993) examined another display developed by TiNi Alloy, Co. for the potential of presenting object shape and texture during dexterous telemanipulation operations. The array also contained 30 pins arranged in a 5x6 array. The pins were spaced at 3 mm and displaced 1-2.5 mm (see Table 4-2 for more details of the display's capabilities). The pins were L-shaped, cantilever beams moved by 100 μm diameter, 15

mm long Nitinol fibers (see Figure 4-5). With this display, subjects were able to identify static and dynamic patterns. However, noticeable irregularities in performance of the device were noted; standard deviations of pin resting positions ranged from 0.3 to 0.6 mm. These irregularities were attributed to differences in pre-stress of the SMA wire and pin resting positions (Hasser and Weisenberger, 1993).

Figure 4-6. An 8x8 SMA-activated array developed by Taylor et al. (1998) to present static displays of object shape (taken from Taylor, 2001).

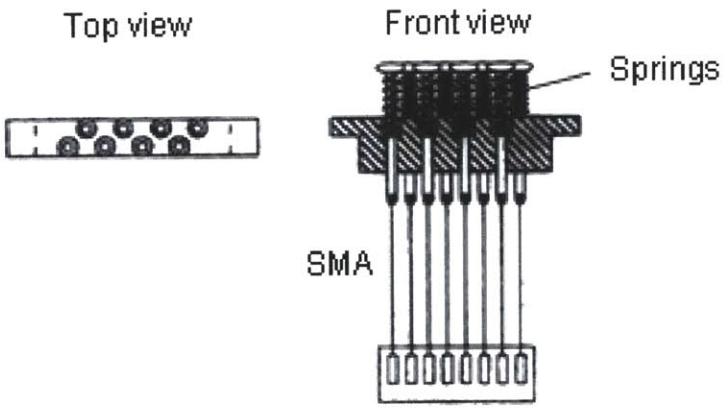

Figure 4-7. Schematic of the actuator mechanism in a 64-element tactile display developed by Taylor et al. (1998) (adapted from Taylor et al., 1998). The shape memory alloy wires retract the pins while the springs provide a biasing force.

Taylor et al. (1998) built a fingertip tactile display to complement information presented visually during virtual reality and computer interactions (see Figure 4-6). The display was designed to convey the shape of an object, and to present surface details such as edges, peaks, troughs, smoothness and sharpness. In tests with the display, 5 out of 6 subjects

were able to recognize static patterns with 100% accuracy; one subject erred in identifying one of the patterns. The array contains 8 units of 8 pins placed next to each other to form a 64-element array. The pins in each unit are spaced by 2.54 and 5.08 mm and are actuated by 101.6 μm (0.004") diameter, 120 mm long NiTi SMA wires (see Figure 4-7). Resistive feedback was used to control the height of individual pins, which could displace a maximum of 3.2 mm. A bandwidth of only 1.4 Hz was achieved for mid-range displacements (values were lower for larger displacements), even with a fan blowing air over the wires to assist with heat transfer during cooling. To increase the bandwidth, the authors proposed decreasing the diameter of the NiTi fiber and using forced cooling (e.g., circulating a cold fluid with high thermal conductivity) (Taylor et al., 1998).

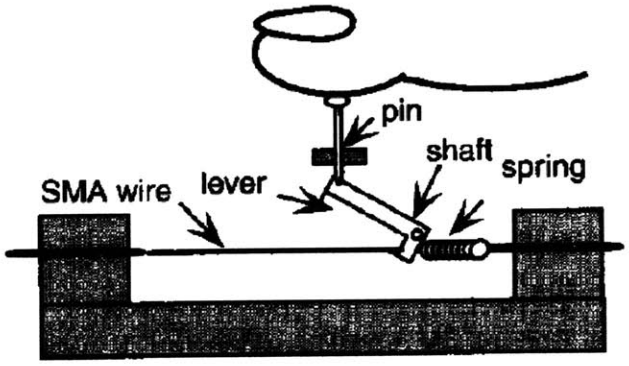

Figure 4-8. Actuation mechanism in a tactile display for the fingertip developed by Howe et al. (1995a) (from Howe et al., 1995b).

Similar in aim to Hasser and Weisenberger (1993), Howe et al. (1995) constructed a 4x6 array tactile display for dexterous telemanipulation operations. The pins in the array were displaced by Nitinol wires with a diameter of 75 μm, length of 30 mm, and transition temperature of 90°C (see Figure 4-8). The pins were spaced 2.1 mm apart and displaced 3 mm with 1 N of force. The authors used position feedback to reduce the hysteresis characteristic of shape memory alloys, and proportional derivative feed-forward control to increase significantly the bandwidth of the system; heating and cooling times of 65 ms (versus 1200 ms and 500 ms respectively) were attained with the control in place. Forced air across the wires also facilitated cooling, increasing the bandwidth to 6-7 Hz. Liquid cooling was recommended to reduce cooling times further (Howe et al., 1995).

A controllable, high bandwidth, SMA-driven tactile array was developed by Wellman and Peine (1997) to present small-scale object shape and texture to the fingertip for use in teleoperation and virtual environments (see Figure 4-9). The system reproduces remotely felt textures by controlling the pin height in the array, displaying tactile information such as corners, edges, and textures (see Figures 4-10 and 4-11). The array consists of a line of 10 pins with 2 mm spacing. Two 75 μm Nitinol wires with a 90°C transition temperature activate each pin to produce over 3-3.5 mm displacement, 1-1.5 N force, and 35 kN/mm pin stiffness. The wires were limited to 4-4.5% strain. Previous experiments conducted by Wellman and Peine (1997) showed no noticeable loss in performance for Nitinol that underwent on the order of 10^4 cycles at 4.8% strain under a 2 N load. (They also note that the number commonly quoted for the lifetime of Nitinol is approximately 10^6 cycles at 2% strain).

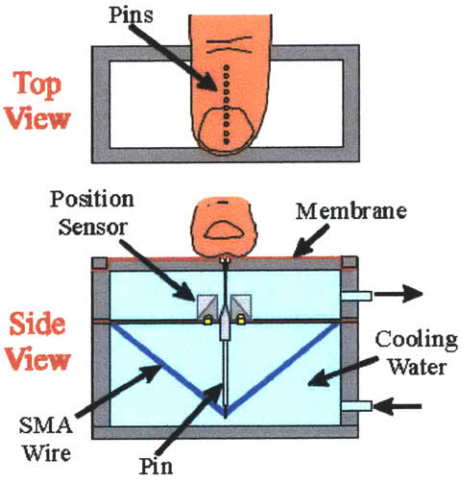

Figure 4-9. Schematic diagram of SMA-activated tactile display with position sensing and liquid cooling (from Wellman and Peine, 1997 and Peine et al., 1997).

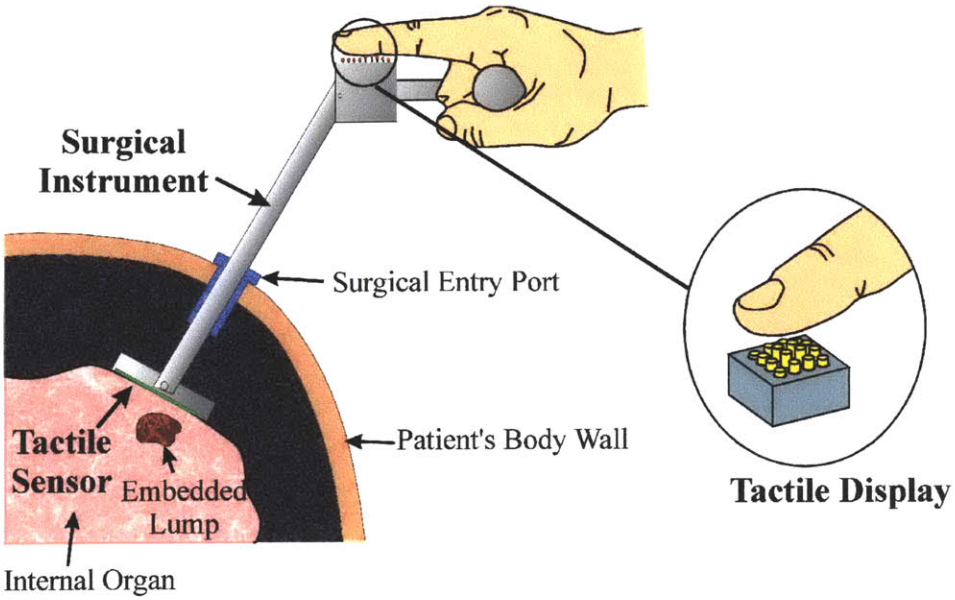

Figure 4-10. Application of a fingertip tactile array reported by Wellman and Peine (1997). The system reproduces remotely felt textures by controlling pin heights, displaying tactile information such as corners, edges, and textures (Harvard BioRobotics Laboratory, 2001).

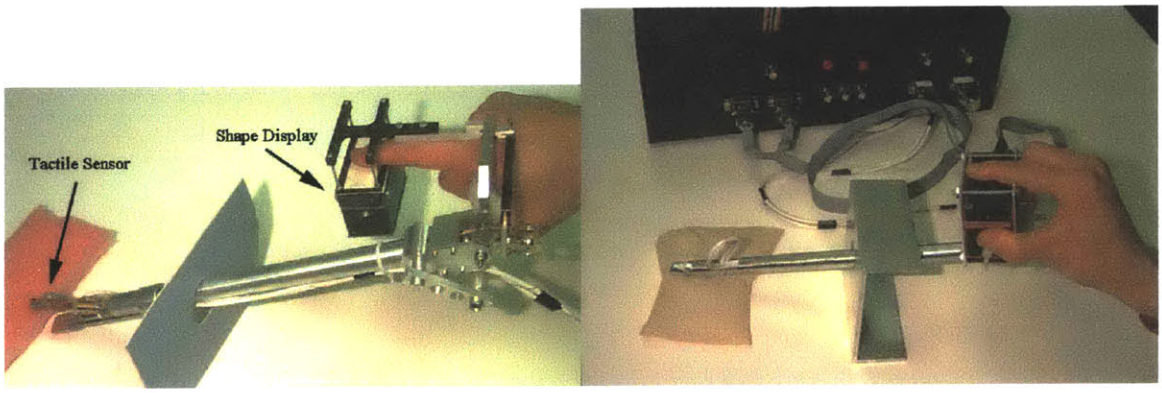

Figure 4-11. Implementation of the schematic shown in Figure 4-10 (Harvard BioRobotics Laboratory, 2001).

Wellman and Peine (1997) achieved a remarkable bandwidth of 40 Hz with their system using two different strategies. Heat transfer during cooling was facilitated by using two fibers with a smaller diameter versus one larger fiber to increase the ratio of available surface area to volume. Water, selected for its high thermal conductivity and heat

capacity, was also slowly recirculated around the wires to speed the cooling process. Ethylene glycol was added to the water (8:1 by volume) to increase the boiling temperature to 110°C, and 0.02% or less by weight of Surfynol 75 was added to encourage bubbles to migrate out of the system (Wellman and Peine, 1997). Liquid cooling greatly influenced the bandwidth; forced-air cooling resulted in a bandwidth of 5-6 Hz, while free convection produced only 1 Hz. A simple proportional, feed-forward controller using position feedback was also used to keep the wire between its minimum and maximum transition temperature. The pin position was always at a height above resting in order to keep the wire near the transition temperature. The controller improved the response time of the system, and reduced the hysteresis of the SMA to less than 0.1 mm (Wellman and Peine, 1997).

The results from these studies highlight certain issues that need to be taken into account when using SMA fibers. As mentioned earlier, a major problem in using Nitinol is its low bandwidth, which results from the long cooling times required to reset the system. Cooling of the wires by free convection to the surrounding air resulted in bandwidths below 3 Hz. However, Wellman and Peine (1997) and Peine et al. (1997) showed that circulation of a water bath around the wires increased the bandwidth to 40 Hz. Another strategy used to speed up the heat transfer process was to increase the ratio of the fiber's surface area to its volume by reducing the diameter of the Nitinol wires (Wellman and Peine, 1997; Peine et al., 1997). For better controllability, resistivity and position feedback have proven effective at reducing the hysteresis behavior of shape memory alloys, as well as improving the response time of the system (Hasser and Weisenberger, 1993; Peine et al., 1997; Taylor et al., 1998; Wellman and Peine, 1997).

5 Preliminary Tests of NiTi Shape Memory Alloy

Initial tests were conducted to determine the feasibility of using NiTi shape memory alloy fibers to actuate a pin that stimulates the skin on the torso. A Nitinol wire 254 μm (0.01") in diameter (Figure 5-1, Dynalloy, Inc., Flexinol^{TM}) was threaded through a pin of non-conducting material as shown in Figure 5-2. A current pulse applied across the wire heats the SMA and causes it to contract, displacing the pin upward with significant force. This particular SMA fiber has a transition temperature of 90°C and can generate a maximum of 180 MPa and 4% strain. A 101.6 μm superelastic wire (Figure 5-1, SportsWire LLC) also threaded through the pin, but electrically isolated from the SMA, returns the pin to its original position as the SMA cools. The superelastic wire eliminates the need for an active force to reset the SMA. Experiments were run to determine the force, displacement, and repeatability of the SMA output in this configuration.

Figure 5-1. NiTi shape memory alloy and superelastic fibers used in experiments. The SMA fiber is 254 μm in diameter (Dynalloy, Inc., Flexinol^{TM}), has a 90°C transition temperature, and can generate a maximum of 180 MPa stress and 4% strain. The superelastic wire has diameter 101.6 μm.

5.1 Method

A number of different input waveforms was used to stimulate the SMA (see Figure 5-3). A discrete waveform was created in Mathcad and fed through a digital/analog board (National Instruments, PCI-6052E) to control a power supply (Kepco, BOP 20-20D). The power supply then applied a current pulse across the SMA fiber (see Figure 5-4). The

current pulse duration was varied from 0 to 2.5 seconds, and the amplitude was varied from 0.5 to 1.7 Amps.

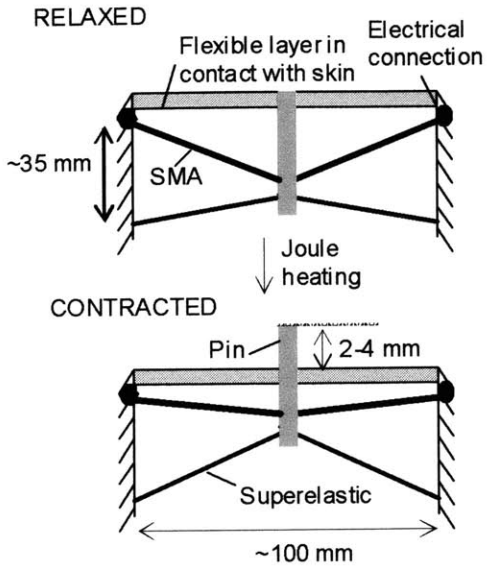

Figure 5-2. Sketch of the mechanism used in preliminary experiments. The shape memory alloy contracts when heated, displacing the pin upward. The superelastic wire passively resets the system.

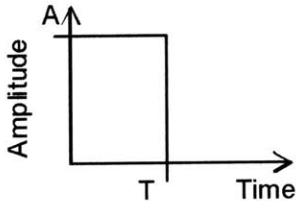

Figure 5-3. Waveform of current input; T is the duration of the pulse and A is the amplitude of the pulse.

The time course of the resulting force and displacement outputs of the SMA were recorded using a force transducer (Shimpo, DFS-20) and displacement transducer (Keyence, LX2-12). The analog voltages from each transducer were transmitted via the analog/digital board to a computer (see Figure 5-4). The voltage signals were then sampled and filtered in Mathcad (using an FIR low pass filter with sampling frequency 500 Hz or 1 kHz, 4096 or 8192 samples, and 50 Hz cut-off frequency). During the force measurements, the force transducer was mounted so it barely touched the top of the pin

(10 mm^2 surface area) when the SMA was in its resting position. As the SMA contracted, the pin pressed against the force transducer and was thus not allowed to displace. During measurements of pin displacement, the pin was allowed to move freely (see Figure 5-5).

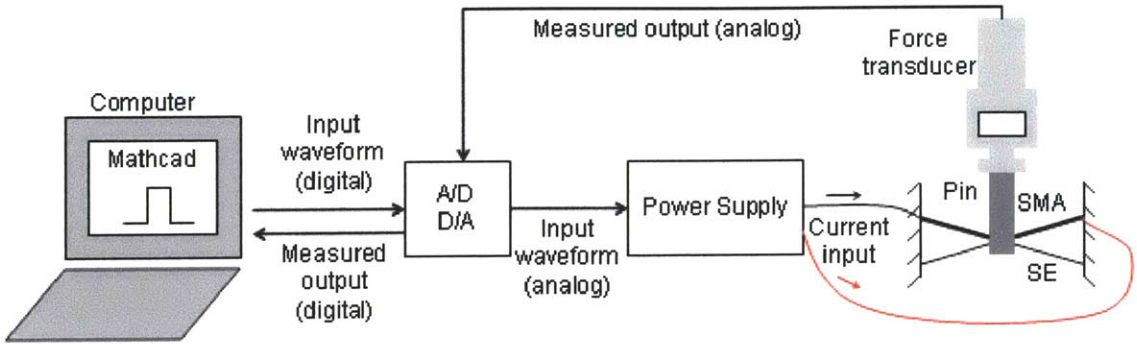

Figure 5-4. Schematic of the equipment used to send a current pulse through the SMA wire and record the resulting force and displacement (the force transducer shown here can be replaced by the displacement transducer).

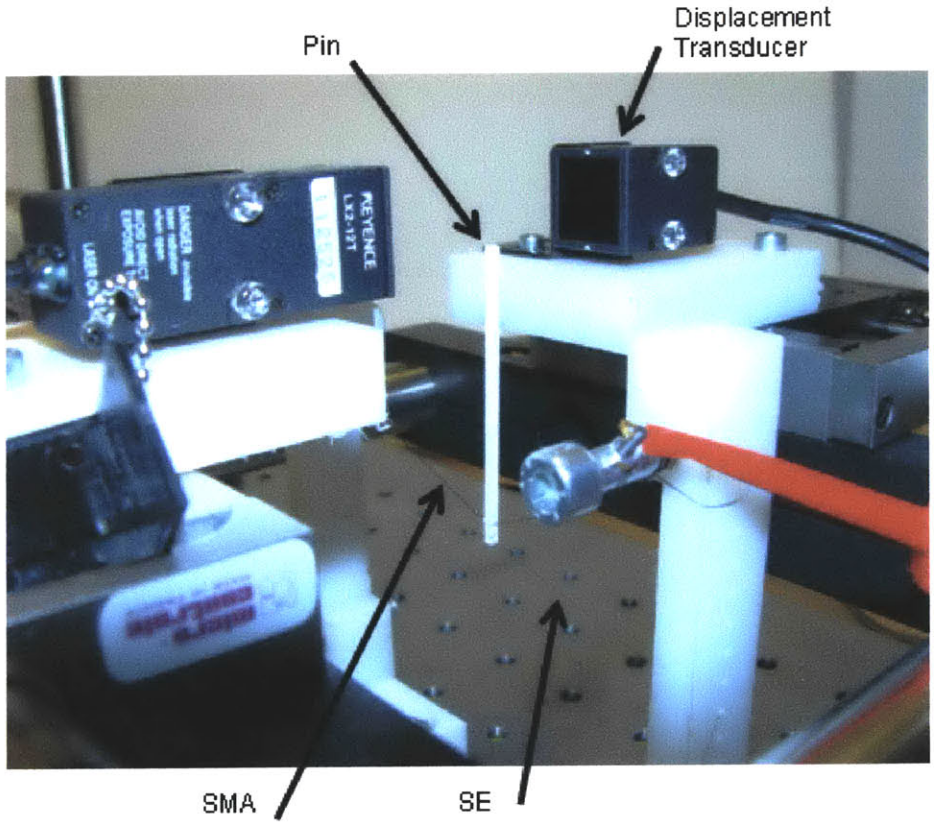

Figure 5-5. Experimental setup to measure the vertical displacement of the pin.

5.2 Results

Typical force and displacement outputs of the SMA stimulated by a 1 second, 1 Amp pulse are shown plotted over time in Figure 5-6.

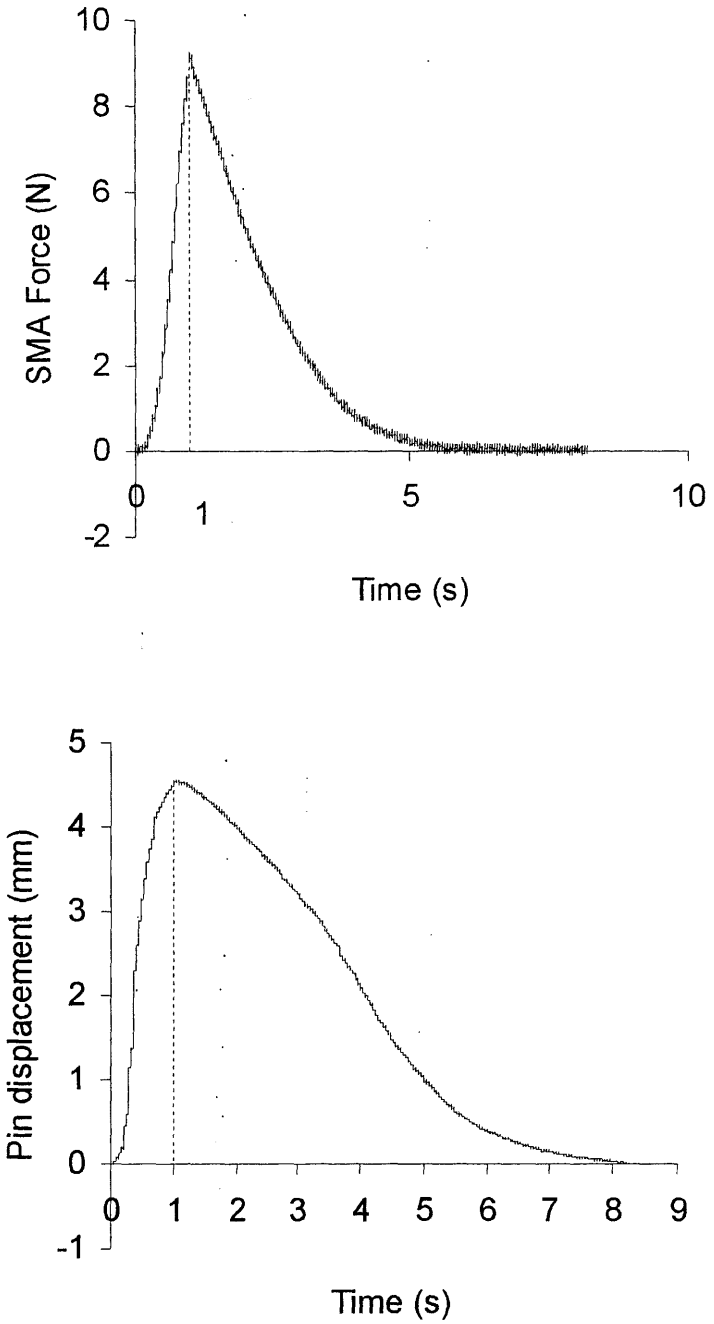

Figure 5-6. Typical curves of pin displacement and SMA vertical force output over time.

5.2.1 Force Output

The input pulse amplitude was varied from 0.8 to 1.2 Amps, and the pulse duration from 0 to 2.5 seconds for measurements of the SMA force output (see Figure 5-7). The force increases with increasing pulse duration, and plateaus at about 1.5 seconds in duration. The force also increases with increasing pulse amplitude, but plateaus at about 1.2 or 1.3 Amps. Longer duration or higher intensity input pulses degrade the output, lowering the force generated by the SMA.

5.2.2 Displacement Output

In measurements of displacement, the pulse duration was first set at 1 second while the pulse amplitude was varied from 0.5 to 1.7 Amps (see Figure 5-8). The pulse duration was then varied from 0.5 to 2 seconds while the pulse amplitude was fixed at 1 Amp (see Figure 5-9). The output pin displacement was affected in a similar manner as the force output by the parameters of the input waveform. The peak displacement increased with higher pulse amplitudes or longer durations, but leveled off after reaching 1.2 Amps or 1.3 seconds.

5.2.3 Repeatability

A single Nitinol fiber was stimulated by a 1 second, 1 Amp pulse for over 3,000 cycles without degradation of the output (see Table 5-1 for a summary of the results). First, the peak force of the SMA was recorded for over 2,000 cycles. The mean of these values was 9.64 N and the standard deviation 0.49 N. The force output did not degrade significantly; the mean was 9.43 N for the first 100 cycles, and 9.47 N for the last 100 cycles (see Figure 5-10). The peak pin displacement was then measured for almost 800 cycles, and had a mean of 3.67 mm with a standard deviation of 37 μm (see Figure 5-11). As with the force output, the peak pin displacement did not decay significantly; in the first 100 cycles the mean was 3.68 mm, and in the last 100 cycles the mean was 3.65 mm. The resting position of the pin had a standard deviation of 17 μm (see Figure 5-12).

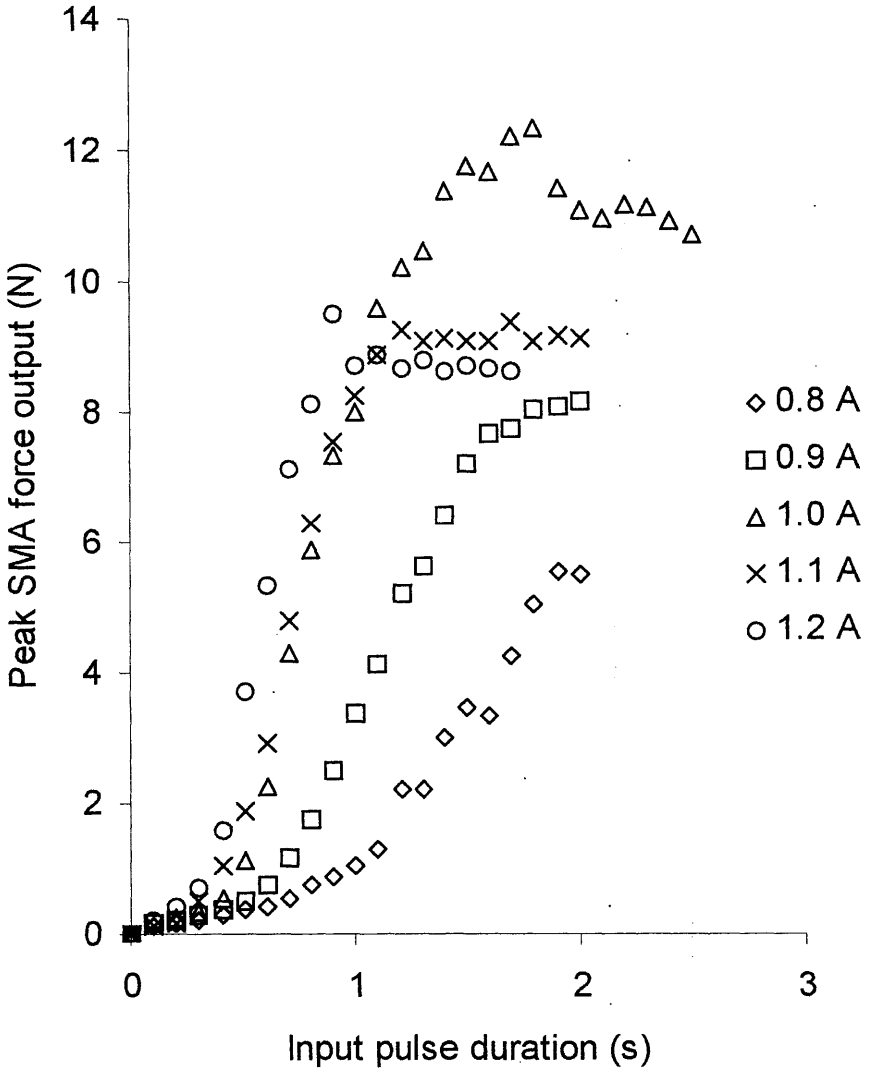

Figure 5-7. Peak SMA force output as a function of input current pulse duration and pulse amplitude.

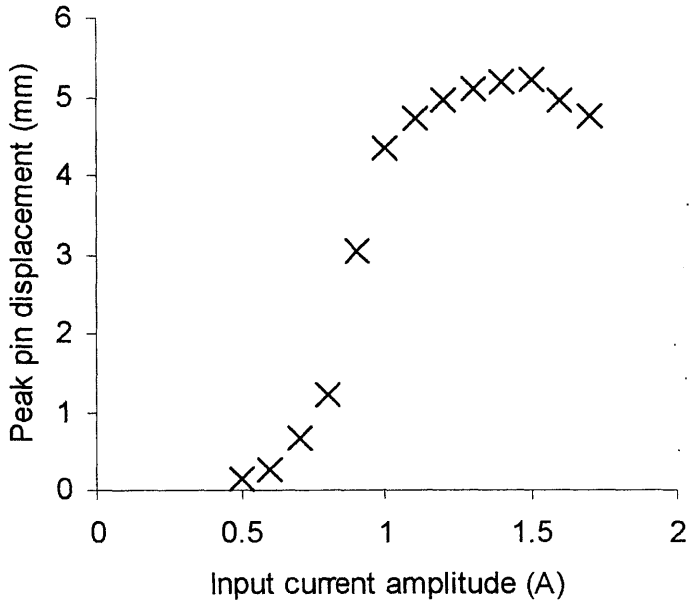

Figure 5-8. Peak pin displacement as a function of input current pulse amplitude.

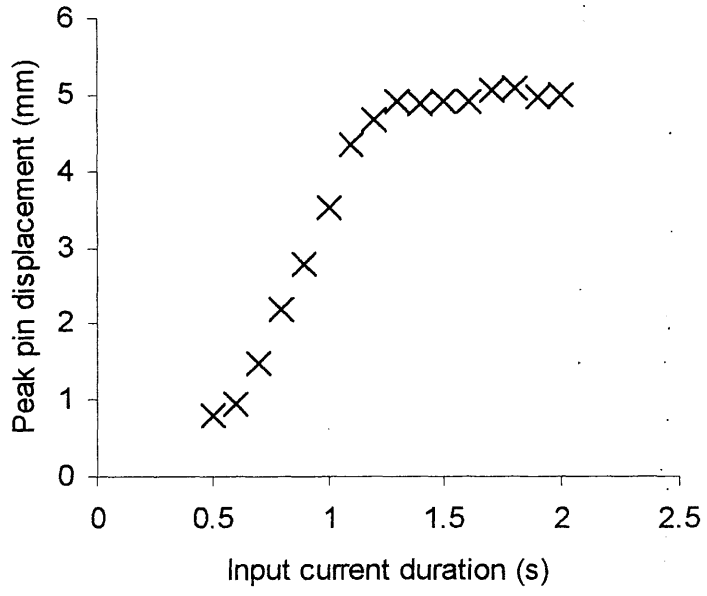

Figure 5-9. Peak pin displacement as a function of input current pulse duration.

Table 5-1. Results from repeatability tests of a single Nitinol fiber.

		Mean	**Standard deviation**
Peak SMA force output:	Overall (2,215 cycles)	9.64 N	0.49 N
	First 100 cycles	9.43 N	0.15 N
	Last 100 cycles	9.47 N	0.34 N
Peak pin displacement:	Overall (753 cycles)	3.67 mm	37 μm
	First 100 cycles	3.68 mm	35 μm
	Last 100 cycles	3.65 mm	36 μm
Pin resting position:	Overall (753 cycles)		17 μm
	First 100 cycles		11 μm
	Last 100 cycles		9 μm

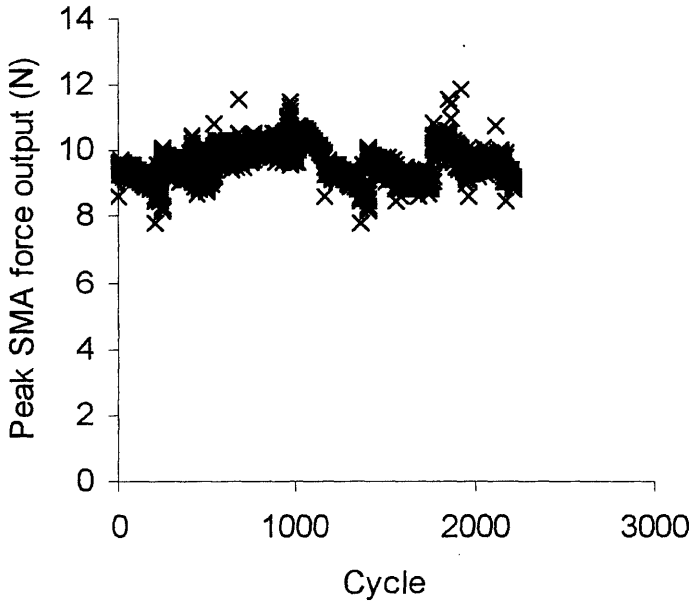

Figure 5-10. Repeatability test of a single Nitinol fiber: peak force output of the SMA for 2,215 cycles.

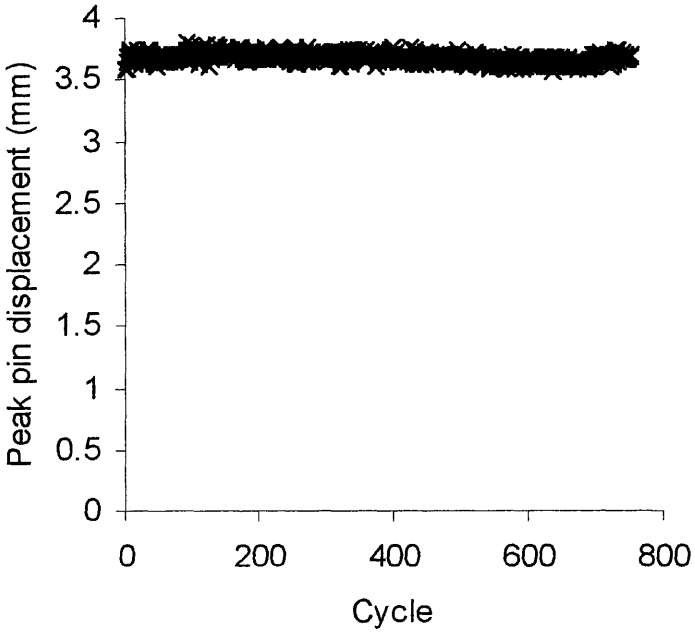

Figure 5-11. Repeatability test of a single Nitinol fiber: peak pin displacement for about 800 cycles.

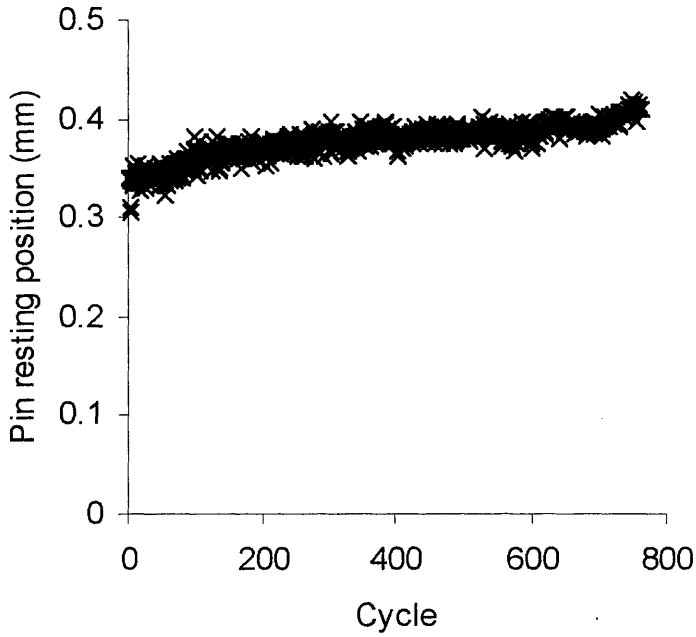

Figure 5-12. Repeatability test of a signal Nitinol fiber: pin resting position for about 800 cycles.

5.3 Discussion

The results achieved thus far prove that the SMA fiber can generate significant displacements and pressures greatly surpassing the sensitivity thresholds of the torso. A pulse 1 Amp in amplitude and 1 second in duration produced an average peak displacement of 3.7 mm and force of 9.6 N. This peak force translates to a pressure over 15 times the touch threshold on the torso (9 N of force transmitted by a pin with an area of 10 mm^2 equates to 900 kPa of pressure, while the touch threshold for the torso is 20-61 kPa). Furthermore, the SMA was able to go through thousands of cycles without degradation of the output. These results indicate promise in using Nitinol to generate a wide range of outputs for a haptic device that stimulates the skin on the torso.

6 Design and Construction of the Tactor

6.1 Design Goals

Our objective is to design a robust, versatile actuator for a Tactile Vest, a wearable device that provides haptic feedback to the torso. The actuator should be perceptually robust, yet thin, lightweight, and flexible, making the device comfortable and invisible to the user until a stimulus occurs. The actuator should also be able to generate at least twice the touch threshold in the torso, or about 120 kPa, and displace the skin 2-4 mm. Inter-element spacing of the stimulators can be greater than or equal to the two-point threshold for the torso (32-41 mm, Weinstein, 1968).

Table 6-1. Design parameters of the tactor unit for the Tactile Vest.

Pressure	≥ 120 kPa
Displacement	2-4 mm
Interelement spacing	≥ 32-41 mm
Size	minimize
Weight	minimize
Power requirement	minimize
Bandwidth	maximize
Flexibility	maximize

6.2 The Design

Shape memory alloys were selected to actuate the tactor unit as shown in Figure 6-1 for their capacity to generate large stresses and strains, flexibility, lightness, and small size. Current applied across the SMA wire causes the fiber to contract, rotating the pin around the pivot rod (see Figure 6-1). The superelastic wire resets the system without the need for activation energy. Based on this mechanism, the actuator unit was designed as shown in Figure 6-2. The unit consists of the pin (see Figure 6-3), pivot rod, SMA and superelastic wires, assorted hardware for the mechanical and electrical connections, and the base: a rigid section that anchors the SMA, superelastic wire, and pivot rod (see Figure 6-3). Holes were drilled in the base, and the SMA and superelastic wires wound through these holes, so that both ends of the wire exit the base at a uniform position. A

casing enclosing the entire unit was also constructed in order to protect the skin from heat and current in the SMA wire (Figure 6-4). The tactor unit, including the casing, has an overall height of 17 mm, length 42 mm, and width 22 mm.

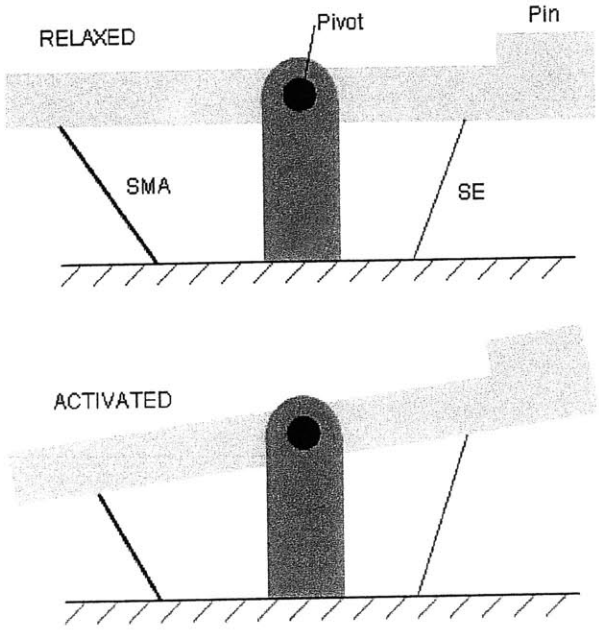

Figure 6-1. Sketch of the actuator mechanism.

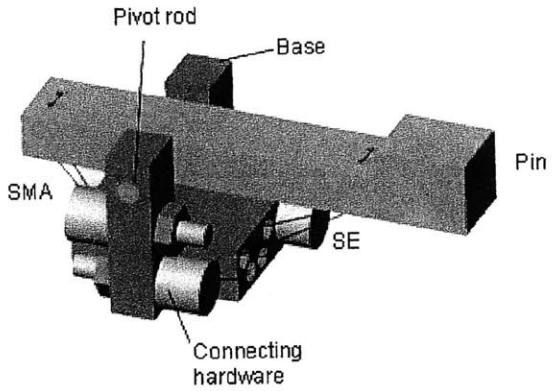

Figure 6-2. Implementation of the actuator mechanism shown in Figure 6-1. In this design, the overall height of the tactor unit is 15 mm, length is 40 mm, and width is 18 mm.

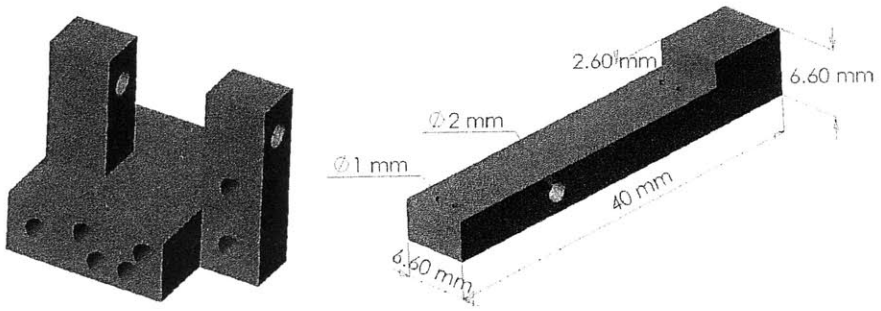

Figure 6-3. Sketch of the base (left) and pin (right) for the tactor unit. The base anchors the SMA, superelastic wire, and pivot rod, and has length of 15 mm, width 18 mm, and height 15 mm.

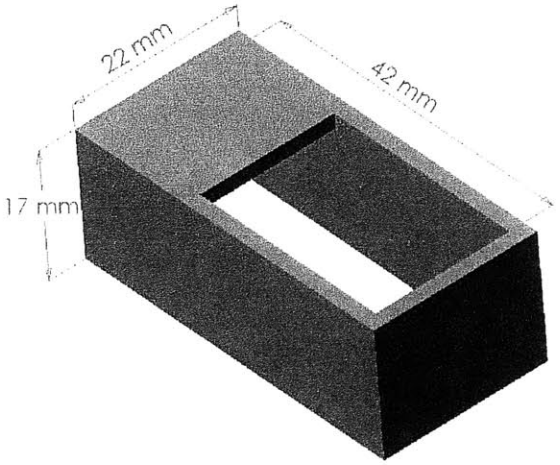

Figure 6-4. Casing for the tactor unit shown in Figure 6-2.

6.2.1 Securing the SMA and superelastic wires

The SMA and superelastic fibers were wound around a bolt, taking advantage of the capstan effect to secure the fiber mechanically, while allowing the wire tension to be adjusted by turning the bolt. As the fiber contracts or stretches, its inner loops tighten and better secure the fiber (the capstan effect). However, the fiber can relax quickly enough to loosen the attachment, and thus an extra mechanism is needed to secure the fiber. The wire was therefore looped once around a couple washers, and tightened with a nut (see Figure 6-5).

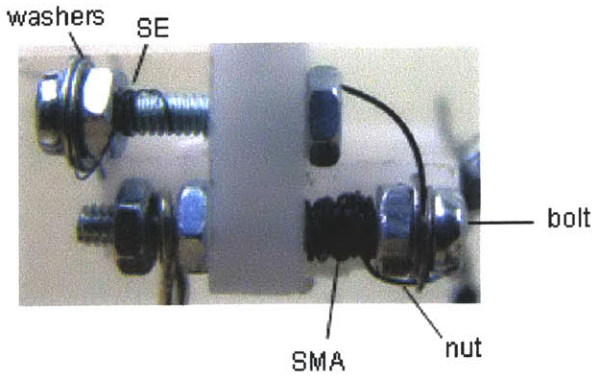

Figure 6-5. Winding the superelastic and SMA wires around a bolt takes advantage of the capstan effect while allowing the wire tension to be adjusted.

6.3 Materials

The base and pin contact the NiTi fiber, which carries current and cycles through temperatures reaching 90°C. The materials for these components must therefore be electrically non-conducting and able to resist high temperatures. Delrin and Macor (Corning, Inc.) were selected as candidate materials for the base and pin. Delrin is an easily machineable plastic (see Appendix C for a few material properties of Delrin), and Macor is a machineable glass ceramic with very high temperature resistance capabilities (see Appendix C for a few material properties of Macor). However, Macor is very brittle, and chips and fractures very easily (see Figure 6-6). As a result, Delrin was selected as the material for the pin and base despite its lower operating temperatures.

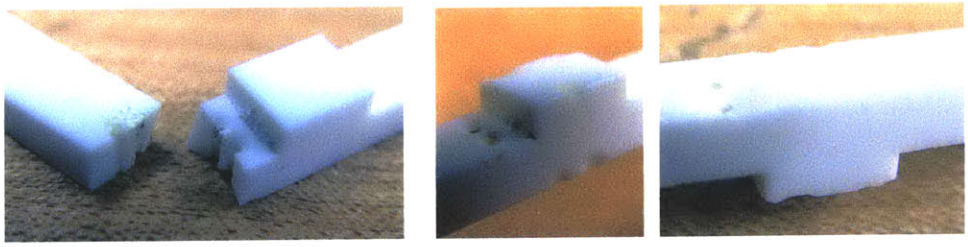

Figure 6-6. Attempts at machining pins from Macor (Corning, Inc.). The Macor is very brittle, and easily chips and fractures.

As mentioned earlier, NiTi fibers were selected to actuate the tactor unit for their ability to produce large stresses and strains, as well as for their small size and flexibility. Tables 6-2 and 6-3 contain the specifications for the NiTi fibers selected. See Chapter 4 for a detailed description of shape memory alloys and Nitinol.

Table 6-2. Specifications for the NiTi shape memory alloy fiber (Flexinol^{TM}, Dynalloy, Inc.).

Property	Value
Diameter	254 μm
Density	6.5 g/cm^3
Maximum generated stress	180 MPa*
Maximum generated strain	4%
Transition temperature	90°C
Resistance	19.7 Ω/m
Lifetime	~10^6 cycles at 2% contraction
	~10^4 cycles at 4.5% contraction

*Equivalent to 9.12 N force for a 254 μm diameter wire

Table 6-3. Specifications for the NiTi superelastic fiber (SportsWire, LLC).

Property	Value
Diameter	101.6 μm
Density	6.5 g/cm^3
Plateau stress	450 MPa*
Maximum strain	8%
Transition temperature	5-18°C

*Equivalent to 3.6 N force for a 101.6 μm diameter wire

6.4 Construction of the Tactor Unit

Four tactors as described above were constructed to create a 2x2 or 4x1 array (see Figures 6-7 through 6-10).

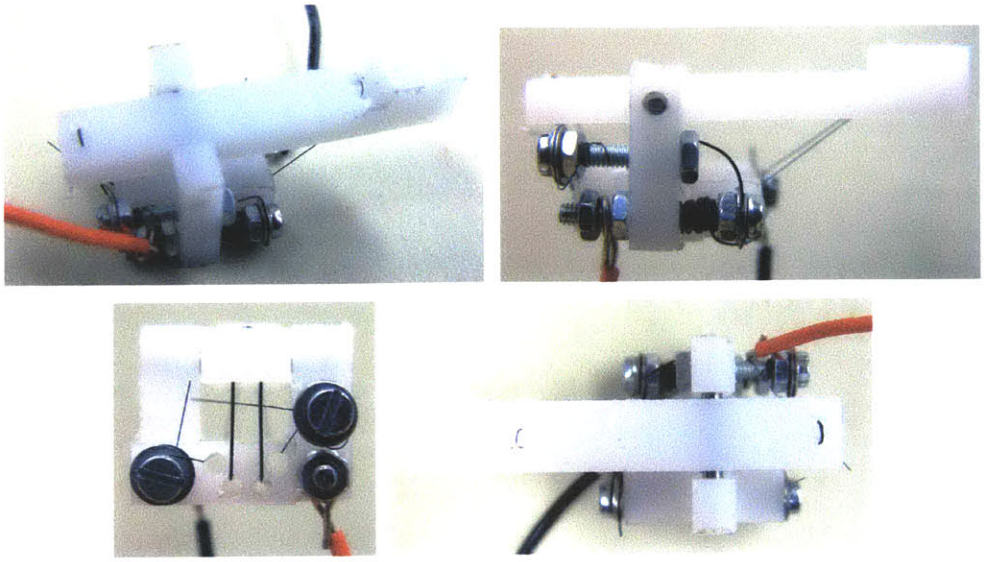

Figure 6-7. The tactor unit.

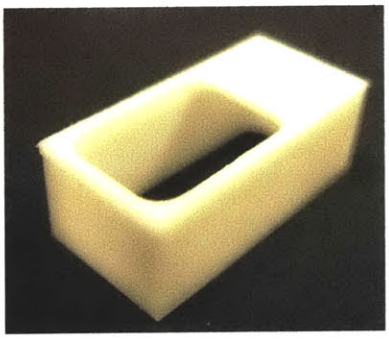

Figure 6-8. Casing for the tactor unit.

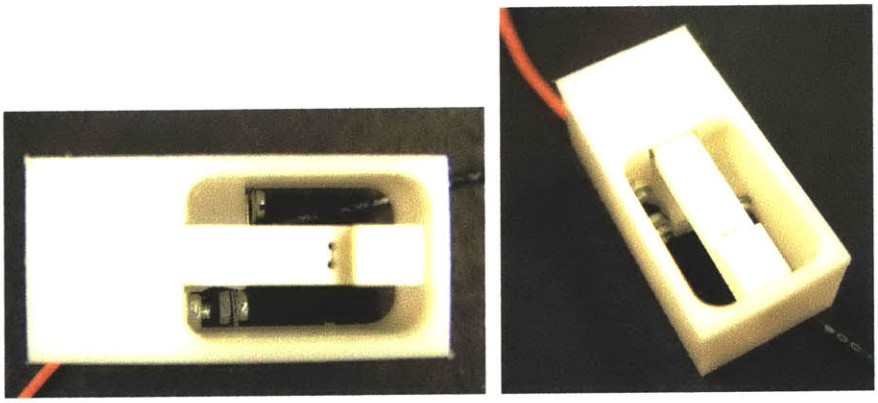

Figure 6-9. The completely assembled tactor unit including the casing. The complete unit has overall height 17 mm, length 42 mm, and width 22 mm.

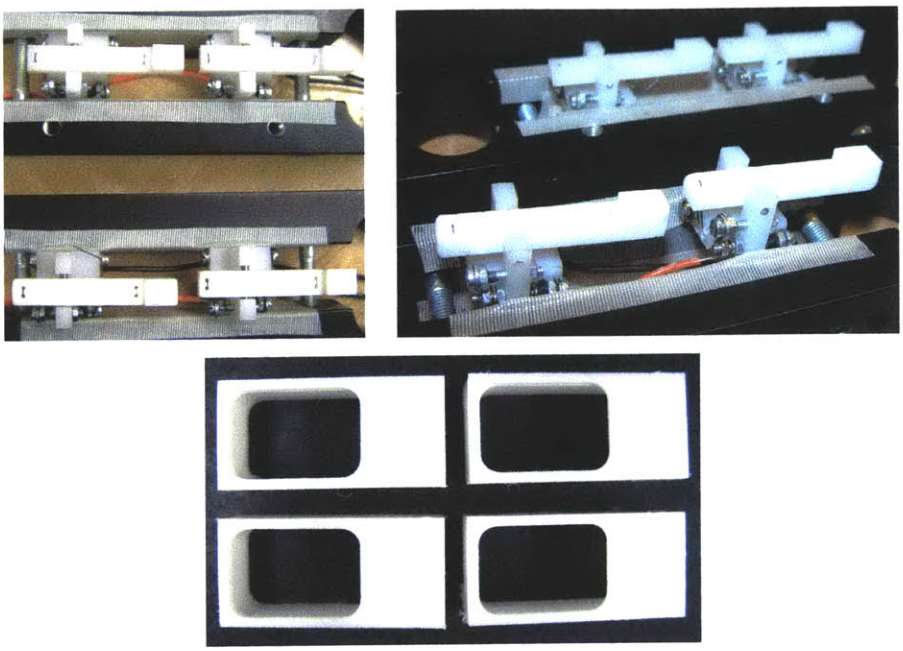

Figure 6-10. Four tactors and casings were built to form a 2x2 array.

6.5 Power requirements

For the NiTi fiber selected, a 1 Amp, 1 second current pulse will adequately heat the wire to produce a contraction. The resistance of a 100 mm long fiber is roughly 2 Ω. Therefore, about 2 Watts of power is required per contraction of the 254 μm diameter shape memory alloy.

6.6 Predicted outputs

Using the dimensions described above, simple kinematics, and assuming 4% strain of the SMA, a vertical displacement of 3.9 mm and force of 7 N (132 kPa for a pin 52.8 mm^2 in area) was predicted. According to the specifications for the total heating and cooling times of the 254 μm NiTi fiber at 21°C ambient temperature, the operating frequency is 0.22 Hz (1 second heating time, 3.5 seconds cooling time).

The next chapters evaluate the performance of the tactor unit array.

7 Performance of the Tactor

The force and displacement outputs of the tactors designed and constructed as described in Chapter 6 were measured individually.

7.1 Method

A current pulse was applied across the NiTi fiber in the tactors to heat the fiber to its transition temperature of 90°C. Different stimulating inputs were created by varying the duration and amplitude of the current pulse. As described in Chapter 5, a discrete waveform was created in Mathcad and fed through a digital/analog board (National Instruments, PCI-6052E). This time, however, instead of directly controlling a power supply, the analog voltage signal (V_{in}) was sent through an op-amp circuit (see Chapter 8 for more details on this circuit). The op-amp circuit amplified the voltage signal and generated a current pulse (I_{load}) across the NiTi fiber (see Figure 7-1).

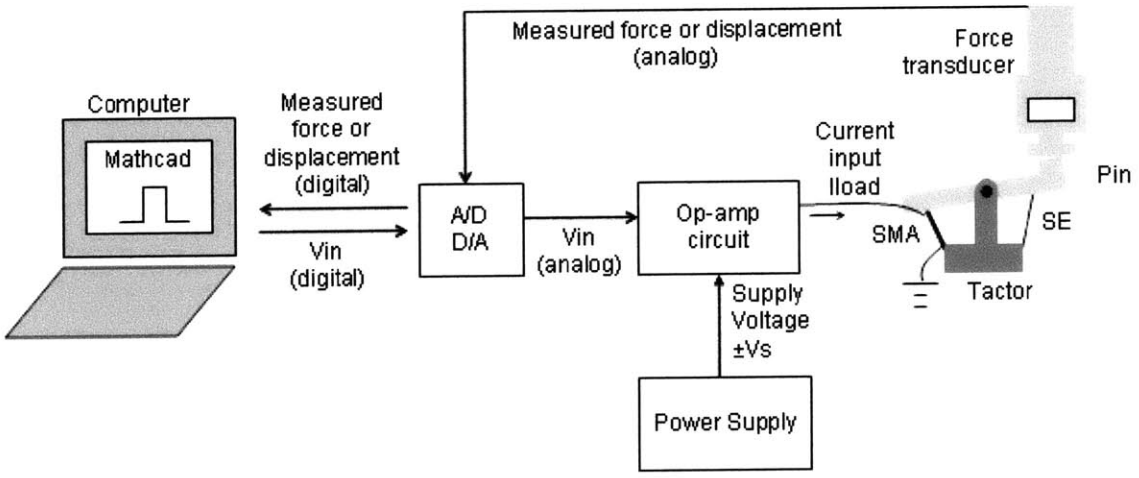

Figure 7-1. Schematic of the equipment used to measure the force and displacement of the tactor for the Tactile Vest. V_{in} is the input voltage signal generated in Mathcad.

The time course of the resulting force output of the SMA was recorded using a force transducer (Shimpo, DFS-20). As before, the force transducer was mounted so it barely touched the top of the pin when the NiTi fiber was in its resting position. As the SMA contracted, the pin pressed against the force transducer and thus did not displace (see

Figure 7-2). The analog voltage from the transducer was transmitted via the analog/digital board to a computer, where it was sampled and filtered in Mathcad (using an FIR low pass filter with sampling frequency 500 Hz, 4096 samples, and 50 Hz cut-off frequency). For displacement measurements, the net movement of the pin was manually read from a ruler placed next to the pin. During the measurements of displacement, the pin was allowed to move freely.

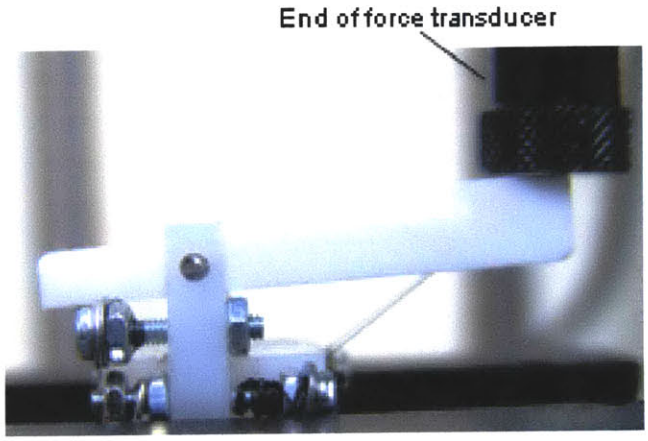

Figure 7-2. Equipment set-up to measure the force output of the tactor.

7.2 Results

The parameters for the input current pulse applied across the NiTi fiber were varied by controlling the amplitude and duration of the voltage signal, V_{in}, sent by the computer to the op-amp circuit (see Figure 7-1). Figures 7-3 and 7-4 show the current sent through the SMA fiber (I_{load}) as a function of the controlling voltage amplitude and pulse duration. The input voltage amplitude was varied between 0-2 V, and the pulse duration was set at 0.5, 0.7, and 1.0 seconds. In general, I_{load} was independent of the pulse duration. However, the current rose linearly with increasing V_{in}, then plateaued (see Figure 7-3). Variations in the current applied across the SMA fiber are probably due to differences in the overall resistance of the fibers in each tactor; the fibers may not have been wound identically during mechanical attachment and adjustment of the tension of the fiber, which may confer differences in resistivity.

Typical force measurements of each tactor over time are shown in Figures 7-5 and 7-6. (In a few of the graphs, a negative force output is shown. This is due to the difference in

resting positions of the pin at the start and finish of contraction. Since the force transducer is zeroed at the start of the cycle, a more relaxed finishing position will produce a negative force output.) For identical input parameters (i.e., identical input voltage amplitudes and pulse durations), the peak force and displacement output was averaged over the four tactor units, and is shown plotted in Figures 7-7 and 7-8. The individual peak force and displacement outputs of each tactor are shown in Figures 7-9 to 7-14. Depending on the input parameters and the tactor, the peak force output ranged between 5-9 N and the displacement between 0-3 mm. The average maximum pin displacement was 3 mm and the average maximum force output 7 N (or equivalently, 133 kPa for a pin contact area of 52.8 mm^2). For the same input voltage amplitude, the shortest pulse duration of 0.5 s produced significantly lower outputs compared to the 0.7 s and 1 s pulse durations. On the other hand, the 0.7 s pulse duration produced outputs very close to those resulting from the longer, 1 s stimulus (see Figures 7-15 and 7-16).

The bandwidth of the four tactors, for all stimulus waveforms used, remained below 0.3 Hz (see Figure 7-17). The rise time of the NiTi fibers was dependent on the input pulse duration and the cooling time generally decreased with increasing pulse duration (see Figures 7-18 to 7-20).

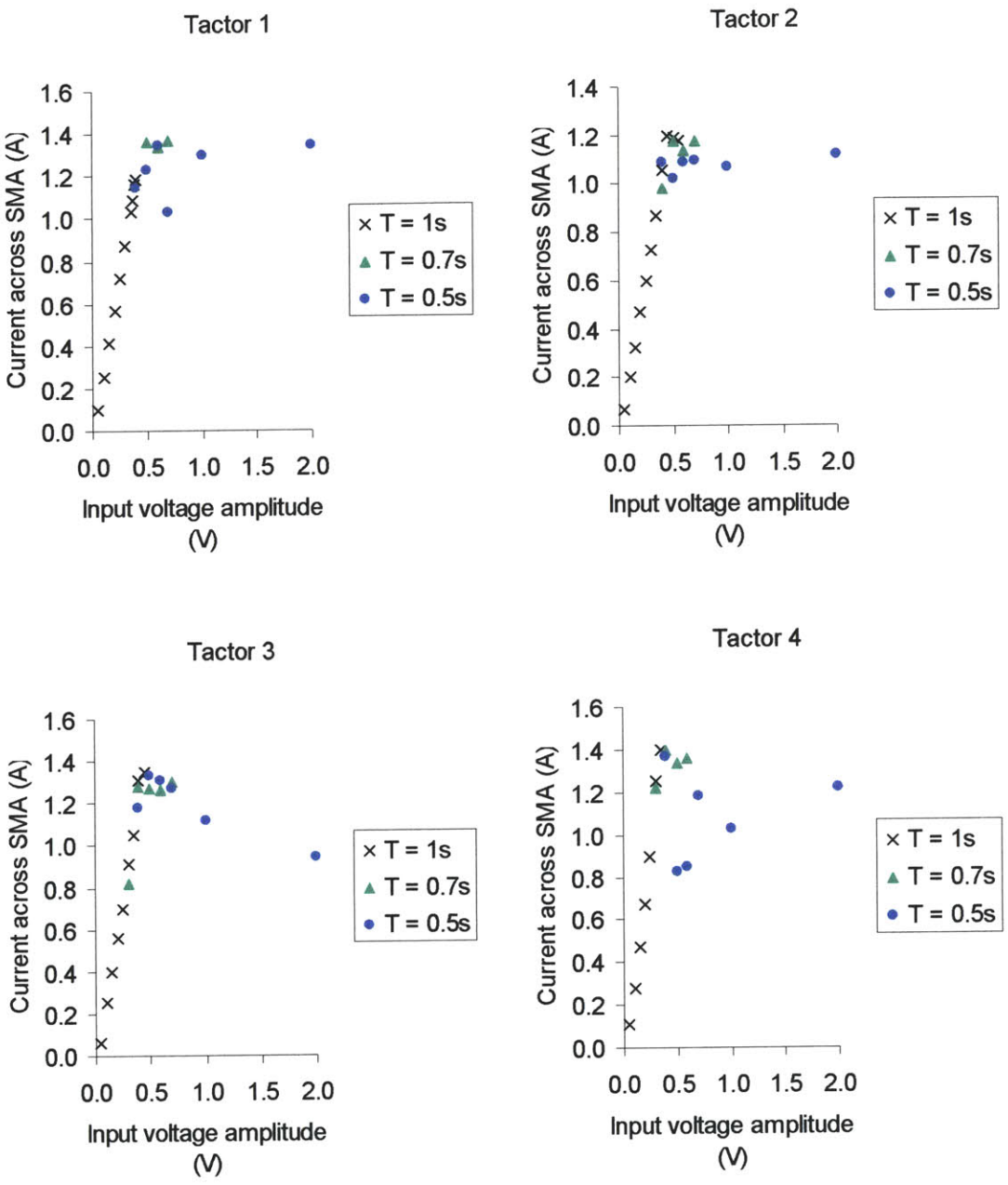

Figure 7-3. Current applied across the SMA fiber (I_{load}) as a function of the controlling voltage amplitude (V_{in}), for Tactors 1-4 (T = pulse duration).

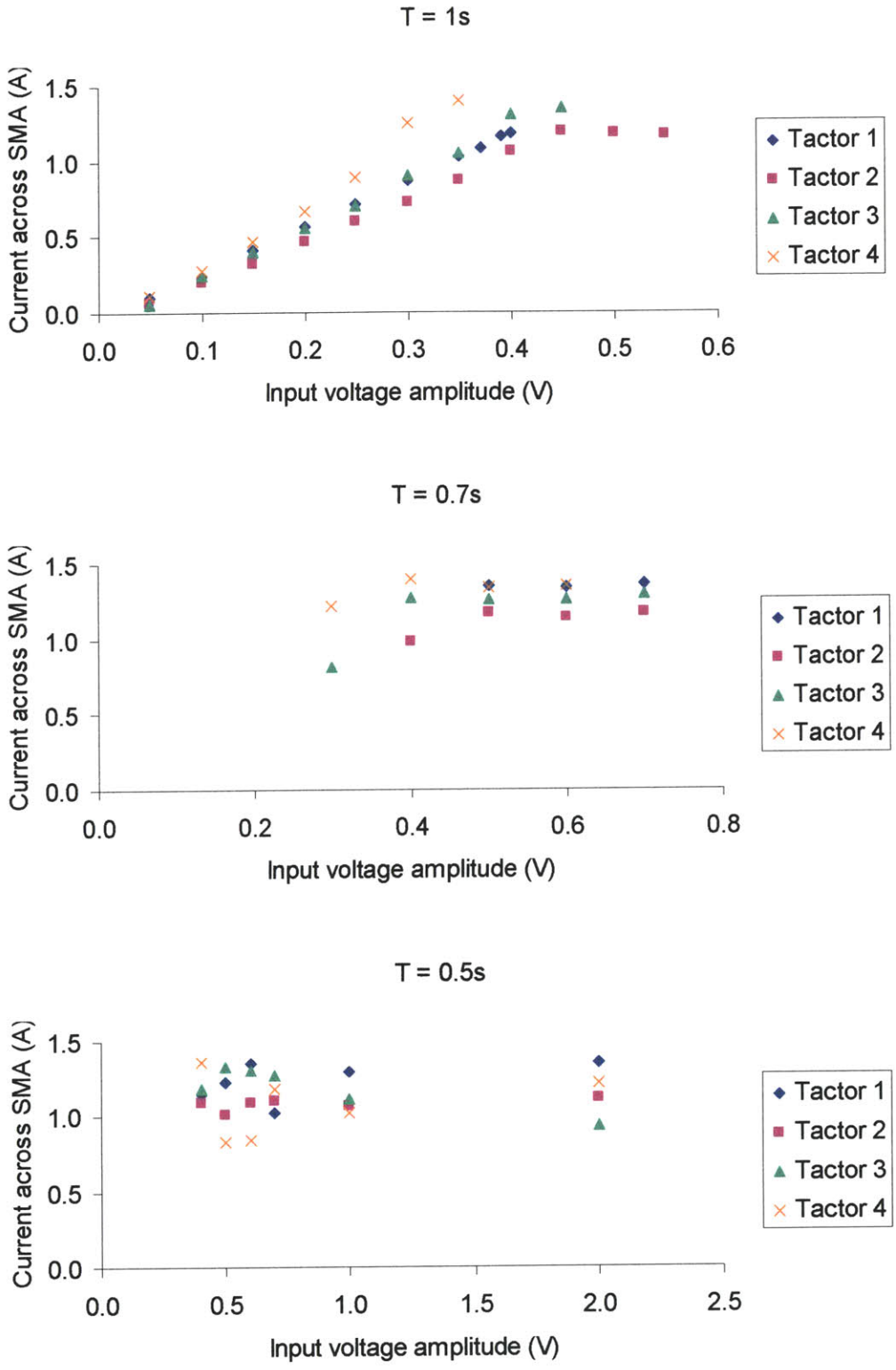

Figure 7-4. Current applied across the SMA fiber (I_{load}) as a function of the controlling voltage amplitude (V_{in}), for pulse durations (T) 1.0, 0.7, and 0.5 seconds.

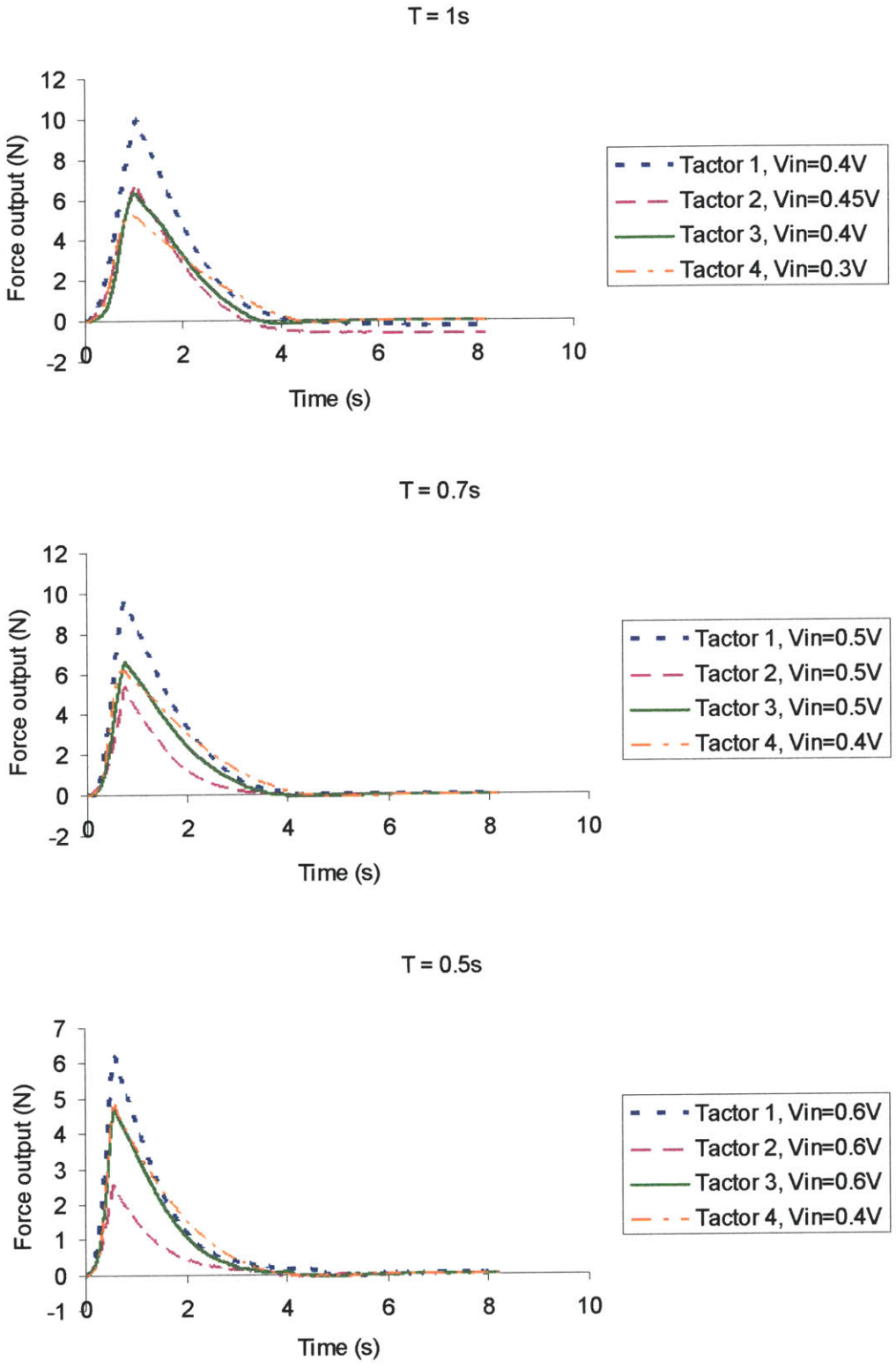

Figure 7-5. The force output of all four tactors over time for pulse durations (T) 1.0, 0.7, and 0.5 seconds.

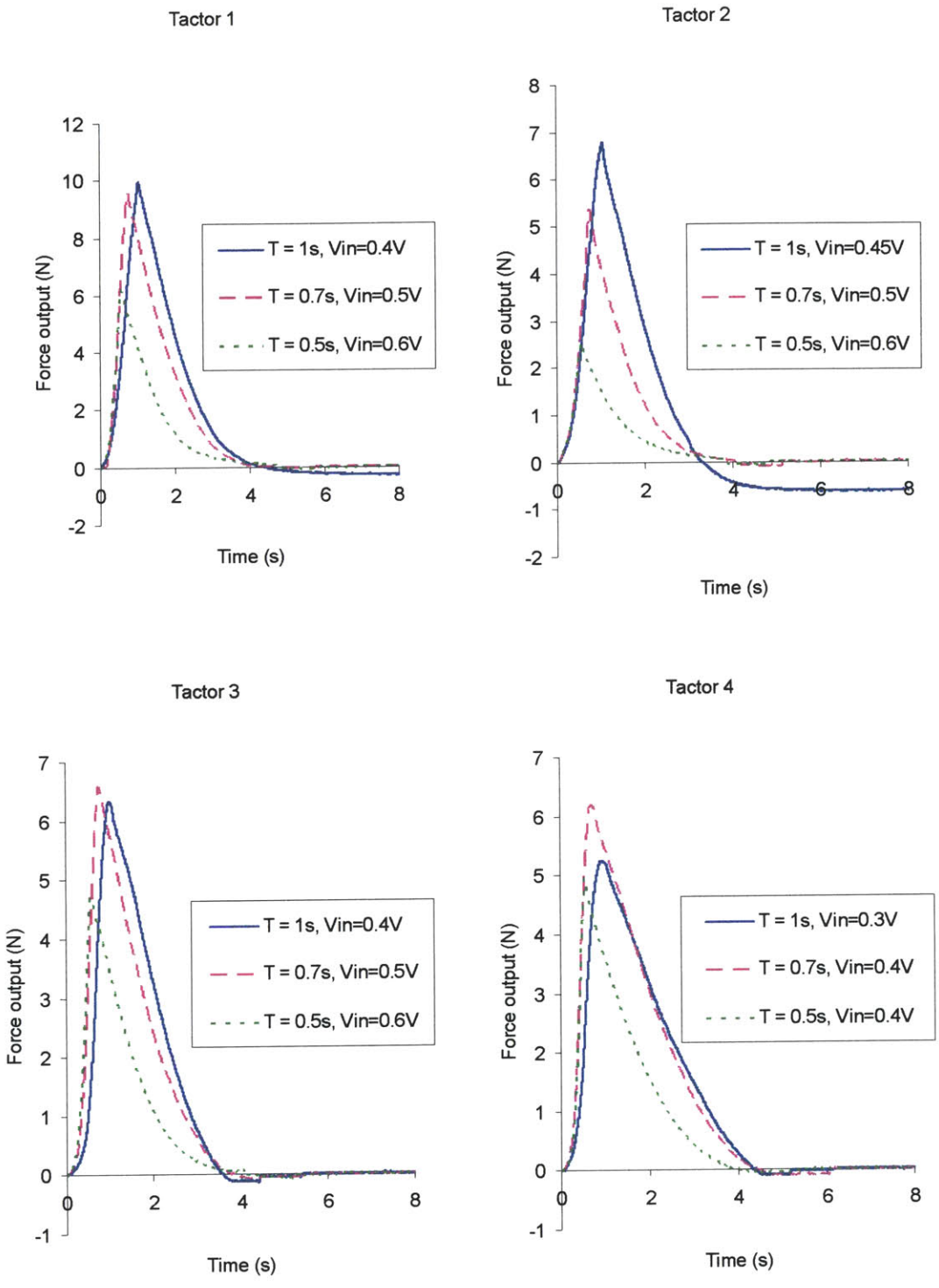

Figure 7-6. The force output of tactors 1-4 over time.

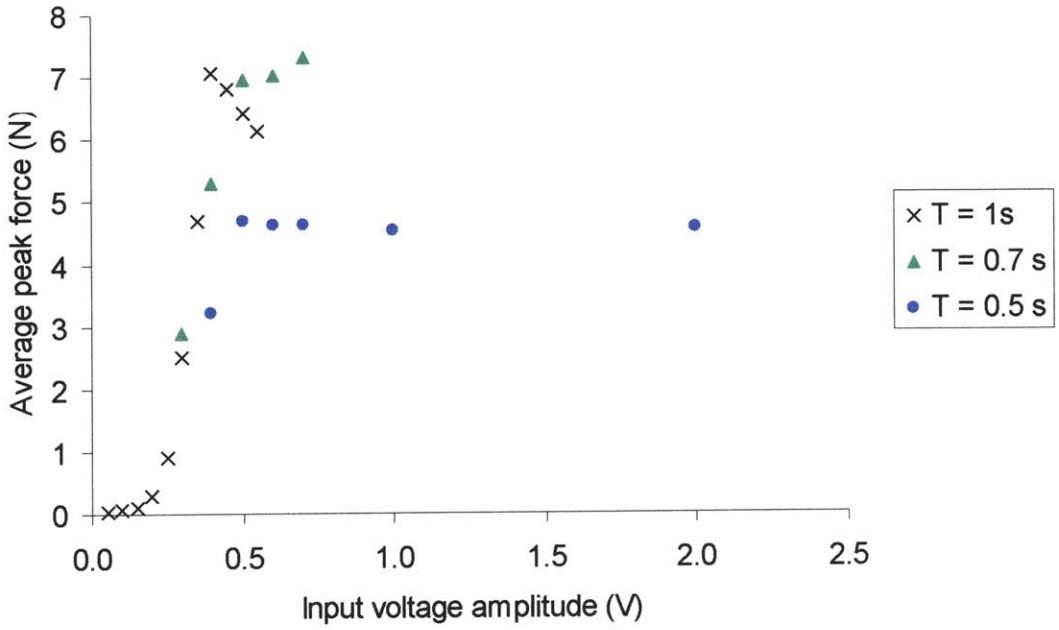

Figure 7-7. Peak force outputs averaged over all four tactors (T = pulse duration).

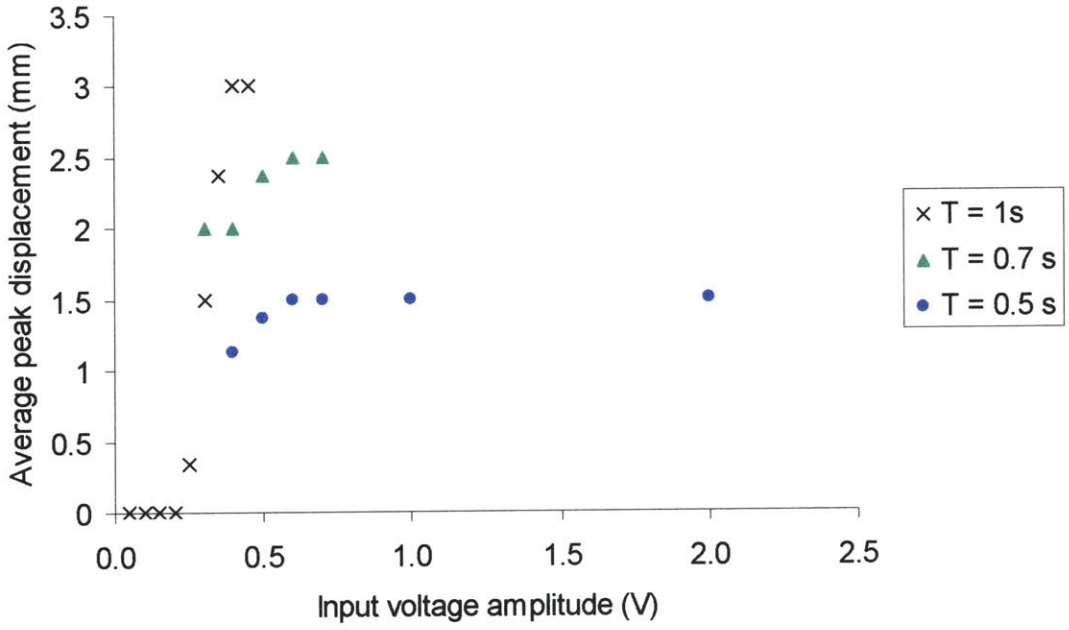

Figure 7-8. Peak displacement outputs averaged over all four tactors (T = pulse duration).

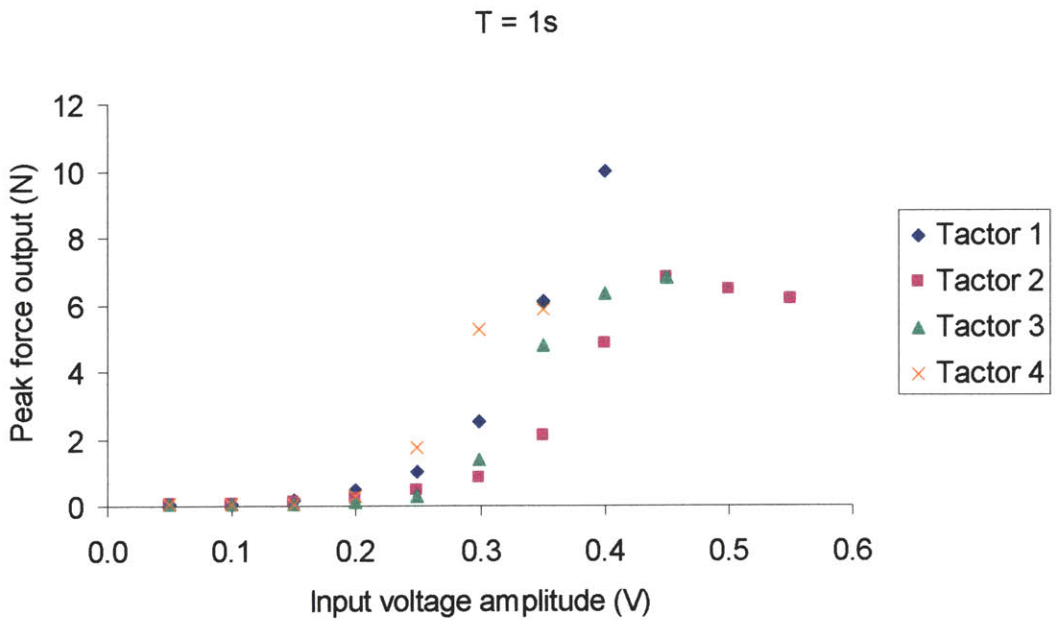

Figure 7-9. Peak force output of the tactor as a function of the controlling input voltage (V_{in}) for all four tactors, with pulse duration (T) 1 second.

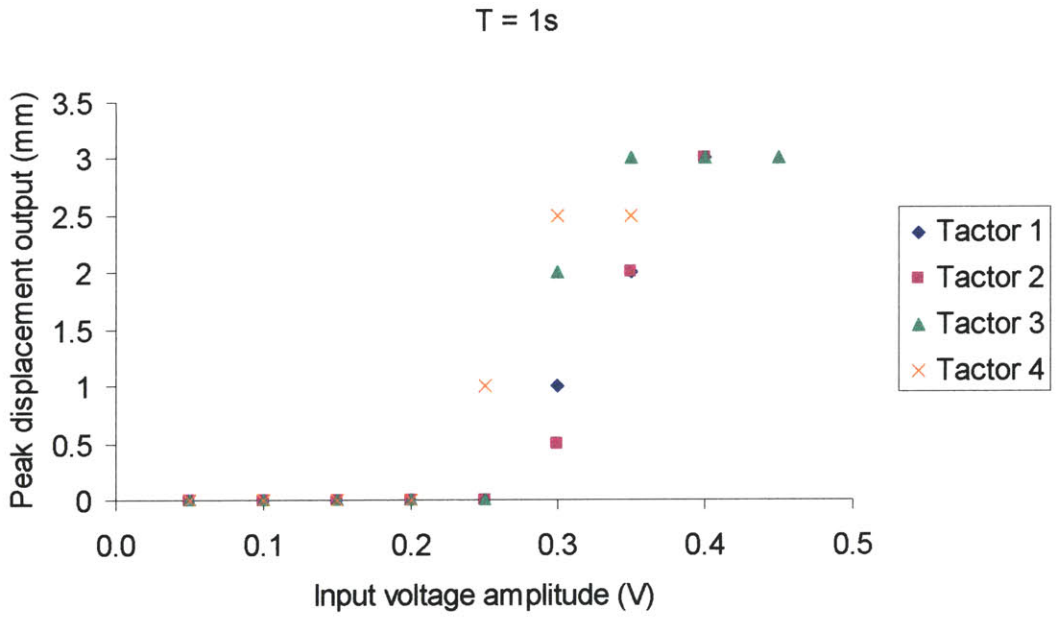

Figure 7-10. Peak displacement output of the tactor as a function of the controlling input voltage (V_{in}) for all four tactors, with pulse duration (T) 1 second.

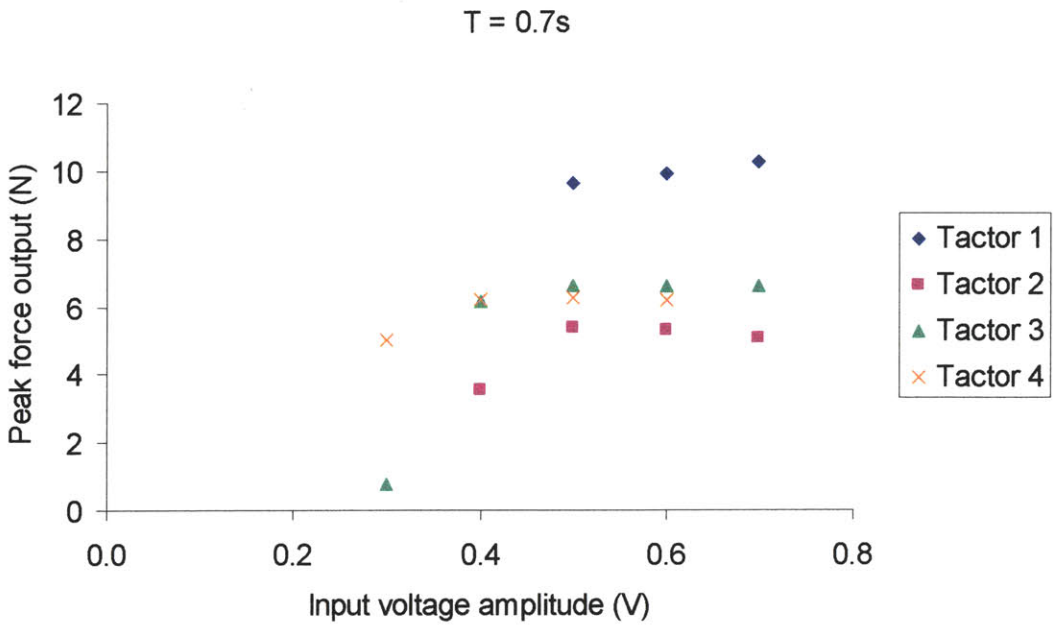

Figure 7-11. Peak force output of the tactor as a function of the controlling input voltage (V_{in}) for all four tactors, with pulse duration (T) 0.7 seconds.

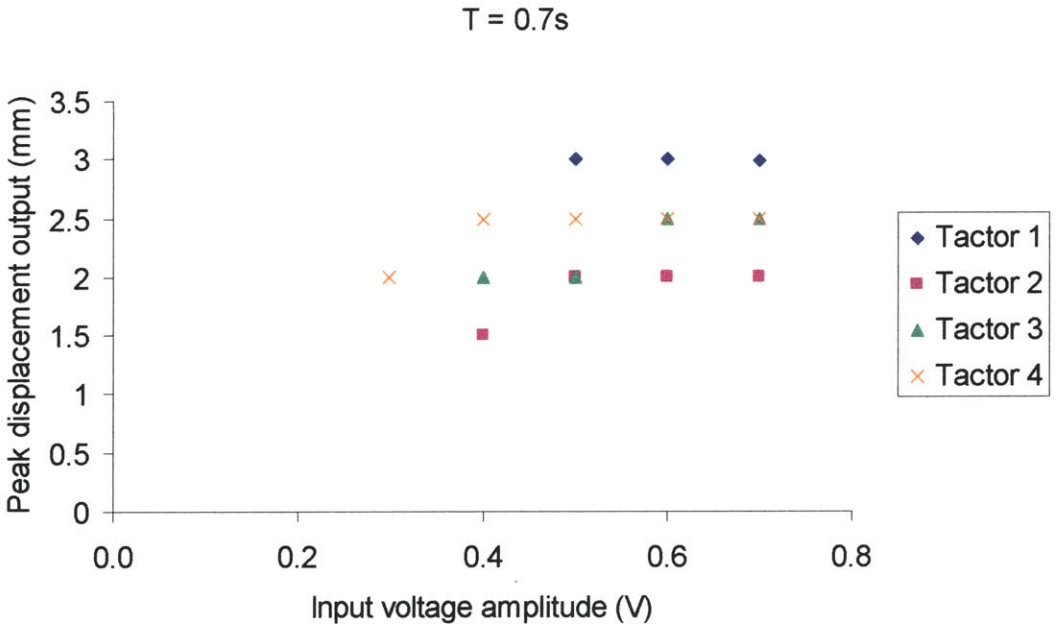

Figure 7-12. Peak displacement output of the tactor as a function of the controlling input voltage (V_{in}) for all four tactors, with pulse duration (T) 0.7 seconds.

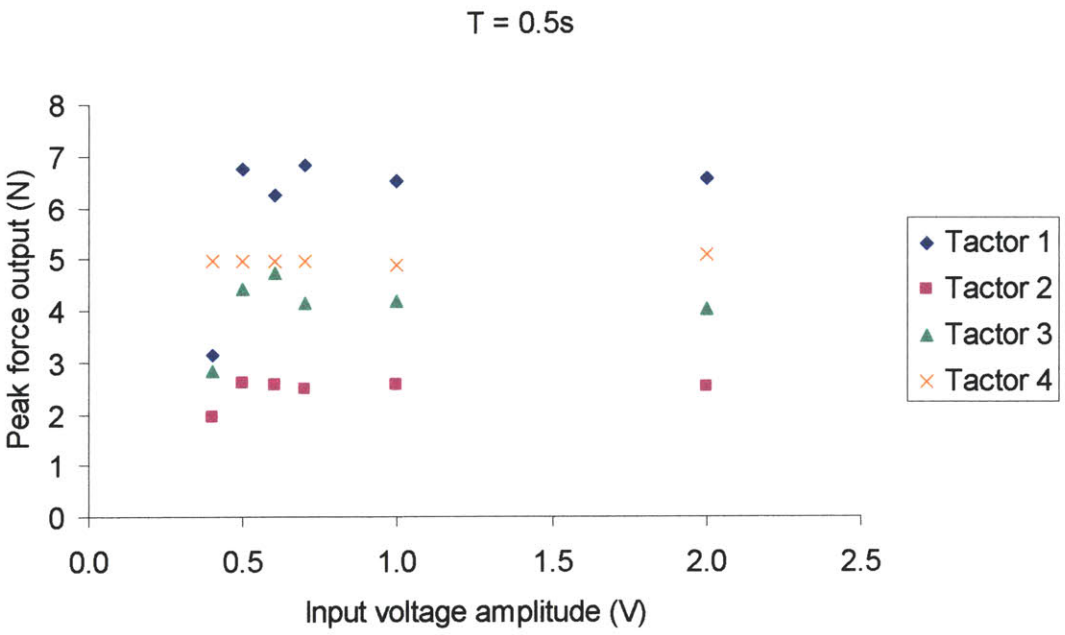

Figure 7-13. Peak force output of the tactor as a function of the controlling input voltage (V_{in}) for all four tactors, with pulse duration (T) 0.5 seconds.

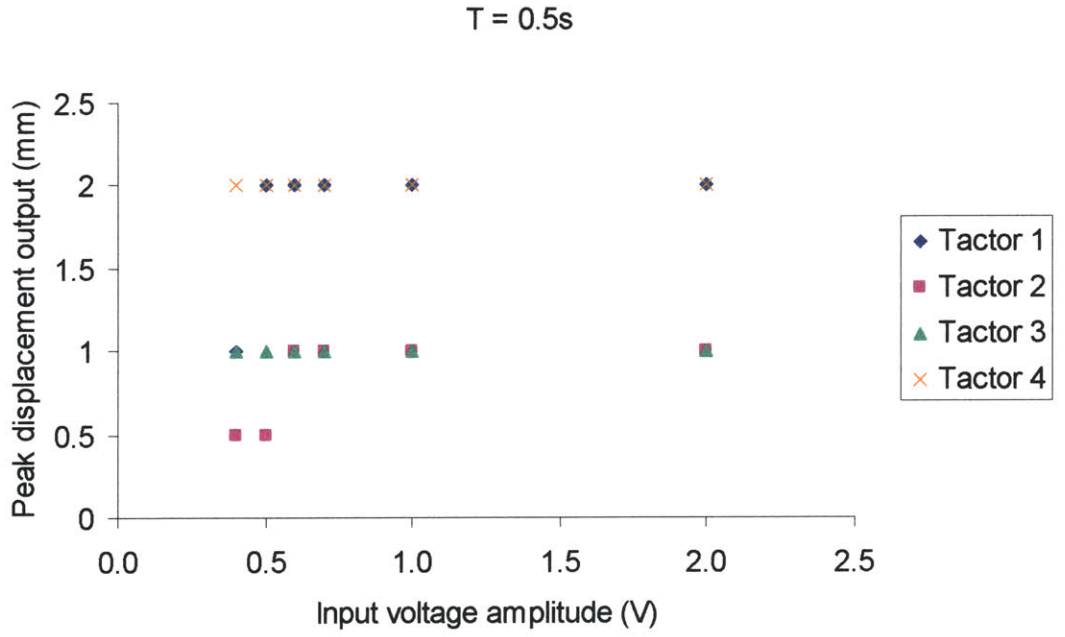

Figure 7-14. Peak displacement output of the tactor as a function of the controlling input voltage (V_{in}) for all four tactors, with pulse duration (T) 0.5 seconds.

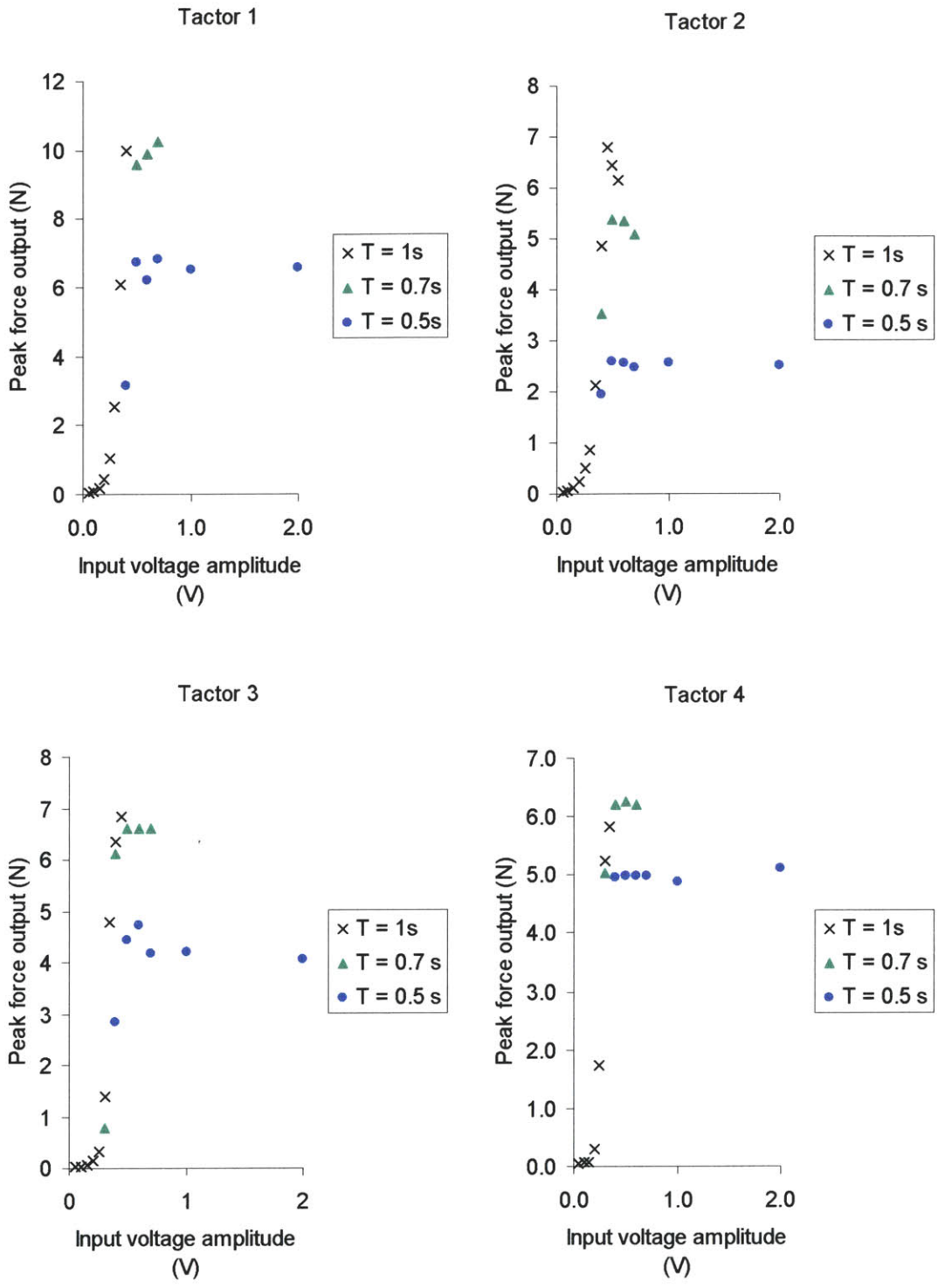

Figure 7-15. Peak force output of tactors 1-4 as a function of the controlling input voltage (V_{in}) and pulse duration (T).

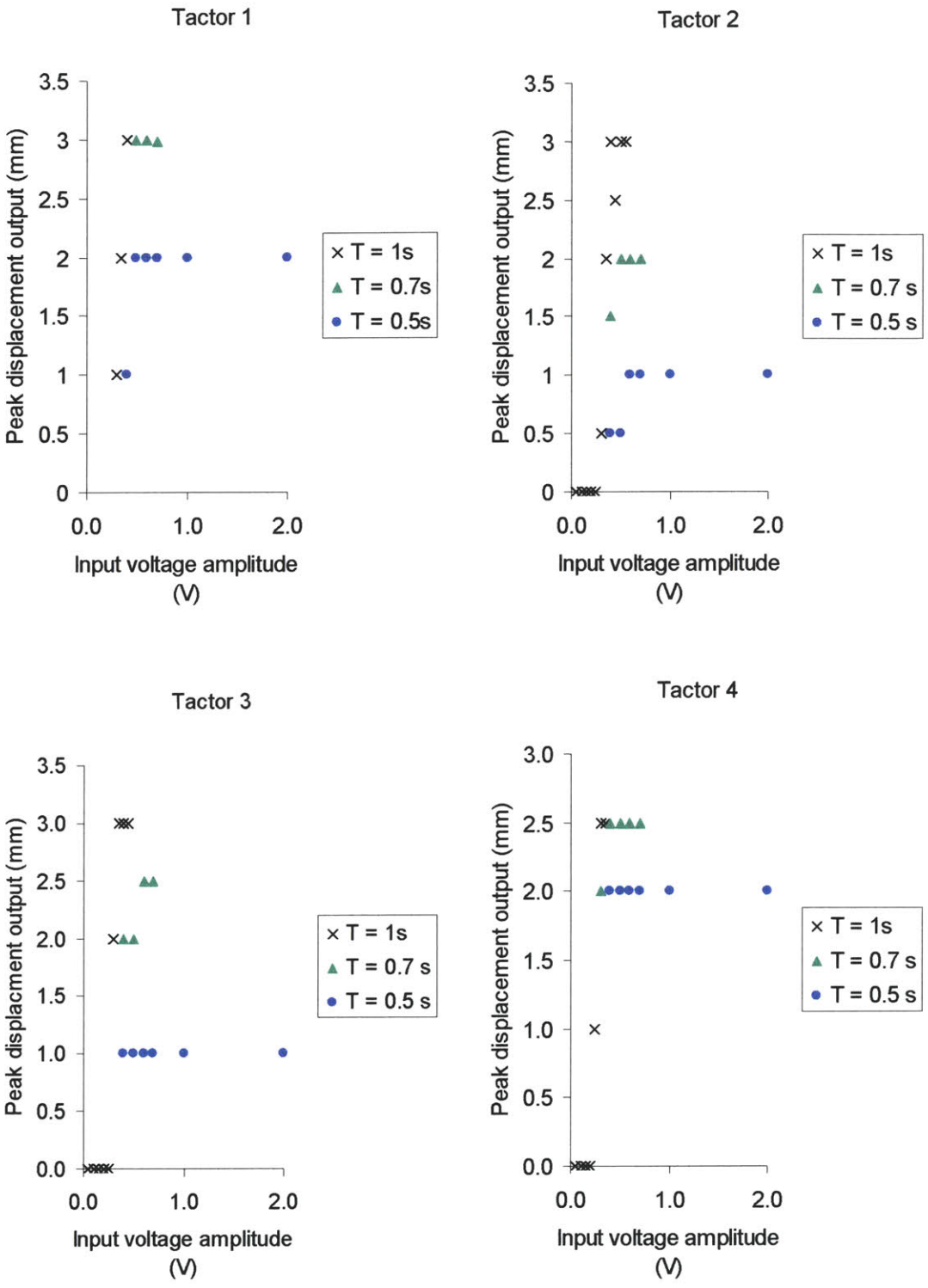

Figure 7-16. Peak displacement output of tactors 1-4 as a function of the controlling input voltage (V_{in}) and pulse duration (T).

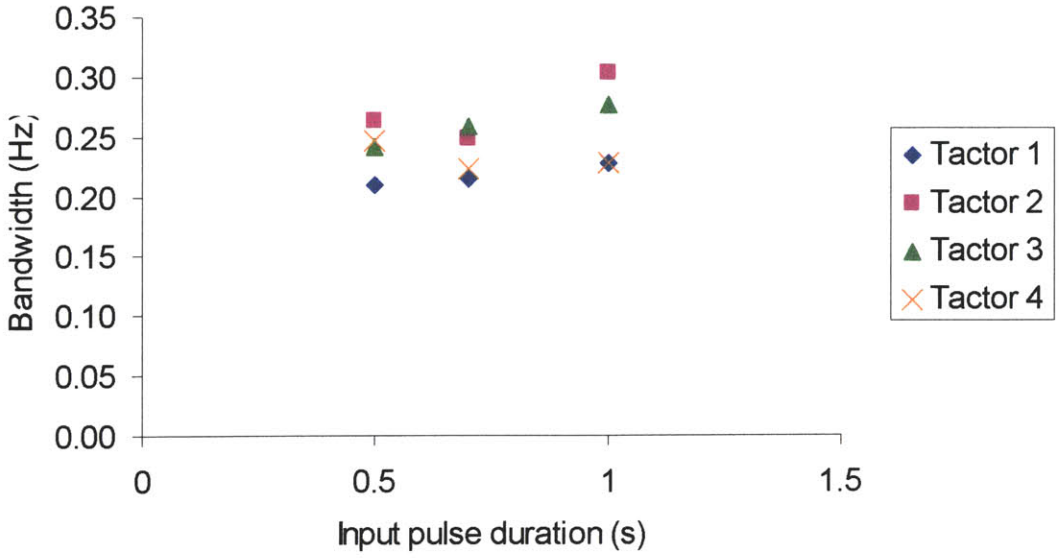

Figure 7-17. The bandwidth for the force output curves shown in Figures 7-6. In general, the bandwidth of the four tactors, for all stimulus waveforms used, remained below 0.3 Hz.

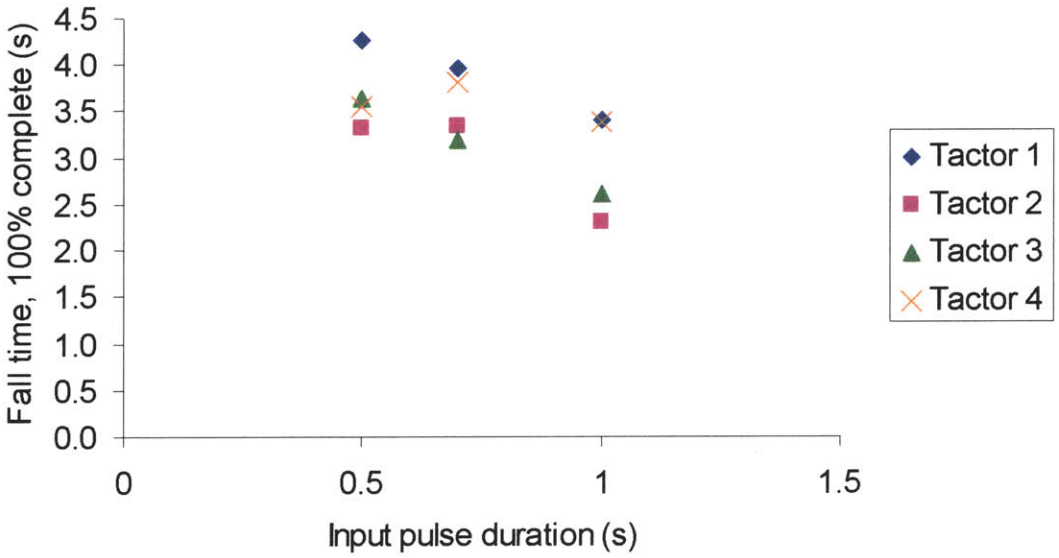

Figure 7-18. Cooling time of the NiTi fibers at 100% completion. The cooling time decreases for increasing pulse duration.

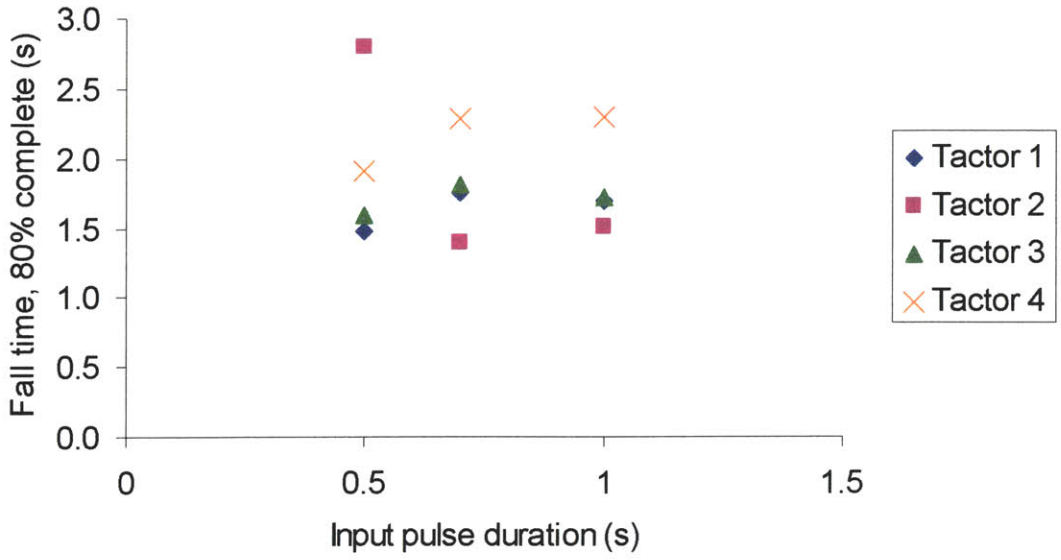

Figure 7-19. Cooling time of the NiTi fibers at 90% completion. The cooling time decreases for increasing pulse duration.

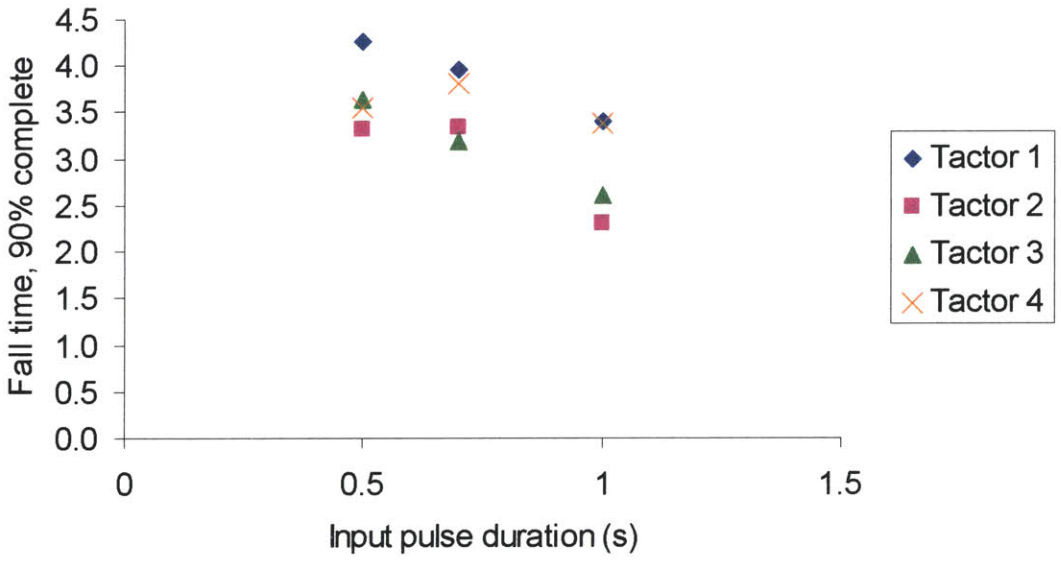

Figure 7-20. Cooling time of the NiTi fibers at 80% completion. The cooling time decreases for increasing pulse duration.

7.3 Discussion

The experimental results demonstrate that the tactor can produce adequate pressure and displacement to stimulate the torso (see Table 7-1). These outputs were achieved using input voltage amplitudes ≥ 0.4 V and pulse durations ≥ 0.7 s. In order to shorten the time of contraction while obtaining the same outputs, it is possible to drive the tactor with a shorter input pulse duration (e.g., 0.7 s versus 1.0 s) and higher pulse amplitude (e.g., 0.5 V versus 0.4 V).

Table 7-1. Desired and achieved outputs of the tactor for the Tactile Vest.

Parameter	Goal	Achieved
Pressure	$\geq$ 120 kPa	95-170 kPa*
		133 kPa* average
Displacement	2-4 mm	0-3 mm
		3 mm average
Bandwidth	maximize	<0.3 Hz

*Converted from units of force using a pin area of 52.8 mm^2.
Larger outputs of pressure are possible by decreasing the pin area.

The same input parameters (voltage amplitude and pulse duration) produced force and displacement outputs that varied greatly between the four tactors. This variation is most likely due to differences in the pre-tension of the NiTi fibers, as well as to disparities in the overall resistance of the fibers and connecting hardware. The initial tensioning of the SMA wire has a considerable impact on the stress and strain generated by the fiber. The wire must be pulled taut enough to deform slightly the SMA from its original shape, so it can then contract and return to its original form upon heating (see Chapter 4 for more details on the shape memory effect). A slack NiTi fiber produces negligible amounts of displacement and stress.

The variations in current applied across the wires also have an effect on the output. In the configuration used here, a voltage is created across the NiTi wire to generate a current across the SMA. Differences in the overall resistance of the fiber and connecting hardware cause variations in the amount of current produced for the same input voltage. A solution to this problem is to convert the driving voltage to a current first, and thus

control the current across the NiTi fiber. (Many attempts were made to implement an op-amp circuit (see Appendix D) that converted voltage to current, but none were successful.) For a given wire tensioning and input current amplitude, the SMA fiber is able to produce repeatable, predictable outputs (see Chapter 5). Therefore, initial preparation of the tactors is required to make certain of the tension of the SMA wires and to determine the proper input power parameters.

The maximum bandwidth achieved was 0.3 Hz. Chapters 4 and 5 discuss several ways of increasing the bandwidth of the SMA fibers (e.g., circulating a fluid around the wires to facilitate heat transfer or pre-conditioning the wires to produce a fast-twitch fiber). Another way to compensate for the low operating frequencies of the SMA is to take advantage of the SMA's compact size and the poor spatial resolution of the torso. Several tactors may be packed closely together, making it likely that the tactors are perceived as a single source of stimuli. In addition, more than one pin along with its actuating NiTi fiber can be packed into a single tactor unit and activated sequentially to produce a higher resultant bandwidth.

8 The Wearable Tactor Array

An array of four tactors was incorporated into a wearable device, and preliminary tests conducted using this device.

8.1 Powering the Array

In order to control an array of tactors (versus just one), circuitry in addition to the previously used equipment is required (see Figure 8-1). A discrete waveform (V_{in}) was created in Mathcad, and fed through one of four channels (0, 1, 2, or 3) of a digital/analog board (National Instruments, PCI-6713). The four channels were each connected to an op-amp circuit (see Figure 8-3), which led to one of the four tactors. The op-amp circuit applied an amplified version of the input voltage signal across the NiTi fiber, producing a current across the SMA wire.

The circuit components were selected as follows (see Figure 8-3). An op-amp (PA16A, Apex Microtechnology) was chosen for its ability to handle large amounts of current (±5 A max.). The R_1 and R_2 resistors had resistances of 999 Ω and 4.99 kΩ respectively, which resulted in a gain of 5. The supply voltage to power the op-amp was set at ±12 V. A circuit for each of the four tactors was built (see Figure 8-5) to activate the NiTi fibers individually.

With this set-up, the tactors can be activated sequentially or simultaneously, simply by controlling the waveform fed to each channel on the D/A card (see Figure 8-1). Figure 8-6 contains samples of stimulating waveforms.

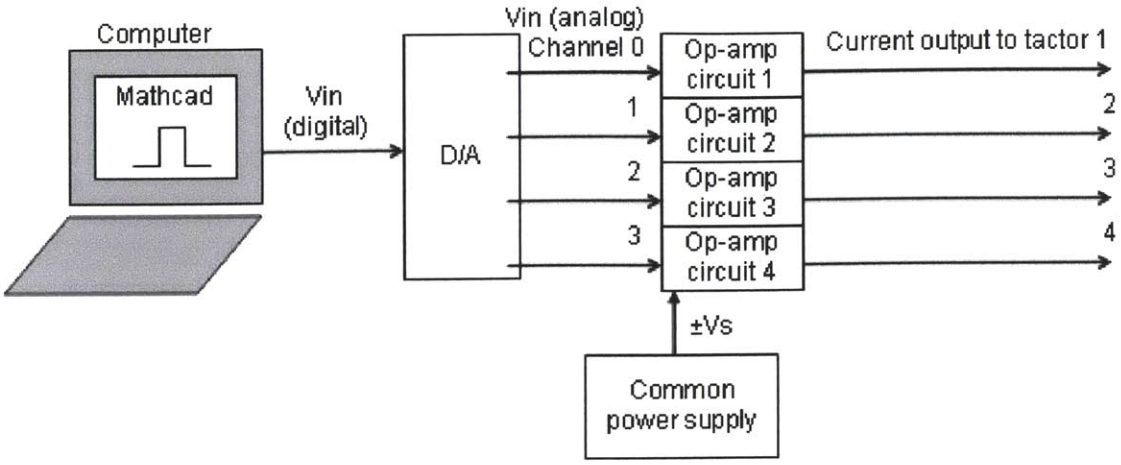

Figure 8-1. Set-up to power an array of four tactors.

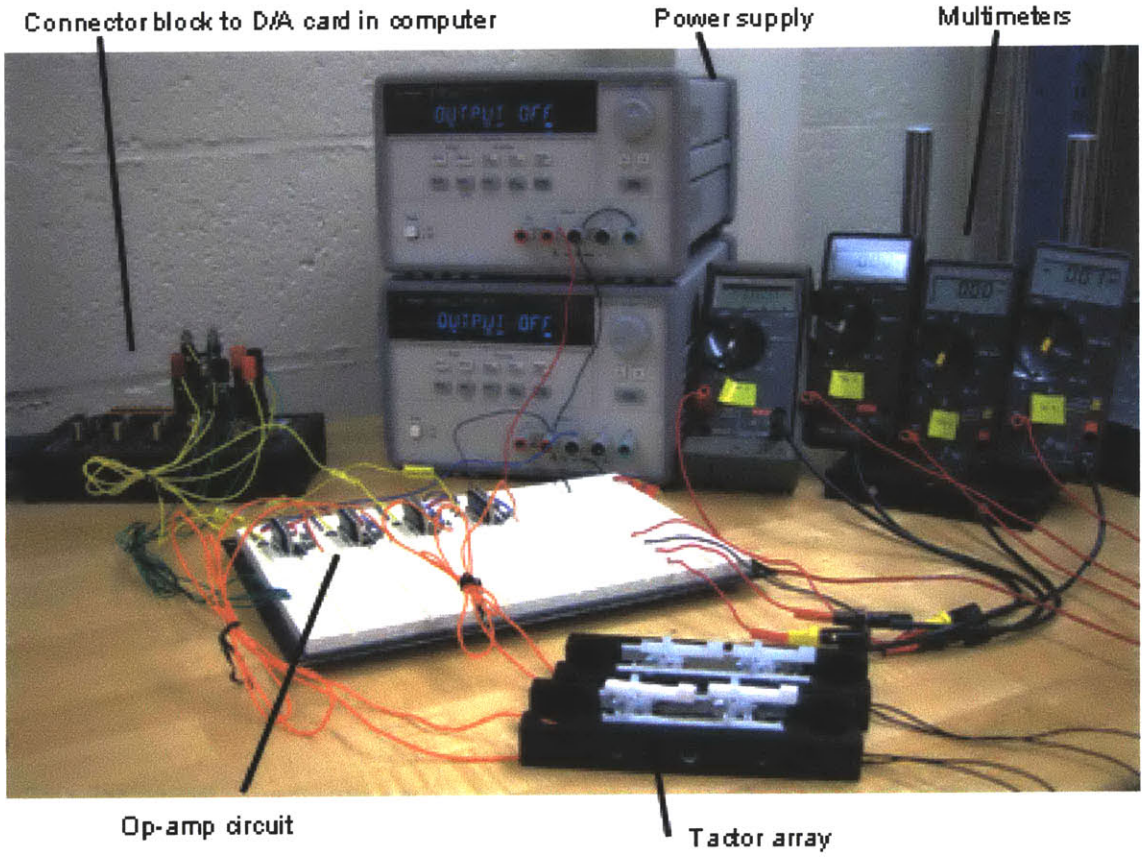

Figure 8-2. Photo of set-up diagrammed in Figure 8-1 (the computer is not shown).

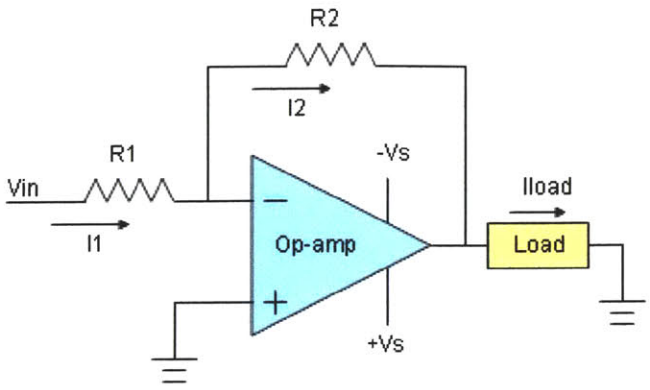

Figure 8-3. Inverting amplifier. This op-amp circuit amplifies the input voltage V_{in} to generate a current (I_{load}) across the NiTi fiber (the load). $\pm V_s$ is the supply voltage from the common power source that powers the op-amp. The gain for this circuit is -R2/R1.

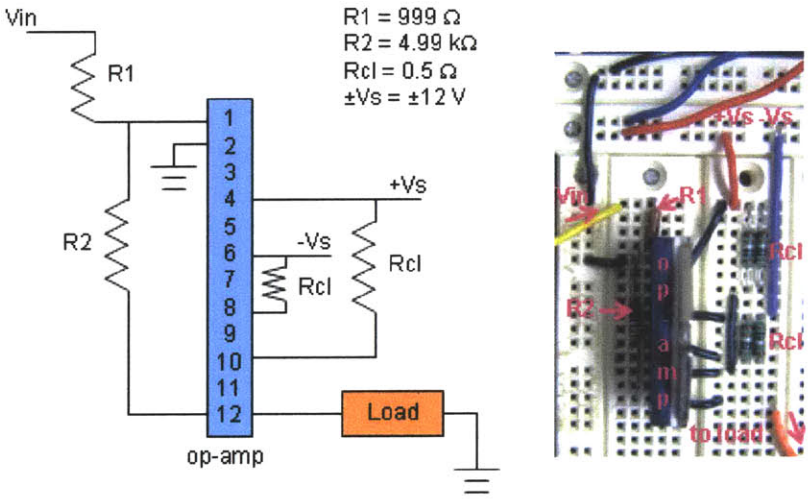

Figure 8-4. Implementation of the circuit drawn in Figure 8-3. Two current limiting resistors (R_{cl}) limit the current flowing through the op-amp.

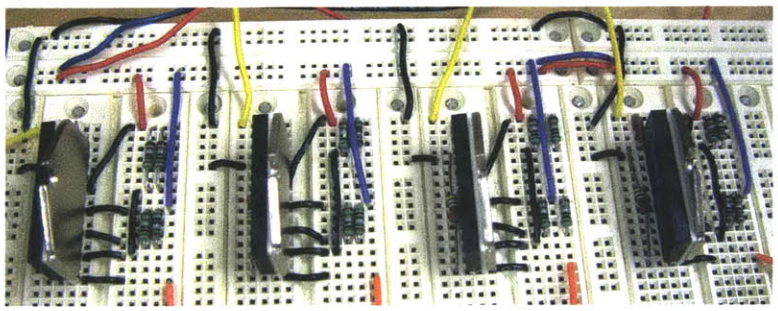

Figure 8-5. The op-amp circuits to power each of the four tactors.

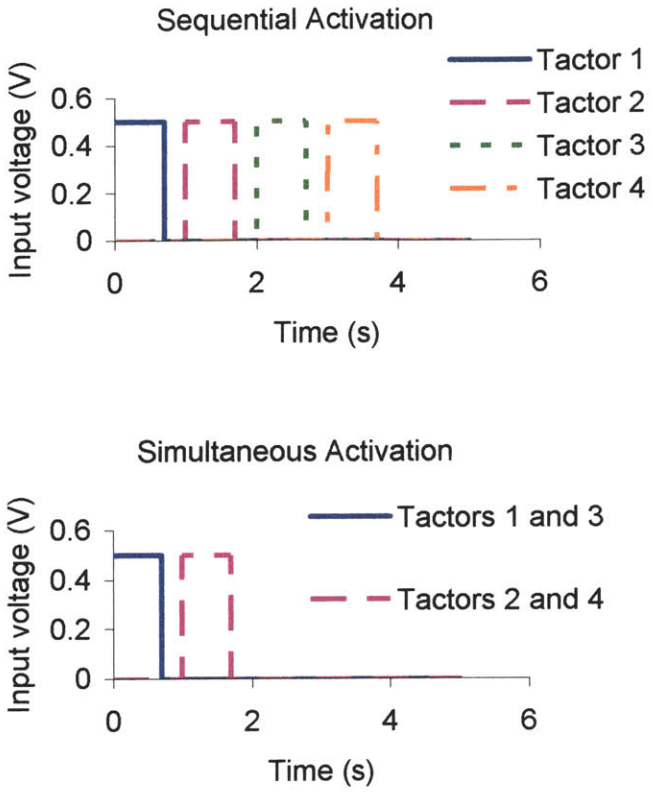

Figure 8-6. Sample stimulating waveforms that activate the tactors sequentially (top) or simultaneously (bottom). The input voltage amplitude, pulse duration, and inter-stimulus interval are variable.

8.2 Making the Tactors Wearable

A stretchable fabric (see Figure 8-7) was used to form a fitting garment around the torso. The tactors were attached to the outside of this garment so that fabric lay between the skin and the pins. Squares of Velcro tape were affixed to the outside of the garment and the top face of the tactors (see Figure 8-8); the tactors were thus detachable and could be moved to different locations. The tactors were arranged linearly and in a 2x2 array (see Figure 8-9). Figure 8-10 shows the tactors situated on a model of the torso. A stretchable bandage (see Figure 8-11) was wound around the array and torso to hold the tactors firmly against the skin.

Figure 8-7. Two types of stretchable fabric. The black fabric is a spandex-like material, and the tan fabric is a nylon-like material (Powernet, Darlington Fabrics).

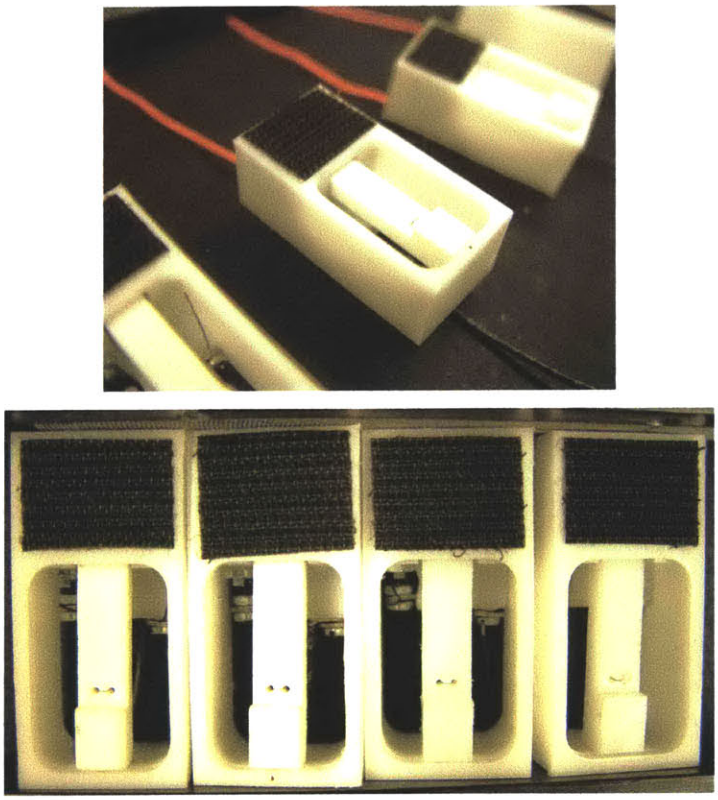

Figure 8-8. Velcro tape was placed on the tops of the four tactors for attachment to the fitted garment.

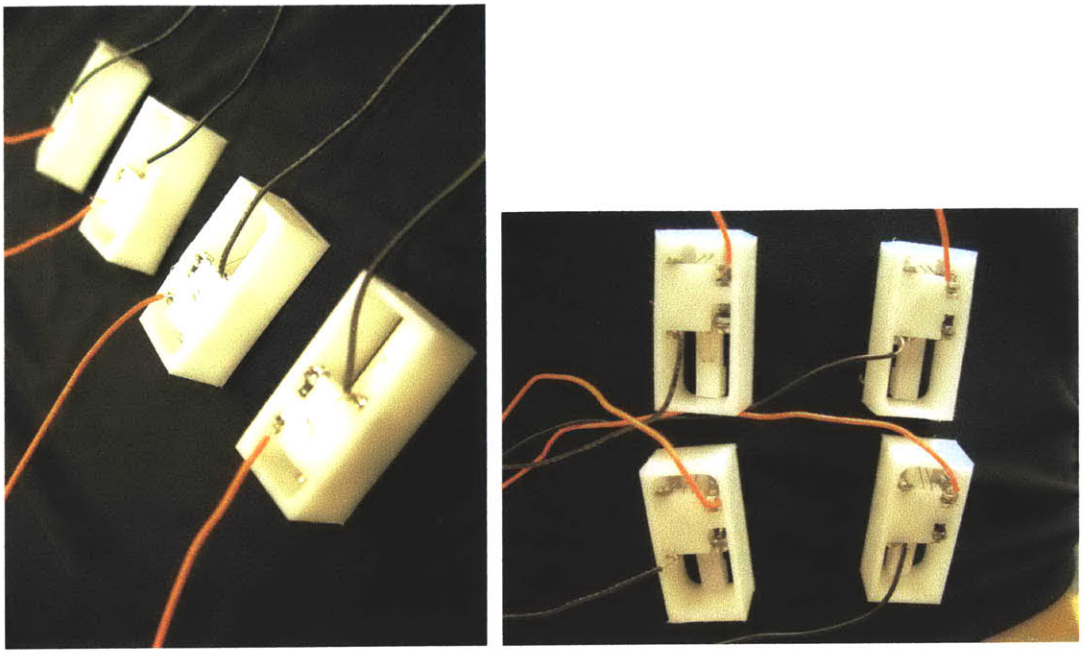

Figure 8-9. The tactors attached to the fitted garment.

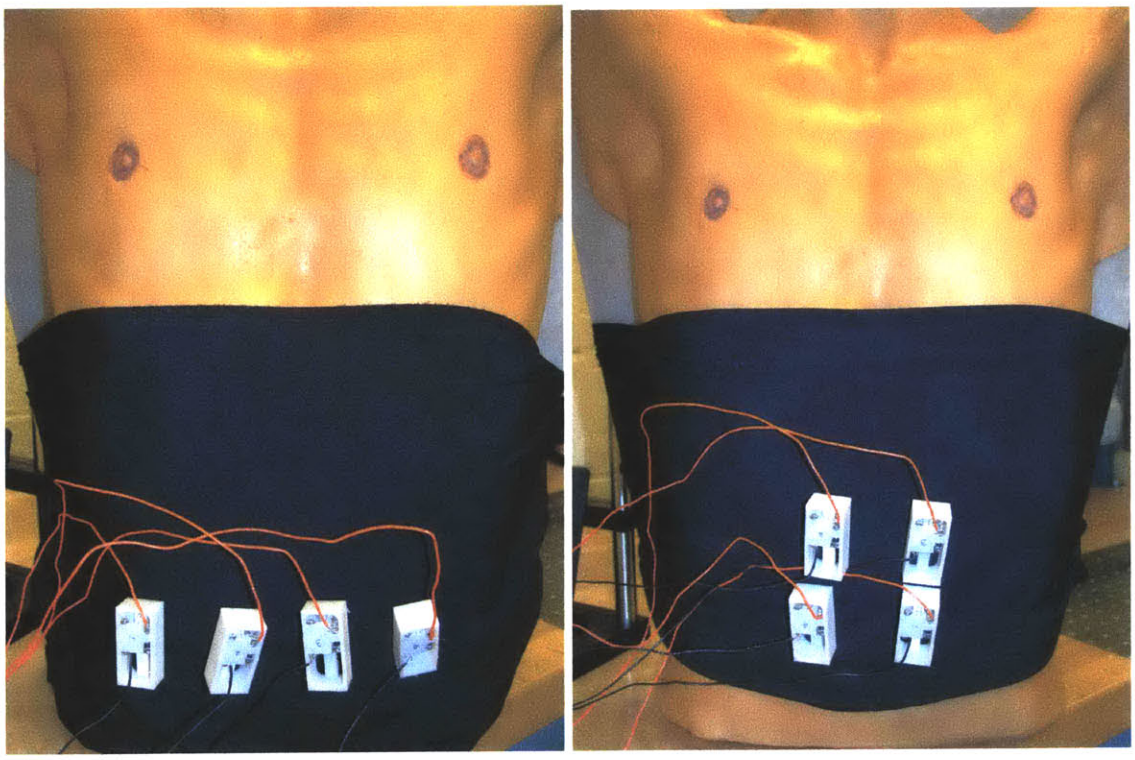

Figure 8-10. The four tactors arranged in a row and a 2x2 array on a model of the torso.

Figure 8-11. A stretchable bandage was used to hold the tactors securely against the skin (Rol-flex cohesive flexible bandage, Smith & Nephew Rolyan Inc.).

8.3 Preliminary Tests

A few preliminary tests were run on the wearable array of tactors. Stimulus parameters that produced displacements of 2.5-3 mm and 5-9 N in force as found in Chapter 7 for each of the tactors were used (see Table 8-1). The tactors were sequentially and simultaneously activated, and placed 50 mm apart in 4x1 and 2x2 arrays against the stomach and back (see Figure 8-12). Only one subject (the author) was tested, and a few qualitative observations of the experience follows.

Table 8-1. Stimulus parameters used to activate the wearable array of tactors, and the outputs achieved previously from these inputs (see Chapter 7).

	V_{in}	T	Force	Displacement
Tactor 1	0.40	1.0	9.9	3
Tactor 2	0.45	1.0	6.8	3
Tactor 3	0.40	1.0	6.3	3
Tactor 4	0.30	1.0	5.2	2.5

The tactile sensations from the tactor activations were not well localized, but felt as firm sensations of pressure, as if someone were gently prodding the skin with a finger. Stimulations from the tactors were easily felt on the stomach, but harder to feel on the back. On the back, stimulations were occasionally missed and the subject had to concentrate in order to feel the activations. Stimulation of the fleshier areas of the back

was more easily felt, while tactors situated along the spinal chord were difficult to detect. When the tactors were placed in a linear configuration and sequentially activated against the stomach, with 0 s between activations, the resulting sensation felt peculiarly like a moving stimulus across the surface, not as isolated points of stimulation.

9 Conclusion

The torso provides a large, relatively unused space for sensory input. The torso is fairly sensitive to touch with pressure thresholds of 20-61 kPa (Weinstein, 1968), second only to the face in sensitivity. In contrast, spatial resolution on the torso is very poor. The two-point threshold is 32-41 mm and point localization is 8.5-12 mm. By comparison, the fingertips have a two-point threshold of 2-4 mm and point localization threshold of 1-2 mm (Weinstein, 1968). However, when the total area of skin available is considered, the torso is able to accommodate over two times more information than the fingertip. The data must simply be presented on a rougher grid.

When tactile information is presented to the torso the limbs are free for other tasks and sensory overload of the eyes and ears is reduced. Torso-based haptic displays have proved useful as sensory substitution devices (Kaczmarek et al., 1991; Kaczmarek and Bach-y-Rita, 1995), balance prostheses (Wall and Weinberg, 2003; Wall et al., 2001), and in improving situation awareness for pilots controlling aircraft (Rupert, 2000; Rupert et al., 1993), and have also shown potential in providing navigation and orientation cues in unusual environments such as under water or during extra vehicular activities in space (Rochlis and Newman, 2000; Traylor and Tan, 2002). A torso-based tactile display may also be used as an alerting mechanism or to focus the user's attention in a certain direction (Lindeman and Yanagida, 2003). A Tactile Vest may aid in situation awareness (e.g., a buzz felt on one side could indicate the approach of a person or vehicle from that direction) using a communication modality that is not seen or heard by anyone else (Rupert, 2000).

Researchers working on devices providing haptic feedback to the torso have noted the need for improved actuator technology. Specifically, the ideal actuator would provide easily felt signals, be light in weight, flexible, and its outputs controllable to render a wide range of stimuli. The results obtained thus far have shown that shape memory alloys have the ability to fulfill the requirements of such an actuator. In preliminary tests, a NiTi fiber 254 μm in diameter was able to displace a pin 3.7 mm and generate over 900 kPa in

pressure (converted from 9.6 N of force transmitted by a pin with an area of 10 mm^2) on average in response to a current pulse with an amplitude of 1 Amp and a duration of 1 second. Furthermore, the SMA underwent thousands of cycles without degradation of its output. The standard deviation of the force output for a single NiTi fiber over 2,000 cycles was 0.49 N, and the standard deviation of the displacement output for the same fiber over almost 800 cycles was 37 μm.

A tactor for a wearable torso-based haptic display, the Tactile Vest, was designed and built using shape memory alloys as the actuator. The overall size of the tactor was 42 mm x 22 mm x 17 mm. The tactor was able to generate adequate pressure and displacement to stimulate the torso. On average, the tactor produced 133 kPa in pressure and 3 mm in displacement at bandwidths $\leq$3 Hz. These outputs were achieved using input voltages $\geq$0.4 V and pulse durations $\geq$0.7 s. The discrepancy between the stress and displacement generated by the tactor unit versus the NiTi fiber in the preliminary tests is most likely due to the difference in geometry of the two configurations. The design of the tactor unit was more compact and involved rotating the pin versus direct vertical displacement.

Four tactors were manufactured to form a 2x2 or 4x1 array, and were attached to a fitting garment worn around the torso. In preliminary tests with one subject using the array, the tactor activations were described as firm sensations of pressure, as if someone were gently prodding the skin with a finger. Tactor stimulations were more difficult to feel on the back as compared to the stomach, especially over firmer skin such as that covering the spinal chord. Stimulations were occasionally missed when they were presented over the bony areas of the back, and concentration was sometimes required to feel the stimuli.

In the development and construction of the wearable tactor array, a number of important design issues that have to be taken into consideration when working with shape memory alloys arose. Initial preparation and testing of the tactors is necessary in order to control the initial tension of the NiTi fibers precisely and to determine the minimal input power parameters. A slack NiTi fiber produces negligible amounts of displacement and stress. In tests of the tactor array, the same input parameters produced force and displacement

outputs that varied widely between the four tactors. These variations were attributed mainly to differences in the pre-tension of the SMA fiber. A minute adjustment in wire tension sometimes increased the pin displacement by up to 1 mm.

In order to produce more uniform outputs across the tactors, current control is also recommended in preference to voltage control to activate the NiTi fibers. In preliminary tests of the SMA fiber, the SMA outputs were repeatable and predictable for a given wire tension and current amplitude. The circuitry used in experiments with the tactor array created a voltage across the NiTi wire, which generated a current across the SMA. Any differences in the overall resistance of the NiTi fiber and connecting hardware in the tactors were reflected by a difference in current output across the SMA wire.

Another factor that needs to be taken under consideration, especially in devices that contact the skin, is the temperature of the SMA fiber during contraction. (The transition temperature of the Nitinol used was 90°C.) Delrin was used for the pin and supporting structure of the tactor. The Delrin came into contact with the SMA, and was able to resist the high temperatures of the NiTi fiber. In preliminary tests of the wearable tactor array, the Delrin adequately insulated the skin from the heat and current generated in the NiTi fiber. Other materials that may be used in place of Delrin are high temperature, machineable ceramics (e.g., Macor).

9.1 Future Directions

Work to maximize the bandwidth of the system should also be conducted. Possibilities include pre-conditioning the SMA wires to produce a fast-twitch fiber, adding a circulating fluid to facilitate cooling, decreasing the diameter of the SMA to increase the ratio of surface area to volume to speed up heat transfer, or using an alloy with a lower transition temperature to reduce the amount of heat to dissipate. The compact size of SMAs and poor spatial resolution of the torso may also be exploited to work around the low operating frequencies of the NiTi fiber. A number of pins and SMA fibers could be packed into a single tactor, and yet be perceived as a single source of stimuli. A higher resultant bandwidth will result by activating these pins sequentially.

Further testing of the wearable array using human subjects is also required. Optimal placement of the tactors, stimulation parameters, and the types of information that can be conveyed by this device are yet to be determined. Additional research on the properties of the touch receptors in the torso would also be helpful. Information on the function and sensitivity of these mechanoreceptors as well as their innervation density and location would assist in determining the optimal manner of stimulating the torso. Determination of the torso's sensitivity to deviations in displacement of the skin and applied pressure is also needed to determine whether the variation of SMA performance is noticeable to the user. Performance of the NiTi fiber varied with a standard deviation of 0.49 N in force, 37 μm in peak displacement, and 17 μm in resting position. If the torso can detect these variations, feedback of the system output (e.g., pin position) may be necessary to control the output of the SMA wire better.

The flexibility and comfort of the Tactile Vest would be improved if the tactor was reduced in size. Using a flexible material (e.g., an electrically and thermally insulating fiberglass fabric) to encase the tactor instead of Delrin would greatly reduce the overall dimensions of the tactor. Work on making the controlling circuitry and power supply portable would also open many more possibilities, allowing the subject to be mobile rather than forced to sit at a desk. Lindeman and Yanagida (2003) have already developed a battery-powered wireless system with 16 controllable outputs based on pancake pager motors.

In conclusion, an array of tactors based on shape memory alloys was successfully constructed for the Tactile Vest. The array was incorporated into a wearable garment, and produced tactile sensations of pressure against the skin. This device has great potential for use in a wide range of applications yet to be explored.

Appendix A: Touch threshold unit conversion

The touch threshold refers to the minimum energy required for a stimulus to be felt by the subject. These measurements are typically made using the nylon myofilaments Semmes-Weinstein monofilaments, which are a modern variant of Von Frey hairs. They are normally calibrated in units of force (log 0.1 mg). Using data from Levin et al. (1978), these values were converted to units of pressure (kPa).

Levin et al. (1978) analyzed two sets of Von Frey hairs. They measured the stress and force corresponding to each filament in a set. The measured stress was plotted against the measured force, and a line fitted to the data (see Figure A-1 for plot). The resulting equation from the best-fit line was used to convert the touch threshold measurement from units of force (g) to units of pressure (g/mm^2).

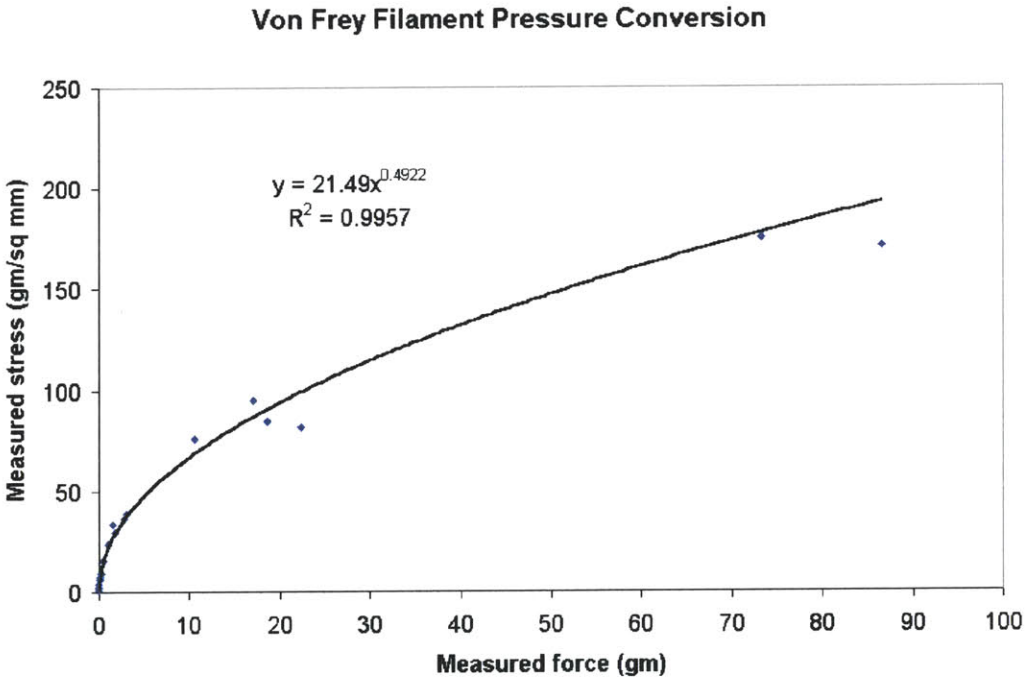

Figure A-1. Plot used to convert touch threshold measurements made using Von Frey hairs from units of force to units of pressure.

The following example illustrates the conversion of the touch threshold measurement in units of force (log 0.1 mg) to units of pressure (kPa):

1. Original measurement using Von Frey hair:

   F = **2.8** log 0.1 mg

2. Convert to units of grams:

   $\log^{-1}(\mathbf{2.8})$ * 1 g / $(0.1*10^3$ mg) = **0.063** g

3. Plug into equation found from best-fit line:

   21.49 * $(\mathbf{0.063})^{0.4922}$ = **5.5** g/sq mm

4. Convert to kPa:

   5.5 g/sq mm * (1 kg / 1000 g) * (10^6 mm^2 / 1 m^2) * 9.81 m/s^2 * (1 kPa / 1000 Pa) = **54** kPa

Appendix B: Spatial resolution and touch sensitivity

Values from various authors for the two point, point localization, and touch thresholds were compiled in the following tables.

Table B-1. Two point and point localization thresholds for various parts of the body. The two-point threshold test determines the minimum distinguishable distance between two points, and the localization test measures the smallest distance at which the subject can tell whether the second of two touches is either distal or proximal to the first touch.

Part of Body			**Threshold**		**Ref**
			Two-pt	**Pt local**	
Torso	Belly, navel level	males	36	8.5	[6]
		females	32	9	
		0 yrs old	14	4.0	[5]
		20 yrs old	19	5.1	
		40 yrs old	24	6.5	
		60 yrs old	31	8.3	
		80 yrs old	40	11	
	Back	males	40	12	[6]
		females	41	10.5	
	Breast	males	32	9	[6]
		females	39	11	
Face	Lip, upper	0 yrs old	1.3		[5]
		20 yrs old	1.6		
		40 yrs old	1.8		
		60 yrs old	2.2		
		80 yrs old	2.5		
	Tongue, tip	0 yrs old	0.71		[5]
		20 yrs old	0.89		
		40 yrs old	1.1		
		60 yrs old	1.4		
		80 yrs old	1.7		
	Cheek, perioral	0 yrs old	5.9	2.1	[5]
		20 yrs old	7.3	2.4	
		40 yrs old	9.1	2.6	
		60 yrs old	11	2.9	
		80 yrs old	14	3.3	
Hand	Finger, tip		1	0.15	[4]
			2		[3]
			2.3		[2]
			2.5	1.5	[1]
		0 yrs old	0.77		[5]
		20 yrs old	1.1		
		40 yrs old	1.5		
		60 yrs old	2.0		
		80 yrs old	2.8		
	Finger, base	0 yrs old	2.7		[5]

Part of Body			Threshold		Ref
			Two-pt	Pt local	
		20 yrs old	3.5		
		40 yrs old	4.5		
		60 yrs old	5.9		
		80 yrs old	7.6		
	Palm, center		10		[3]
			11		[1]
		0 yrs old	5.0	1.9	[5]
		20 yrs old	6.3	2.3	
		40 yrs old	8.0	2.7	
		60 yrs old	10	3.3	
		80 yrs old	13	3.9	
Arm			40		[3]
	Forearm, ventral	0 yrs old	15	7.0	[5]
		20 yrs old	17	7.3	
		40 yrs old	21	7.7	
		60 yrs old	25	8.0	
		80 yrs old	29	8.4	
	Upper arm, lateral	0 yrs old	16		[5]
		20 yrs old	21		
		40 yrs old	28		
		60 yrs old	36		
		80 yrs old	47		
Leg	Thigh		67		[2]
	Thigh, ventral	0 yrs old	12		[5]
		20 yrs old	16		
		40 yrs old	21		
		60 yrs old	29		
		80 yrs old	38		
	Calf, lateral	0 yrs old	29	8.9	[5]
		20 yrs old	31	9.3	
		40 yrs old	33	9.8	
		60 yrs old	36	10.3	
		80 yrs old	39	10.7	
Foot	Sole, center	0 yrs old	7.5	2.1	[5]
		20 yrs old	10	2.7	
		40 yrs old	14	3.5	
		60 yrs old	18	4.5	
		80 yrs old	24	5.8	
	Toe, hallux	0 yrs old	2.5	0.88	[5]
		20 yrs old	4.0	1.4	
		40 yrs old	6.3	2.2	
		60 yrs old	10	3.4	
		80 yrs old	16	5.3	

References: 1. Burdea (1996), 2. Caldwell and Tsagarakis (2000), 3. Gardner et al. (2000), 4. Srinivasan (1994), 5. Stevens and Choo (1996) 6. Weinstein (1968)

Table B-2. Touch threshold of various parts of the body.

Body Part			Units of pressure (kPa)	Units of force (log 0.1 mg)	Ref
Torso	Anterior		24	2.08	[2]
	Breast	males	54	2.8	[3]
		females	39	2.5	
	Back	males	61	2.9	[3]
		females	20	1.9	
	Belly	males	54	2.8	[3]
		females	20	1.9	
Face	Nose	Males	16	1.7	[3]
		females	15	1.65	
	Upper lip	Males	20	1.9	[3]
		females	15	1.65	
	Cheek	males	22	2.0	[3]
		females	15	1.65	
	Forehead	males	22	2.0	[3]
		females	16	1.75	
Hand	Palm	males	85	3.2	[3]
		females	41	2.55	
			83	3.18	[1]
	Fingertip		61	2.90	[1]
	Thumb	males	54	2.8	[3]
		females	34	2.4	
	Pointer	males	61	2.9	[3]
		females	34	2.4	
	Middle	males	54	2.8	[3]
		females	31	2.3	
	Ring	males	48	2.7	[3]
		females	29	2.25	
	Pinky	males	48	2.7	[3]
		females	27	2.2	

References: 1. Burdea (1996), 2. Saddiki-Traki et al. (1999), 3. Weinstein (1968)

Appendix C: Material properties of Delrin and Macor

Table C-1. Material properties of Delrin (McMaster-Carr Supply Company, 2003).

Property	SI/Metric	English
Operating temperature	-29 °C to +82°C	-20°F to 180°F
Melting point	175°C	347°F
Coefficient of friction	0.35	0.35
Tensile strength	69 MPa	10,000 psi
Dielectric strength	20 V/μm	500 V/mil
Durometer	Rockwell M: 94	Rockwell M: 94
Coefficient of thermal expansion		6.8×10^{-5} in/in/°F

Table C-2. Material properties of Macor (Corning Inc., 2003).

Property	SI/Metric	English
Density	2.52 g/cm^3	157 lbs/ft^3
Porosity	0%	0%
Young's modulus, 25°C	66.9 GPa	9.7×10^6 psi
Poisson's ratio	0.29	0.29
Shear modulus, 25°C	25.5 GPa	3.7×10^6 psi
Hardness		
Knoop, 100g	250	250
Rockwell A	48	48
Vickers	400	400
Moh's	4.5	4.5
Flexural strength, 25°C	94 MPa	13,600 psi
Compressive strength	345 MPa	50,000 psi
Tensile strength	90 MPa	
Fracture toughness	1.53 MPa m$^{0.5}$	1,390 psi in$^{0.5}$
Coefficient of kinetic friction, 25°C		
Against steel	0.12	0.12
Against aluminum	0.15	0.15
Against Macor	0.15	0.15
Continuous operating temperature	800°C	1472°F
Maximum no load temperature	1000°C	1832°F
Coefficient of expansion		
-200 – 25°C	74×10^{-7}/°C	41×10^{-7}/°F
25 – 300°C	93×10^{-7}/°C	52×10^{-7}/°F
25 – 600°C	114×10^{-7}/°C	63×10^{-7}/°F
25 – 800°C	126×10^{-7}/°C	70×10^{-7}/°F
Specific heat, 25°C	0.79 kJ/kg°C	0.19 Btu/lb°F
Thermal conductivity, 25°C	1.46 W/m°C	10.16 Btu in/hr ft^2 °F
Thermal diffusivity, 25°C	7.3×10^{-7} m^2/s	0.028 ft^2/hr
Thermal shock resistance	25-100°C	25-100°C
Dielectric constant, 25°C		
1 kHz	6.03	6.03
8.5 GHz	5.67	5.67
Dielectric strength (at 12 mil thickness and 25°C)		
(AC) avg.	9.4 kV/mm	785 V/mil
(DC) avg.	62.4 kV/mm	5206 V/mil
DC volume resistivity, 25°C	$>10^{16}$ ohm-cm	$>10^{16}$ ohm-cm

Appendix D: Voltage to Current Op-Amp Circuit

The circuit shown in Figure D-1 was initially used to convert the input voltage signal (V_{in}) from the computer to a current applied across the NiTi fiber. The circuit could not be made to work after many tries, and one of the op-amps was ruined during these attempts. It was hypothesized that the large amounts of power fed back into the op-amp caused the circuit to blow out. Other voltage-to-current-converting circuits were not tried.

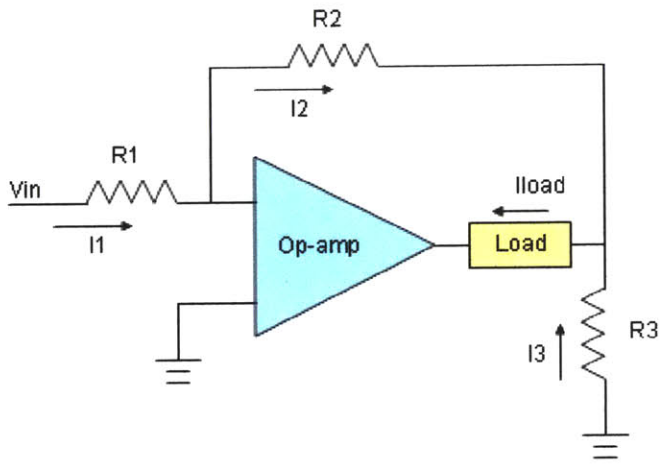

Figure D-1. Voltage to current op-amp circuit.

References

Anquetil, P.A., Yu, H., Madden, J.D., Madden, P.G., Swager, T.M., and Hunter, I.W. (2002). Thiophene based molecular actuators. SPIE 9th Annual Symposium on Electroactive Materials and Structures, San Diego, CA, March 18-21, 2002, 4695, 424-434.

Ascoli, G. (2001). Mechanical sensory systems: audition; somatosensation; pain. Physiological Psychology, Class 7. http://www.krasnow.gmu.edu/ascoli/Teaching/Psyc372_01/Cla7.html, retrieved May 2003.

Bliss, J.C., Katcher, M.H., Rogers, C.H., and Shepard, R.P. (1970). Optical-to-tactile image conversion for the blind. IEEE Transactions on Man-Machine Systems, MMS-11(1), March 1970, 58-65.

Bolanowski, S.J., Gescheider, G.A., and Verrillo, R.T. (1994). Hairy skin: psychophysical channels and their physiological substrates. Somatosensory and Motor Research, 11(3), 279-290.

Burdea, G. (1996). Force and touch feedback for virtual reality, New York: John Wiley & Sons.

Caldwell, D.G. (1992). Polymeric gels: pseudo muscular actuators and variable compliance tendons. Proceedings of the 1992 IEEE/RSJ International Conference on Intelligent Robots and Systems, Raleigh, NC, July 7-10, 1992, 950-957.

Caldwell, D.G. and Tsagarakis, N. (2000). Integrated haptic feedback. In Burdea, Grigore C. and Srinivasan, Mandayam A. (Eds.), IEEE Virtual Reality 2000: Workshop 2, Haptics in Virtual Environments, Hyatt Regency Hotel, New Jersey, March 19, 2000, 7-14.

Cholewiak, R.W. and Collins, A.A. (2000). The generation of vibrotactile patterns on a linear array: influences of body site, time, and presentation mode. Perception & Psychophysics, 62(6), 1220-1235.

Corning, Inc. (2003). http://www.corning.com, retrieved May 2003.

ForeThought Development, LLC. (2000). The Videotact: exploiting tactile perception. http://my.execpc.com/~dwysocki/videotac.html, retrieved May 2003.

Gardner, E.P., Martin, J.H., and Jessel, T.M. (2000). The Bodily Senses. In Kandel, E.R., Schwartz, J.H., and Jessel, T.M. (Eds.), Principles of Neural Science, New York: McGraw-Hill, Health Professions Division, 430-449.

Geldard, F.A. and Sherrick, C.E. (1972). The cutaneous "rabbit": a perceptual illusion. Science, 178, 178-179.

Gray, H. (2001). Anatomy of the human body, Philadelphia: Lea & Febiger, 1918. On Bartleby.com, 2001, www.bartleby.com/107/, retrieved May 2003.

Harvard BioRobotics Laboratory. (2001). http://biorobotics.harvard.edu, retrieved May 2003.

Hasser, C.J. and Weisenberger, J.M. (1993). Preliminary evaluation of a shape-memory alloy tactile feedback display. Advances in Robotics, Mechatronics, and Haptic Interfaces, ASME 1993, DSC-Vol. 49, 73-80.

Howe, R.D., Kontarinis, D.A., and Peine, W.J. (1995). Shape memory alloy actuator controller design for tactile displays. Proceedings of the 34th IEEE Conference on Decision & Control, New Orleans, LA, December 13-15, 1995, 3540-3544.

Hunter, I.W. and Lafontaine, S. (1992a). A comparison of muscle with artificial actuators. Solid-State Sensor and Actuator Workshop. 5th Technical Digest, IEEE, 178-185.

Hunter, I.W. and Lafontaine, S. (1992b). Shape memory alloy fibres having rapid twitch response. US patent 5,092,901.

Johnson, K.O. (2001). The roles and functions of cutaneous mechanoreceptors. Current Opinion in Neurobiology, 11(4), 455-461.

Kaczmarek, K.A. and Bach-y-Rita, P. (1995). Chapter 9: Tactile Displays. In Barfield, W. and Furness, T.A. III (Eds.), Virtual Environments and Advanced Interface Design, New York: Oxford University Press, Inc, 349-414.

Lafontaine, Serge R. Fast Shape Memory Alloy Actuators (PhD Thesis). Department of Biomedical Engineering, McGill University, Montreal, July 1997.

LaMotte, R.H. and Srinivasan, M.A. (1987). Tactile discrimination of shape: responses of slowly adapting mechanoreceptive afferents to a step stroke across the monkey fingerpad. Journal of Neuroscience, 7(6), 1655-1671. (Cited by Burdea, 1996.)

Levin, S., Pearsall, G. and Ruderman, R.J. (1978). Von Frey's method of measuring pressure sensibility in the hand: an engineering analysis of the Weinstein-Semmes pressure aesthesiometer. The Journal of Hand Surgery, 3(3), 211-216.

Lindeman, R.W. and Yanagida, Y. (2003). Empirical studies for effective near-field haptics in virtual environments. Virtual Reality 2003, IEEE Proceedings, 287-288.

McMaster-Carr Supply Company. (2003). http://www.mcmaster.com, retrieved June 2003.

Naval Aerospace Medical Research Laboratory (NAMRL). (2000). Tactile Situation Awareness System (TSAS): information through the sense of touch. http://www.namrl.navy.mil/accel/TSAS/index.htm, retrieved April 2003.

Okamura, A. (2001). ME/CS 530.651 Haptics for Virtual Reality, http://pegasus.me.jhu.edu/~allisono/courses/530.651-2001, retrieved May 2003.

Olausson, H., Lamarre, Y., Backlund, H., Morin, C., Wallin, B.G., Starck, G., Ekholm, S., Strige, I., Worsley, K. Vallbo, A.B., Bushnell, M.C. (2002). Unmyelinated tactile afferents signal touch and project to insular cortext. Nature Neuroscience, 5(9), 900-904.

Peine, W.J., Wellman, P.S., and Howe, R.D. (1997). Temporal bandwidth requirements for tactile shape displays. Proceedings of the Sixth Annual Symposium on Haptic Interfaces for Virtual Environment and Teleoperator Systems, ASME International Mechanical Engineering Congress and Exposition, Dallas, TX, November 15-21, 1997, DSC-Vol 61, 107-114.

Rochlis, J.L. and Newman, D.J. (2000). A tactile display for International Space Station (ISS) Extravehicular Activity (EVA). Aviation, Space, and Environmental Medicine, June 2000, 71(6), 571-578.

Rupert, A.H. (2000). An instrumentation solution for reducing spatial disorientation mishaps: a more "natural" approach to maintaining spatial orientation. IEEE Engineering in Medicine and Biology, March/April 2000, 71-80.

Rupert, A.H., Guedry, F.E., and Reschke, M.F. (1993). The use of a tactile interface to convey position and motion perceptions. Presented at an AGARD Meeting on Virtual Interfaces: Research and Applications, October 1993, 20-1 – 20-7.

Saddiki-Traki, F., Tremblay, N., Dykes, R.W., Derraz, S., El-Khamlichi, A., and Harrison, M. (1999). Differences between the tactile sensitivity on the anterior torso of normal individuals and those having suffered complete transection of the spinal cord. Somatosensory and Motor Research, 16(4), 391-401.

Schmidt, R.F. (1983). Somatovisceral sensibility: cutaneous senses, proprioception, pain. In Schmidt, R.F. and Thews, G. (Eds.), Human Physiology, New York: Springer-Verlag, 211-233.

Shape Memory Applications, Inc. (1999). www.sma-inc.com, retrieved September 2002.

Srinivasan, M.A. (1994). Haptic interfaces. In Durlack, N.I. and Mavor, A.S. (Eds.), Virtual Reality: Scientific and Technical Challenges, Report of the Committee on Virtual

Reality Research and Development, National Research Council, National Academy Press.

Stark, B., Carlstedt, T., Hallin, R.G., and Risling, M. (1998). Distribution of human Pacinian corpuscles in the hand: a cadaver study. Journal of Hand Surgery (British and European Volume), 23B(3): 370-372.

Stevens, J.C. and Choo, K.K. (1996). Spatial acuity of the body surface over the life span, Somatosensory and Motor Research, 13(2), 153-166.

Taylor, P.M., Moser, A., and Creed, A. (1998). A sixty-four element tactile display using shape memory alloy wires. Displays, 18(3), 163-168.

Traylor, R. and Tan, H.Z. (2002). Development of a wearable haptic display for situation awareness in altered-gravity environment: some initial findings. Proceedings of the 10th International Symposium on Haptic Interfaces for Virtual Environment and Teleoperator Systems (in conjunction with IEEE VR), Orlando, FL, March 24-25, 2002, 159-164.

Vallbo, A.B., Olausson, H., and Wessberg, J. (1993). Unmyelinated afferents constitute a second system coding tactile stimuli of the human hairy skin. Journal of Neurophysiology, 81(6), 2753-2763.

Wall, C. III. and Weinberg, M.S. (2003). Balance prostheses for postural control: preventing falls in the balance impaired by displaying body-tilt information to the subject via an array of tactile vibrators. IEEE Engineering in Medicine and Biology Magazine, March/April 2003, 84-90.

Wall, C. III, Weinberg, M.S., Schmidt, P.B., and Krebs, D.E. (2001). Balance prosthesis based on micromechanical sensors using vibrotactile feedback of tilt. IEEE Transactions on Biomedical Engineering, October 2001, 48(10), 1153-1161.

Wellman, P.S. and Peine, W.J. (1997). Mechanical design and control of a high-bandwidth shape memory alloy tactile display. In Casals, A. and de Almeida, A.T. (Eds.), Lecture Notes in Control and Information Sciences, Proceedings of the Fifth International Symposium of Experimental Robotics, Barcelona, Spain, June 15-18 1997, Springer-Verlag, Berlin: 232, 56-66.

Weinstein, S. (1968). Intensive and extensive aspects of tactile sensitivity as a function of body part, sex, and laterality. In Kenshalo, D.R. (Ed.), The Skin Senses, Springfield, IL: Charles C Thomas, 195-222.

Youngblut, C. (1996). Review of virtual environment interface technology. IDA Paper P-3186, produced by Institute for Defense Analysis, http://www.hitl.washington.edu/scivw/publications.html, retrieved May, 2003.